Clinical and laboratory assessment of diabetic microvascular complications

Doctoral thesis

Dr. Gábor Márk Somfai

Semmelweis University
Academic Medical Sciences Programme, 2/10

Tutor:	Professor György Salacz, Ph.D
Co-Tutor:	Dr. Anikó Somogyi, D.Sc.
Official opponents:	Dr. Ágnes Kerényi, Ph.D. Dr. Éva Szökő, D.Sc.
Final exam chair:	Professor János Németh, D.Sc.
Final exam board members:	Professor Péter Kempler, D.Sc. Dr. Tibor Milibák, Ph.D.

Budapest
2008

Table of contents

List of abbreviations

5-HT	5-hydroxytryptamine
A	Adrenaline
ANOVA	Analysis of Variance
AO	Amine Oxidase
aoSSAO	aortic Semicarbazide-Sensitive Amine Oxidase
Ch	Choroid
ChCap	Choriocapillary
CME	Cystoid Macular Edema
CSME	Clinically Significant Macular Edema
DA	Dopamine
DAO	Diamine-oxidase
DM	Diabetes Mellitus
DME	Diffuse Macuar Edema
DRP	Diabetic retinopathy
DRT	Diffuse Retinal Thickening
ECM	Extracellular Matrix
ETDRS	Early Treatment Diabetic Retinopathy Study
FAD	Flavin Adenine Dinucleotide
FD-OCT	Fourier Domain Optical Coherence Tomography
FLA	Fluorescein Angiography
FT	Foveal Thickness
GCL + IPL	Ganglion Cell Layer and Internal Plexiform Layer Complex
hsCRP	high sensitivity C-Reactive Protein
ILM	Inner Limiting Membrane
INL	Inner Nuclear Layer
IQR	Interquartile Range
IS/OS	Inner Segment / Outer Segment
logMAR	Logarithm of the Minimum Angle of Resolution
MV	Macular Volume
NA	Noradrenaline
OCT	Optical Coherence Tomography
OCTRIMA	Optical Coherence Tomography Retinal IMage Analysis Software

ONL	Outer Nuclear Layer
OPL	Outer Plexiform Layer
OR	Odds Ratio
PVD	Posterior Vitreous Detachment
RNFL	Retinal Nerve Fiber Layer
RPE	Retinal Pigment Epithelium
RR	Relative Risk
SAM	Segmentation Accuracy Measure
SD	Standard Deviation
SD-OCT	Spectral Domain Optical Coherence Tomography
SEM	Standard Error of Mean
seSSAO	serum Semicarbazide-Sensitive Amine Oxidase
SMD	Serous Macular Detachment
SNR	Signal-to-Noise-Ratio
SS	Signal Strength
SSAO	Semicarbazide-sensitive amine oxidase
ß-PEA	ß-phenylethylamine
TAS	Total Antioxidant Status
TD-OCT	Time Domain Optical Coherence Tomography
V	Vitreous body
WHO	World Health Organization

1 Introduction and literature review

1.1 The global burden of diabetes

The World Health Organization (WHO) estimates that more than 180 million people worldwide have diabetes. This number is likely to more than double by 2030 according to the projection of WHO. This more than twofold global increase will occur because of population ageing and growth, as well as from obesity, unhealthy diets and a sedentary lifestyle. These latter factors are closely associated with urbanization and industrialization.[1]

Diabetic complications may be classified broadly as macrovascular or microvascular.[2]

Macrovascular complications include heart disease, stroke and peripheral vascular disease (which can lead to ulcers, gangrene and amputation). Other complications of diabetes include infections, metabolic difficulties, impotence, autonomic neuropathy and pregnancy problems.[2]

The three major diabetic microvascular complications include diabetic neuropathy, diabetic retinopathy and diabetic nephropathy. Diabetic microvascular complications result from damage to the small blood vessels in the nerves, eyes and kidneys, and eventually lead to loss of function in these tissues. The walls of the vessels become abnormally thick but weak, followed by bleeding, leakage of protein which slows the flow of blood to the cells. If undetected and untreated, these complications can potentially lead to severe organ damage possibly resulting in limb amputation, blindness, and kidney failure.[3]

Hyperglycemia and hypertension can damage the kidneys' glomeruli. When the kidneys are damaged, protein leaks out of the kidneys into the urine. Damaged kidneys can no longer remove waste and extra fluids from the bloodstream. Diabetic nephropathy is defined as the presence of persistent proteinuria >0.5 gms/24 hours. Overt nephropathy is characterized by progressive decline in renal function resulting in end stage renal disease.[2, 3]

Neuropathy is a heterogenious condition that is associated with nerve pathology. The three major forms in people with diabetes are peripheral neuropathy, autonomic neuropathy, and mononeuropathy. The most common form is peripheral neuropathy, which affects mainly the legs and feet.[2, 3]

In the eye, diabetes may affect almost all anatomical structures: diabetic keratopathy may develop, cataract formation is more rapid and the retina may suffer severe damage leading to the decline and finally the loss of vision.[2, 4]

1.2 Retinal complications of diabetes

As mentioned above, diabetes can affect the eye in a number of ways. The most serious eye condition associated with diabetes involves the retina and more specifically, the network of blood vessels lying within it.

1.2.1 Diabetic retinopathy

Diabetic retinopathy (DRP) is an important cause of blindness, and occurs as a result of long-term accumulated damage to the small blood vessels in the retina. After 15 years of diabetes, approximately 2% of people become blind, and about 10% develop severe visual impairment.[1]

Diabetic retinopathy is composed of a characteristic group of lesions found in the retina of individuals having had diabetes mellitus for several years. The abnormalities that characterise diabetic retinopathy occur in predictable progression with minor variations in the order of their appearance. Diabetic retinopathy is considered to be the result of vascular changes in the retinal circulation. In the early stages vascular occlusion and dilations occur. It progresses into a proliferative retinopathy with the growth of new blood vessels. Macular edema (the thickening of the central part of the retina) can significantly decrease visual acuity. (Fig. 1.)

Figure 1. Color fundus image (left) and Fluorescein Angiography (FLA) late phase image (right) of an eye with moderate diabetic retinopathy and severe diabetic maculopathy. On the color fundus image retinal hemorrhages and microaneurysms can be seen, while the white-colored hard exudates are indicative of diabetic macular edema. On the late phase of the FLA diffuse leakage can be seen in the macula with several microaneurysms scattered around the entire retina.

It is estimated that in 2002 diabetic retinopathy accounted for about 5% of world blindness, representing almost 5 million blind.[5]

According to the survey conducted by Süveges and Schneider in 2002 in Hungary, 60% of patients with diabetes have retinopathy (23% of type 1, and 65% of type 2 diabetics).[6] According to recent data by Németh et al., DRP is the second leading cause of registered blindness in Hungary, with an increasing tendency. Blindness due to retinopathy among Hungarian patients with diabetes was 4,23% - it is worth considering that in Budapest it was 1,98% while int he rest of the country it was 4,86.[7]

1.2.2 Diabetic macular edema

Diabetic patients with long standing diabetes have a high risk for the development of diabetic maculopathy.[4] Diabetic maculopathy is the leading cause of visual impairment in the working-age population in developed countries and thus is one of the major ocular health problems worldwide.[8] Specifically, diabetic maculopathy is very common in people with more severe background DRP. In diabetic maculopathy, fluid rich in fat and cholesterol leaks out of damaged vessels. (see Fig. 1.) If the fluid accumulates near the center of the retina (the macula) there will be distortion of central vision. If too much fluid and cholesterol accumulates in the macula, it can cause permanent loss of central vision.[4]

Fluorescein angiography is more sensitive than biomicroscopy for the qualitative detection of fluid leakage causing macular edema, but angiograms are not indicated for quantitative assessment of macular thickness, which remains subjective and correlates better with visual impairment.[9] Howewer, one of the main requirements in routine clinical assessment of diabetic maculopathy is for quantitative parameters, also as an objective basis for assessing the efficacy of therapy. The Early Treatment Retinopathy Study (ETDRS) criteria for classification of macular edema are based on slit-lamp biomicroscopy of macular thickening, independently of the angiographic findings. This classification arose from the need for quantification, but is still not a complete solution, since basically it only distinguishes between two major types of macular edema: Clinically Significant Macular Edema (CSME) and non-CSME.[10] These considerations illustrate the potential of optical coherence tomography (OCT) as a diagnostic technique that gives morphological and quantitative data on retinal thickness.

1.3 Optical coherence tomography (OCT) imaging of the retina

The eye is a unique organ of the human body because of its transparent media allowing direct visualization of the retina. This is one of the main reasons why ophthalmic imaging techniques are developing so incredibly fast, enabling the assessment of more and more details down to a single photoreceptor cell.

Optical coherence tomography (OCT) is one of the fields where state-of-the-art technology meets clinical demands, helping the clinician ophthalmologist with a new dimension of medical thinking: the high resolution cross-sectional plane of the retina.[11] The possibility to gain information on this never-before seen dimension has changed the current view on vitreoretinal diseases.

1.3.1 Basic Principles of OCT

OCT is an extension of optical coherence domain reflectometry to imaging in two or three dimensions.[12] This imaging technique generates a cross-sectional image by recording axial reflectance profiles while the transverse position of the optical beam on the sample is scanned. Thus, the longitudinal location of tissue structures are determined by measuring the time-of-flight delays of light backscattered from these structures. The optical delays are measured by low coherence interferometry. Light reflected from deeper layers has a longer propagation delay than light reflected from more superficial layers.[12]

Conventional or time domain OCT (TD-OCT) is based on the principle of low coherence interferometry: a powerful tool to "section" a transparent object. Low coherence means that the system employs a wide range of wavelengths. The most straightforward and currently the most common interferometer for OCT is a simple Michelson interferometer (see Fig. 2.).[12] A low-coherence source illuminates the interferometer. The light is split by a 50/50 beam splitter into a sample and a reference path. Light retro-reflected from the reference and the sample is recombined at the beam splitter and half is collected by a photodetector in the detection arm of the interferometer. Half of the light is returned towards the source, where it is lost. In addition, the reference arm light is typically attenuated by orders of magnitude in order to improve signal to noise ratio.

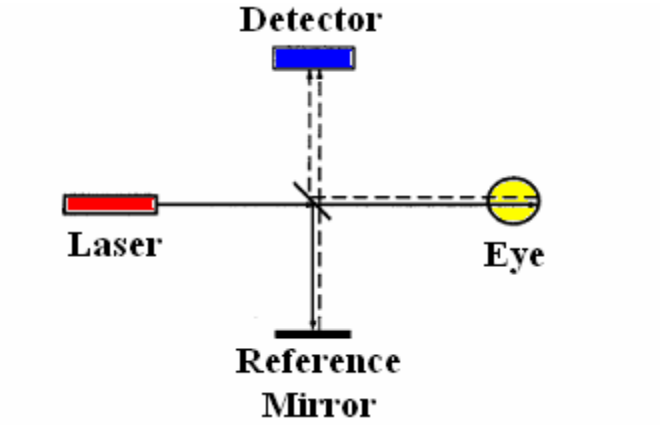

Figure 2. Schematic drawing of the principle of OCT emphasizing how it is essentially a Michelson interferometer. The outgoing light paths are solid lines, while reflected light is drawn as dashed lines.

The axial resolution of an OCT image depends on the coherence length which is a fundamental property of the light source, whereas transverse resolution for OCT imaging is determined by focused spot size, as in microscopy. By rapidly varying the reference arm mirror and synchronously recording the magnitude of the resulting interference signal, a single axial profile or A-scan is obtained which is a graph of the optical reflectivity versus distance in the eye. A sequence of such A-scans is obtained by scanning the probe beam across the entire retina which forms a B-scan tomogram. As a result, a cross-sectional view of the structure similar to a histology section is obtained. The method and also its display in originally greyscale pixels is very similar to that of ultrasound, with the exception that light is used for imaging purposes rather than light, leading to the above mentioned advantages of higher resolution resulting from a shorter wavelength.

OCT can be used for retinal imaging and anterior segment imaging. The OCT for ophthalmic examination is similar to a slit lamp for anterior segment imaging and a fundus camera for retinal imaging. The instrumentation includes a video display for operator viewing of the anterior segment or fundus while obtaining the OCT images and a simultaneous computer display of the tomograms. Images are stored via computer for the diagnostic record.[11]

1.3.2 Interpretation of the OCT image

The OCT signal from a particular tissue layer is a combination of its reflectivity and the absorption and scattering properties of the overlying tissue layers. Strong reflections occur

at the boundaries between two materials of different refractive indices and from a tissue that has a high scattering coefficient along with a disposition to scatter light in the perfectly backward direction.[12] Thus, an OCT image is a map of the reflectivity of the sample. In most tissues, main sources of reflection are collagen fiber bundles, cell walls, and cell nuclei. Dark areas on the image represent homogeneous material with low reflectivity, such as air or clear fluids. The imaging light is attenuated in the sample, so there is an exponential decrease in the intensity of the image with depth. Blood attenuates the signal faster than collagenous tissues, fat and fluids attenuate the signal the least. Figure 3. illustrates an OCT image of a healthy fovea.

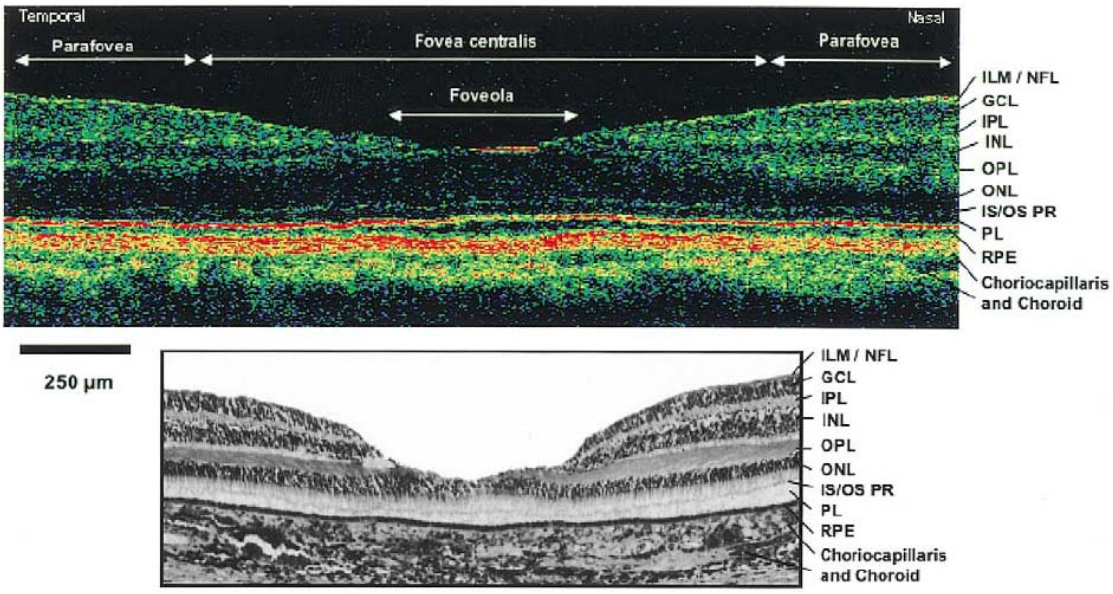

Figure 3. OCT image of the normal human macula. (A) Ultrahigh resolution OCT image showing the various cellular layers of the retina. (B) Comparison of the OCT image (same as shown in A) to a histologic micrograph of the normal human macula. (Image taken from ref. 13).
ILM: Inner Limiting Membrane, NFL (retinal nerve fiber layer), GCL (ganglion cell layer), IPL (internal plexiform layer complex), INL (inner nuclear layer), OPL (outer plexiform layer), ONL (outer nuclear layer), IS/OS PR (photoreceptor inner-outer segment), PL (photoreceptor layer), RPE (retinal pigment epithelium)

In OCT images, the signal strength is represented in false color. High backscatter appears red-orange and low backscatter appears blue-black (see Fig. 3). Thus, cellular layers with different reflectivity are displayed in different colors. It is important to note that OCT image contrast arises from intrinsic differences in tissue optical properties. Thus, coloring of different structures represent different optical properties in false color image and it is not necessarily different tissue pathology (see Fig. 3). Warm colors (red to white) represent areas

of relative high reflectivity, while cold colors (blue to black) represent areas of relative low reflectivity. The exact relationship between the histology of the tissue and the OCT map is still under investigation. Layers with relatively high reflectivity correspond to areas of horizontal retinal elements such as the nerve fiber layer at the retinal surface and the retinal pigment epithelium (RPE) and choroid. Relatively low reflective layers correspond to the nuclear layers and a single layer of photoreceptor inner and outer segments.

A typical example of OCT images of the human macula for normal and pathologic eyes is shown in Figure 4, respectively. The OCT image shown in Fig. 4B is from a subject with cystoid macular edema due to diabetes. This image demonstrates thickening of the macula with several large hyporeflective cystoid spaces in the fovea. When comparing the image of the pathologic subject with the one obtained in the normal subject, the importance of quantifying the structural changes of retinal features and pathologies is obvious.

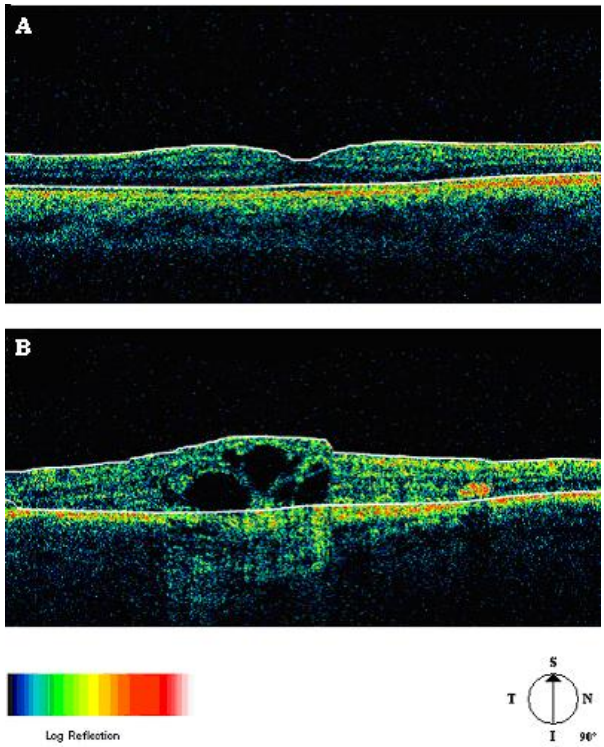

Figure 4. OCT images of the retina for a healthy and pathologic human eye. (A) Image of the retina of a normal subject. Note that the fovea has a characteristic depression with thinning of the retina corresponding to its normal anatomy. (B) OCT image from a subject with cystoid macular edema caused by diabetes. Note the thickening of the macula with several large hypo-reflective cystoid spaces in the central region. The inner and outer retinal boundaries determined by the Stratus OCT^{TM} software analysis are marked in white. The OCT signal strength is represented in false color using the normal visible spectrum scale. High backscatter is represented by red-orange color and low backscatter appears blue-black.

In the retina, the vitreoretinal interface is demarcated by the reflections from the surface of the retina. The retinal pigment epithelium (RPE) and choriocapillaris layer (ChCap) is visualized as a highly reflective red layer and represents the posterior boundary of the retina. Below the choriocapillaris weakly scattered light returns from the choroid and sclera because of attenuation of the signal after passing through the neurosensory retina, RPE, and ChCap. The outer segments of the rods and cones appear as a dark layer of minimal reflectivity anterior to the RPE and ChCap. The intermediate layers of the retina exhibit moderate backscattering (see Fig.3). The fovea appears as a characteristic thinning of the retina. Retinal blood vessels are identified by their increased backscatter and by their blocking of the reflections from the RPE and ChCap (see Fig.3). The larger choroidal vessels have minimally reflective dark lumens.

Below are summarized the OCT features that need to be observed carefully when interpreting the result of a macular OCT image. Before reading it further, we would recommend the Reader to look attentively at figures 4A and 8. Thus, the OCT features of a healthy macula that should be remembered are:

- An intact vitreoretinal interface;
- Contour of the fovea;
- The pattern of the ONL layer (basically representing the photoreceptors), with a cone-shaped thickening underneath the fovea indicating healthy photoreceptors;
- The intact, hyperreflective RPE layer with the IS/OS almost clearly recognizable anteriorly;
- Normal, homogeneous reflection from the choroid, with choroidal vessels sometimes faintly recognizable deeply;

1.3.3 Quantitative measurements on OCT images

OCT can aid in identifying, monitoring and quantitatively assessing various posterior segment conditions including macular edema, age- and non-age related macular degeneration, full and partial-thickness macular hole, epiretinal membrane, intraretinal exudate, idiopathic central serous chorioretinopathy, RPE detachment, detachment of the neurosensory retina, macular lesions associated with optic nerve head pits or glaucoma.

OCT can demonstrate the presence of edema where it is not seen on biomicroscopy or angiographically. A very important feature of the OCT system is that it provides information on the retinal structures. For example, the location of fluid accumulation in relation to the different retinal layers may be determined and the response to treatment without the need to perform invasive studies such as fluorescein angiography may be objectively monitored. At the same time it may be possible to explain why some patients respond to treatment while others do not. OCT has significant potential both as a diagnostic tool and particularly as a way to monitor objectively subtle retinal changes induced by therapeutic interventions. Thus, OCT may become a valuable tool in determining the minimum maintenance dose of a certain drug in the treatment of retinal diseases, and may demonstrate retinal changes that explain the recovery in some patients without angiographically demonstrable improvement and lack of recovery in others.

In the clinical routine, measurement of retinal thickness by the OCT software depends on the identification of the internal limiting membrane and the hyper-reflective band believed to correspond to the retinal pigment epithelium – choriocapillaris interface (or, more precisely, the photoreceptor inner-outer segment border in the case of third generation OCTs). The OCT software calculates the distance between these 2 boundaries across all of the sampled points (usually along 6 evenly spaced radial lines) and interpolates the retinal thickness in the unsampled areas between these lines. As a result, central retinal thickness in the foveal centre can be obtained, along with total macular volume in a 6.0 mm and a 3.5 mm radius. The Stratus OCT has an optional built-in normative database that is very reliable in detecting thickness alterations from the age-adjusted normal values. Besides, there is a possibility to track thickness and volume changes by comparative analyses provided by the software. This enables the clinician to follow retinal changes as they occur either naturally or as a response to therapy.

However, once the various layers can be identified and correlated with the histological structure of the retina, it may seem relevant to measure not only the entire thickness of the retina, but the thickness of the various cellular layers. Moreover, measuring the reflectance of the various retinal layers on OCT images may also be of interest.[14] For example, Drexler et al. have shown in *in vitro*[15] and *in vivo*[16] studies that physiological processes of the retina lead to optical density changes that can be observed by a special M-mode OCT imaging, known as

optophysiology. Thus, it also seems rational that quantitative analysis of reflectance changes may provide clinically relevant information in retinal pathophysiology.

1.3.4 Scanning artifacts, errors and quality on OCT images

Several investigators have demonstrated a relatively high reproducibility of OCT measurements.[17-19] However, quantitative retinal thickness data generated by OCT could be prone to error as a result of image artifacts, operator errors, decentration errors resulting from poor fixation, and failure of accurate retinal boundary detection by the Stratus OCT software algorithms.[20] Therefore, the correct image acquisition along with the accurate and reproducible quantification of retinal features by OCT is crucial for evaluating disease progression and response to therapy.

It is very important to emphasize that usually, image analysis quality largely depends upon the quality of the acquired signal itself. Thus, controlling and assessing the OCT image quality is of high importance to obtain the best quantitative and qualitative assessment of retinal morphology. At present, the Stratus OCT software provides a quality score, identified as the signal strength (SS) but the clinical advantage of this parameter is not really known. The quality score is based on the total amount of the retinal signal received by the OCT system. We note that the SS score should not be used as an image quality score since it is basically a signal strength score. It was previously found that SS outperformed signal-to-noise ratio (SNR) in terms of poor image discrimination.[21] SNR is a standard parameter used to objectively evaluate the quality of acquired images. Stein et al. suggested that SS possibly provides insight into how operators subjectively assess OCT images, and stated that SS is a combination of image quality (SNR) and uniformity of signal strength within a scan.[21] However, additional detail about SS interpretation is not available from the manufacturer because of its proprietary nature. From our experience, if the best attainable image has a SS of less than 6 units, the potential for images to be missing valuable tissue information increases.

On the other hand, certain types of retinal pathology have a propensity to generate poorer quality images and it is difficult to determine whether or not these pathological images are of poor quality, or if these are the best possible quality images that can be acquired in an eye with advanced retinal damage. During the course of scanning patients in our clinics, we have observed several different types of scan artifacts. Some of these artifacts have been

observed previously,[13, 20] and have been also analyzed in a systematic manner[20]. In general, six types of scan artifacts have been identified and classified in two different categories: I) artifacts caused by limitations in the built-in algorithm identifying the retinal boundaries, such as 1) misidentification of the inner retina, 2) misidentification of the outer retina, and 3) artifacts caused by a degraded scan image; II) artifacts derived from poor scan acquisition related to operator error: 4) "off center" artifacts that occurred when the foveal center is misidentified; 5) "cut edge" artifacts, that occurred when the edge of the scan is truncated improperly; 6) "out of register" artifacts, defined as a scan that is shifted superiorly such that the inner retina is truncated.[20]

Finally, it is worth to mention that the retinal thickness values provided by the Stratus OCT mapping software should be carefully reappraised. For example, due to the operator pitfall's errors, the Stratus OCT custom built-in algorithm may fail to locate properly the inner and outer boundaries of the retina (see Fig. 5). Since these boundaries are found by a threshold procedure, their estimated locations could be sensitive to relative differences in reflectance between the outer and deeper retinal structures. Thus, even scans of normal eyes could have inner and outer retina misidentification artifacts under operator errors.

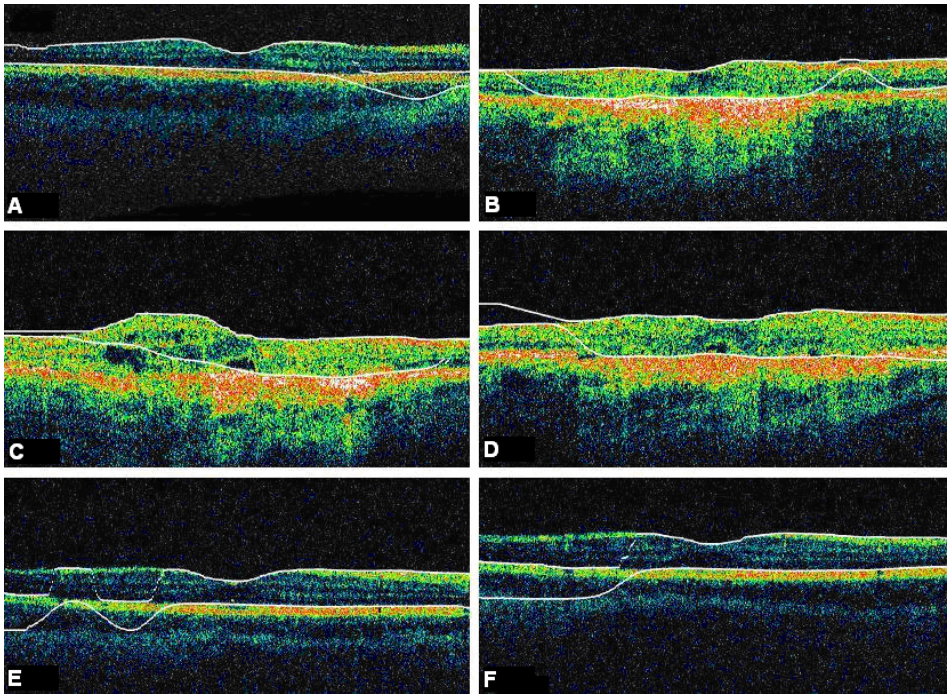

Figure 5. Segmentation results showing the performance of the StratusOCT™ custom built-in algorithm. **(A)** Macular scan obtained for a normal eye under depolarization artifact. Note the misidentification of the outer boundary of the retina (outlined in white). (B-F) Macular scans obtained for different pathological eyes. Note that there are significant errors in the two detected boundaries.

The importance of the above observations lies in the interpretation of OCT scans:

- When looking at an OCT image of bad quality image we loose information on the structure of the neuroretina;
- Retina misidentification artifacts may lead to false thickness and volume measurements affecting all types of analysis, therefore care must be taken to identify them before interpreting any data derived from OCT.

1.3.5 The use of OCT in diabetes

The diagnosis and management of diabetic maculopathy by OCT has become very popular since the introduction of the technology. In 1995, Puliafito, Hee and collaborators shown that OCT was an effective technique for monitoring central foveal thickness in patients with macular edema.[11] Three years later, Hee et al demonstrated for the first time the potentiality of OCT as a method for screening for the early development of DME.[10] This study also reported OCT to be more sensitive than slit lamp biomicroscopy for detection of small changes in retinal thickness (i.e. changes of <100 microns greater than the mean retinal thickness in normal subjects). It is worth to mention that changes of this magnitude are too subtle for the human eye to detect on stereo fundus photographs as well as binocular slit lamp biomicroscopy, the latter presumably being the better way of assessing retinal thickening.[22] Strom et al. found a significant degree of agreement between stereo fundus photographs and OCT for both the area and location of retinal thicknening.[23] Specifically, precise agreement was found in 69 of 82 eyes when comparing measurements of the area of retinal thickening. Shaudig et al also reported OCT as a more sensitive diagnostic method than slit-lamp biomicroscopy to small changes in retinal thickness in diabetic patients without CSME.[24]

In addition, OCT images in macular edema usually show increased retinal thickness, and the presence of low intraretinal reflectivity characterized by Otani and associates in two distinct features: (1) outer retinal swelling represented by an ill-defined, widespread hyporeflective area of thickening, and (2) cystic hyporeflective spaces, with high signal elements bridging the retinal layers.[25] In general, studies with OCT in diabetic subjects revealed that DME includes three basic structural changes, namely, sponge-like retinal swelling or diffuse macular edema, CME and serous detachment (see Fig. 6.)[25], and it was suggested that macular thickening was frequently abnormal when the foveal thickness was greater than 180 microns with OCT.[10, 25-27]

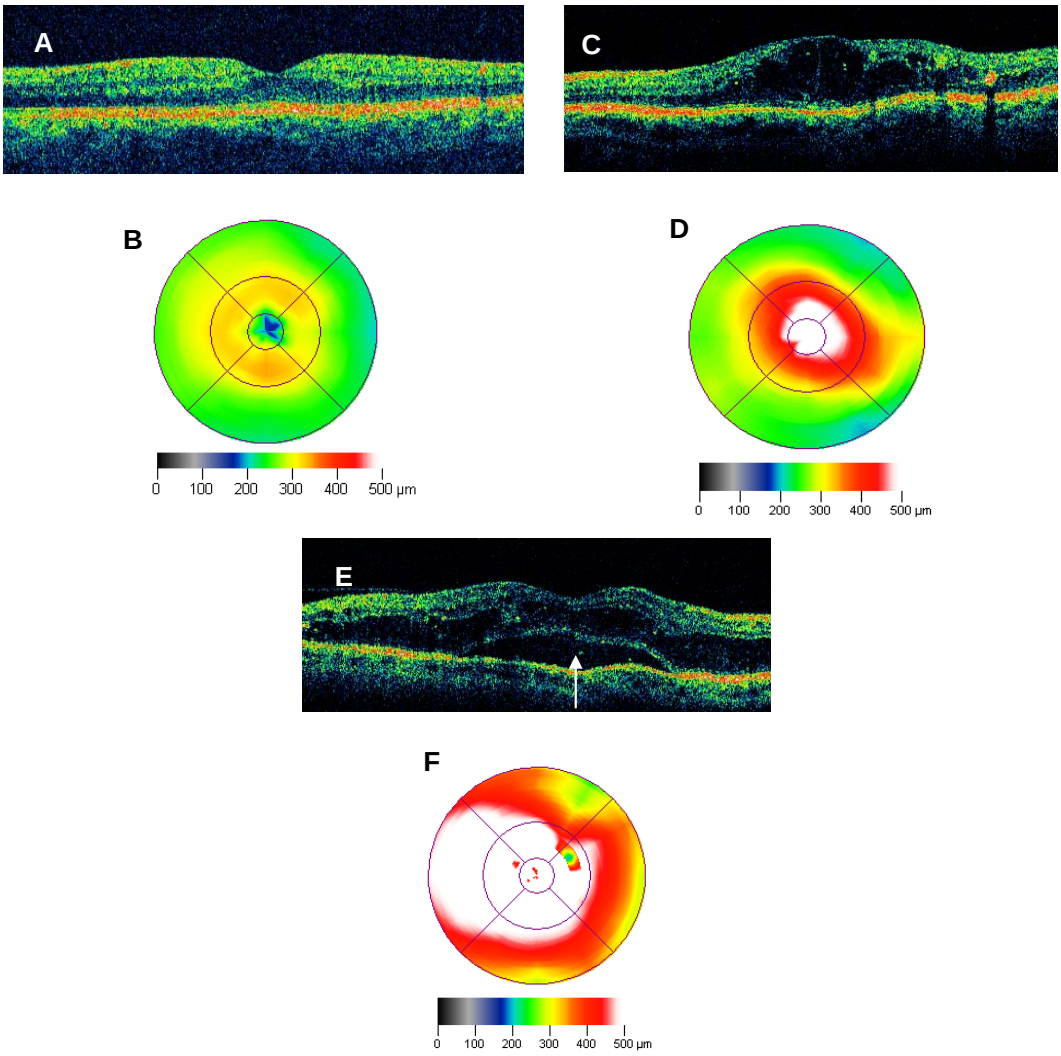

Figure 6. OCT patterns of diabetic macular edema with corresponding macular thickness maps below: diffuse macular edema (A, B), cystoid macular edema (C, D) and serous macular detachment (E, F).

OCT was also useful in the characterization and monitoring of diabetic maculopathy induced by vitreo-retinal traction.[28-30] OCT studies revealed different patterns of diabetic maculopathy and clarified its pathogenesis[25, 31, 32]: sponge-like retinal swelling was the most common appearance (88%), followed by cystoid ME (47%) and serous retinal detachment (15%) (See Fig. 6.).

The utility of OCT has been also demonstrated for monitoring the disease,[10] or to show restoration of the normal foveal profile after vitrectomy for macular edema,[33] or for documenting an early response to laser photocoagulation in clinically significant macular edema (CSME) secondary to diabetes.[34] In this latter study, the authors concluded that the timing of focal laser treatment may be made more objectively with this noninvasive method. In addition, several studies have also demonstrated that OCT can accurately and reliably

quantify macular retinal thickening in diabetic patients in both non-clinically significant DME[24] and clinically significant DME[32, 35].

In another study it was found that OCT can detect early changes in retinal thickness in patients with diabetes.[27] Specifically, their results suggested that abnormal macular thickening may be suspected if the foveal thickness measures more than 180 microns on OCT, which may indicate that the patient is a candidate for more frequent and detailed follow-up.[27] This particular report was the first study showing the usefulness of OCT for the discrimination of DRP. Lattanzio et al. also confirmed the utility of OCT to handle patients with diabetes when objective measurements are needed for checking the course of retinopathy and quantifying the effect of treatments such as anti-edema drugs or laser photocoagulation or vitrectomy.[36] These authors also mentioned that OCT could also be useful for selecting diabetic patients with edematous-exudative maculopathy as candidates for posterior pole laser treatment.

Massin et al. established normal values for macular thickness in healthy subjects and was able to detect early retinal thickening in 12 eyes of 20 diabetic patients (mean age 52 years) with NPDR but no macular edema on biomicroscopy.[37] Goebel et al found that increased retinal thickness detected by OCT was more closely linked with CSME than with angiographically detectable leakage. This study also reported a very good sensitivity (89%) and specificity (96%) of detecting CSME by measuring retinal thickness in the fovea.[26] Furthermore, OCT was also used to evaluate the use of intravitreal triamcinolone for the treatment of DME unresponsive to laser photocoagulation in sixteen eyes of fifteen diabetic individuals with CSME.[38] In this study, quantitative measurement of retinal thickness by OCT showed a reduction from baseline exceeding 55% at the 1-and 3- month follow-up intervals. All eyes also demonstrated a functional response at 1 and 3 months, with an average improvement in visual acuity of 2.4 Snellen lines. They also reported a visual acuity gain average of 1.3 lines at 6 months. Thus, their results based on OCT observations suggested that intravitreal injection of triamcinolone acetonide appears to treat effectively diffuse DME that persist despite laser photocoagulation.[38]

Shaudig et al. also reported a study about the correct classification of macular edema in routine clinical use by using the quantitative assessment of retinal thickness provided by the OCT technology.[39] A study to compare contact lens biomicroscopy with OCT for the detection of diabetic foveal edema in 172 eyes of 95 diabetic patients was lately carried out by Brown et al. Agreement between contact lens examination and OCT for the detection of

diabetic foveal edema was poor when OCT thickening was mild and thus they suggested that contact lens biomicroscopy may be relatively insensitive for the detection of mild foveal thickening apparent on OCT.[40]

In 2005, Gaucher et al. reported results of the different stages of posterior vitreous detachment in diabetic patients (49 eyes of 35 patients) using the OCT 1 system.[30] Their study showed that the stage more frequently found in eyes with DME was perifoveal posterior vitreous detachment PVD with foveolar attachment (stage 1), which seems to be part of a continuous process of vitreous detachment that evolves with aging. Degenring et al. compared OCT and confocal Scanning Laser Tomography (cSLT) for quantitative retinal thickness mapping of the macula and their ability to detect macular edema.[41] Particularly, this study showed that both techniques can differentiate between eyes with and without macular edema, with OCT showing a higher predictive value. In another related study, the retinal morphological changes associated with macular edema of different etiologies was examined with the Humphrey 2000 OCT system (OCT 2). This observational case series study performed on 78 eyes of 78 patients (DME was only present in 27 individuals, mean age 59 years) demonstrated some morphologic differences according to the different etiologies of cystoid macular edema that may be explained by their different pathogenic mechanisms.[42] In this study, the presence of serous retinal detachment was not correlated with poorer visual acuity. Similar results were also obtained by Ozdek et al after examining 195 eyes of 110 patients with different stages of DR with OCT 3 and FA.[43] The authors reported that CME was detected with OCT in 15.4% of eyes, 40% of which was not detected with slit-lamp biomicroscopy and 63.3% of which was not evident in FA. These results indicated the importance of OCT in the follow-up of diabetic patients during the early stages of diabetic maculopathy when the structural changes are not yet evident with slit-lamp biomicroscopy or angiographically.[43]

Sugimoto et al. obtained a high reliability for RNFL thickness measurements in type 2 diabetes patients without DR.[44] This result demonstrated that OCT may also be a useful tool, not only for progressed retinopathy but also for early diabetic retinopathy changes. Moreover, these authors also found that both retinal and RNFL thickness changed significantly in the superior region. Interestingly, this study reported a biometrical difference between the macular and peripapillary's regions. The thickening of the retina seen in the macula region contrasted with the thinning seen for the RNFL in the surrounding papilla. The authors

speculated that the superior RNFL thickness may decrease even in the macular region, but is masked under the existence of edema that causes thickening in the full retinal thickness. Recently, Biallosterski et al.[45] and Nilsson et al.[46] found that the pericentral retinal thickness in diabetic patients seems to be decreased compared to healthy subjects. Conversely, Shaudig et al. found an increasing pericentral retinal thickness in diabetic patients.[24]

Despite some uncertainties regarding the resolution of the thickness map, OCT currently appears to be the most reliable and sensitive technique for detecting and measuring maculopathy changes in diabetic patients.[35, 46-48] The most recent advances of the OCT technology (i.e. UH-OCT, SD-OCT., etc) will definitely play a key role in the future management of patients with diabetic maculopathy. Particularly, Vandijk et al. (2007) analyzed the sensitivity of OCT in the diagnosis of CSME using the time-domain Stratus OCT and the spectral-domain Topcon OCT.[49] A total of 50 patients were included in this study. This study reported a difference in diagnosis of CSME between OCT and biomicroscopy. OCT missed the diagnosis of CSME in 20 patients using the standard Stratus OCT topographic maps. When the maps were optimized with additional scan lines, the diagnosis of CSME was missed in 9 patients. Moreover, spectral-domain OCT missed the diagnosis of CSME in 7 patients. A search of the current literature, however, found no other study case series for diabetic maculopathy using the new OCT applications.

1.3.6 Optical coherence tomography image segmentation: a future avenue in retinal diagnostics

Most of the work cited above provides convincing evidence that only the changes in retinal thickness have been explored in all the studies related to diabetes mellitus reported to date by using OCT measurements. This limitation is mainly due to the fact that the Stratus OCT only reports thickness and volume measurements of the macular region. Moreover, only the inner and outer boundaries of the retina along with the edges of the retinal nerve fiber layer (RNFL) are extracted by the Stratus OCT built-in algorithm.

Recently, Cabrera et al. have shown that the measurement of retinal thickness along with the various cellular layers of the retina can be extracted from the retinal images obtained with the Stratus OCT system using a segmentation algorithm called OCTRIMA (Optical Coherence Tomography Retinal IMage Analysis).[14, 50] A detailed description of the software can be found in reference [[14]], however here we briefly summarize the algorithm.

The program was developed using a custom automatic and/or interactive boundary detection algorithm written for the MATLAB software platform (The Mathworks, Natick, MA). Raw data files of OCT images are exported to a compatible PC. OCTRIMA searches for peaks on each sampling line instead of applying conventional thresholding techniques. The structure coherence matrix is used in this peak finding process instead of the original data. Usually the following two characteristics of a local maximum of a continuous function are used in peak searching algorithms:

1) Near the maximum the curve is convex and so its second derivative becomes negative, having a minimum value around the maximum of the peak.

2) While passing a peak the first derivative changes sign. In our peak finding procedure, the peak is identified at the point where the first derivative changes sign from either positive to negative or negative to positive. A total of 7 boundaries are automatically extracted using the new approach presented herein. The summarized flow of the algorithm is as follows (see also flowchart shown on Fig. 7.):

1. First the DC bias and the background noise level are removed. The DC bias and background noise level are computed from the mean and standard deviation respectively of the first 50 rows in the OCT image, which are assumed to contain only noise.

2. Apply a nonlinear complex diffusion filter to suppress the speckle noise. The resulting denoised image (real part) is then used in the enhanced coherence scheme in order to obtain the structure coherence matrix.

3. Seeks the internal limiting membrane (ILM) on each sampling line by determining the first peak from the inner side of the retinal structure. The automatic peak finding procedure is applied to each image column individually once the structure coherence matrix (1024x512) is obtained. We note that the ILM is usually defined as the first highly reflective rise from the inner side on each sampling line. Then, starting from the ILM, the next peak below is detected and corresponds to the outer boundary of the RNFL.

4. Seeks the outer side of the retinal pigment epithelium (RPE) layer by detecting the maximum intensity level (i.e. the absolute highest peak) on each sampling line. Defines a starting point at the RPE contour in order to detect the next peak above this layer that corresponds to the outer side of the outer nuclear layer (ONL). From there, the subsequent peaks above the ONL are determined to outline the remaining of the layers (i.e. the ganglion cell layer [GCL] along with the inner plexiform layer [IPL], inner nuclear layer [INL], and the outer plexiform layer [OPL]). The inner side of the RPE layer is determined by looking for peaks below the ONL and above the outer side of the RPE layer.

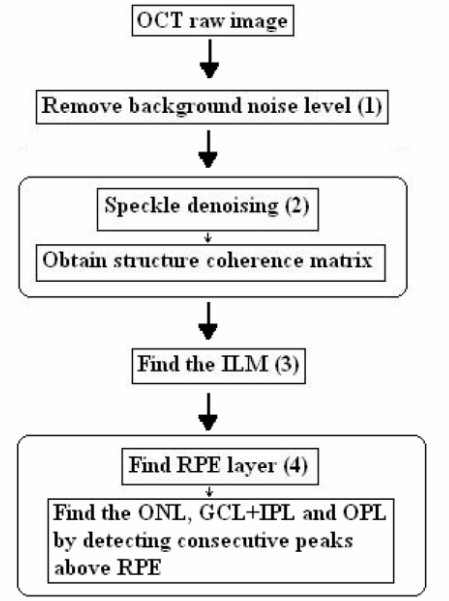

Figure 7. Flowchart of the OCTRIMA software algorithm illustrating the corresponding main processing steps that need to be performed to automatically extract the cellular layers of the retina on OCT images (Taken from: ref. 14)

Thus, the algorithm of the software is able to automatically segment seven specific layers of the retina for the extraction of local reflectance properties and structural information of the retina (See Figure 8). This quantitative approach could provide useful information about the pathological changes in morphology. The quantification of such pathological changes could permit both a better detection and follow up of layers injury as well as understanding of the diseased retina.

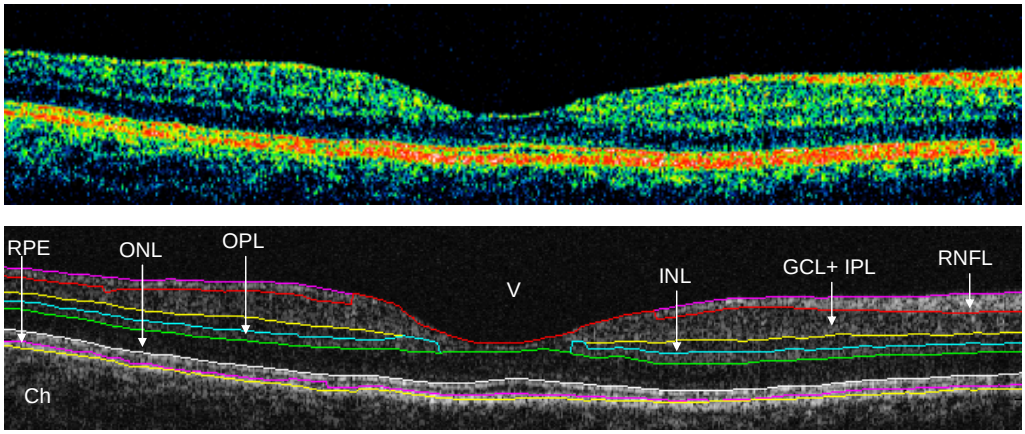

Figure 8. OCT tomogram of a healthy macula before (above) and after segmentation (below) with the OCTRIMA software. The following abbreviations are used for the various layers: RNFL (retinal nerve fiber layer), GCL + IPL (ganglion cell layer and internal plexiform layer complex), INL (inner nuclear layer), OPL (outer plexiform layer), ONL (outer nuclear layer), RPE (retinal pigment epithelium), Ch (choroids), V (vitreous).

1.4 Semicarbazide-sensitive amine oxidase (SSAO) and its role in diabetic microvascular complications

Semicarbazide-sensitive amine oxidase (SSAO) was discovered more than half a century ago during the investigation of amine oxidizing enzymes. The activity of the enzyme belonging to this family was not inhibited by typical monoamine oxidase (MAO) inhibitors, such as clorgyline and deprenyl, for this reason they have been defined by their inhibition with a carbonyl-reactive compound, semicarbazide.[51, 52] This group of enzymes is now classified as amine:oxygen oxidoreductase (deaminating) (copper containing), EC 1.4.3.6, as all of them are inhibited by semicarbazide.

Already in the 1960s it was reported that plasma SSAO activity was elevated in patients with diabetes mellitus[53], in serum or kidney tissues of diabetic patients and animals[54]. It is interesting to note, that the increase of methylamine – a metabolite from one of the reactions catalyzed by SSAO – in the urine of diabetic patients was already observed in a report in 1935. This finding is consistent with later results, discussed in this review..[55, 56]

1.4.1 Enzymatic classification, isoenzymes, the oxidative deamination reaction

There are several enzymes belonging to the SSAO group: diamine oxidases, lysil oxidase, and a group of plasma membrane-bound and soluble amine oxidases, which differ in their substrate specificity and subcellular localization (see Table 1.).

The rest of this work will focus on the characteristics of a group of SSAO enzymes, which are mostly *soluble* or *tissue-bound*, expressed on the cell surface in mammals, and have different preferred substrates like benzylamine and methylamine.[57] These SSAOs are also present in bacteria, yeasts and plants, as well as in mammals and humans.

There are some difficulties because of the large variety of names previouslyly used to describe these enzymes: amine oxidase, copper-dependent (AOC); clorgyline-resistant amine oxidase (CRAO); serum monoamine oxidase; benzylamine oxidase; histaminase; methylamine oxidase etc.[58] Today, the name SSAO is widely accepted to use.

Table 1. Classification of amine oxidases (AOs). FAD: Flavin adenine dinucleotide; DAO: Diamine-oxidase, NA: noradrenaline; DA: dopamine; A: adrenaline; 5-HT: 5-hydroxytryptamine, ß-PEA: ß-phenylethylamine; trypt: tryptamine; ECM: extracellular matrix

Amine Oxidases (AO)						
	FAD-containing AO		Copper Containing SSAO (EC 1.4.3.6)			
	MAO EC 1.4.3.4	PAO	DAO	Cell-surface	Soluble	Lysyloxidase EC 1.4.3.6
Expression	Mitochondria	Intracellular	Intracellular	Extracellular	Serum	Extracellular
Substrates	NA, DA, A, 5-HT, ß-PEA, tyr, trypt	Spermine Spermidine	Putrescine Cadaverine Histamine	Benzylamine Methylamine		Lysine (in collagen and elastin)
Inhibitors	Pargyline Clorgyline Deprenyl		Semicarbazide, hydroxylamine			
Function	Neurotransmission	Cell growth	Degradation of histamine	Amine catabolism Glucose uptake Leukocyte adhesion		Formation of ECM

All SSAOs catalyze deamination of primary amines in a reaction (reviewed in refs. 57, 59, 60):

$$R\text{-}CH_2NH_2 + O_2 + H_2O \rightarrow RCHO + NH_3 + H_2O_2$$

The kinetic reaction consists of two half-reactions. First, the enzyme is reduced by the substrate with simultaneous release of the corresponding aldehyde. In the second part, the enzyme is reoxidated by molecular oxygen with concomitant release of hydrogen peroxide and ammonium. During the oxidative half-reaction, the reduced cofactor recycles back to its oxidized TPQ form. During this process hydrogen peroxide and ammonia are released. [57, 59, 60]

SSAOs only accept primary amines as substrates, although there may be exceptions to this rule.[61] Nevertheless, there appears to be wide variation among the preferred substrates among different species.[57] Benzylamine, an artificial amine, is the preferred substrate for most, if not all, SSAOs, but in addition methylamine, aminoacetone and allylamine are also accepted substrates of the enzyme.[57]

1.4.2 Structure and molecular biology

Most SSAOs are dimeric glycoproteins with molecular masses of 140-180 kDa.[59] SSAOs contain two atoms of copper per dimer. Their prosthetic group, topaquinone (TPQ, 2,4,5-trihydroxyphenyl alanine quinone) is generated from an intrinsic tyrosine of the molecule by a self-processing event that only requires bound copper ion and molecular oxygen.[62] A well characterized E. coli SSAO contains four catalytic domains and displays a mushroom-like shape.[63, 64] A 400 amino acids-long C-terminal ß-sandwich domain contains the active site and forms much of the dimer interface. For a detailed review on structure see reference no. 60 and 61.

Currently full-length cDNA sequences are available from seven mammalian SSAOs. The first SSAO enzyme, encoding the bovine serum amine oxidase (bsSSAO), has been cloned from bovine liver.[65] A human SSAO was then cloned by two independent groups under two different names, human placental amine oxidase (also termed AOC3)[66] and vascular adhesion protein-1 (VAP-1)[67]. Later, a retina-specific SSAO with alternatively spliced variants (designed RAO, or AOC2) has been reported.[68-70] In fact, these three human SSAOs were the only ones from the recently published sequence of the human genome, and they all cluster in the long arm of chromosome 17.[71] Human placenta SSAO and RAO show 65% similarity at the protein level, while there is a lower, though significant similarity (36%) to human kidney amine oxidase (AOC1).[65]

Table 2. Cloned human SSAOs. AOC: amine oxidase, copper-dependent.

AOC1	amiloride binding protein 1 = kidney diamine oxidase
AOC2	retina amine oxidase
AOC3	vascular adhesion protein 1 = human placental amine oxidase
?	human SSAO (pseudogene)

1.4.3 The identity of SSAO with an adhesion molecule, vascular adhesion protein-1 (VAP-1)

An important turning point in SSAO research was its molecular cloning by two independent groups, revealing the identity of human SSAO with an adhesion molecule, vascular adhesion protein-1 (VAP-1).[66, 67]

VAP-1 can be found on smooth muscle cells (both vascular and non-vascular), adipocytes and on endothelial cells[71], and also in intracellular granules of endothelial cells[72] which are translocated lumenally upon elicition of inflammation[73]. It is also known that VAP-1 exists in a soluble form, as well, similarly to SSAO.

Further experiments have shown that the amount of VAP-1 in human serum correlates with detectable SSAO activity[74, 75], moreover, if serum VAP-1 was depleted from sera using anti-VAP-1 antibodies, almost all SSAO activity disappeared simultaneously[74]. According to these findings, more than 95% of the increased SSAO activity seen in diabetes is derived from the soluble VAP-1 molecule.[75] The same results were found in a study by Stolen et al.[76] For the above reasons the same protein is also referred to as SSAO/VAP-1 indicating the similarity in structure and function. We will be using the two expressions according to the literature cited.

1.4.4 The presence and distribution of SSAO

SSAOs are widely expressed in mammals.[57, 72, 73] The most prominent synthesis takes place in smooth muscle (both vascular and non-vascular) and adipocytes, but endothelial cells and follicular dendritic cells are also positive for VAP-1. In contrast, leukocytes, epithelial and fibroblastoid cells are completely devoid of VAP-1. The enzyme is also absent from chondrocytes and odontoblasts, which have been reported to display SSAO activity in other animals. [57, 72, 73]

There has been considerable disagreement as to whether the soluble form is a product of a different gene or a cleavage product of the transmembrane form of SSAO. In man there is evidence that the soluble enzyme is formed by a proteolytic cleavage near the transmembrane region (also called shedding)[77] of the membrane-bound molecule, since the N-terminal sequence of the soluble form isolated from the serum is identical to the membrane distal sequence of VAP-1.[78] Besides, there is additional evidence showing that soluble VAP-1 is mainly produced in the sinusoidal endothelium of the liver by shedding.[78]

In two recent studies it was found that both adipocytes and endothelial cells release a soluble form of VAP-1/SSAO. In the study by Stolen et al. two transgenic mouse models were created with full-length human VAP-1 expressed on either endothelial (mTIEhVAP-1) or adipose tissues (aP2hVAP-1). Under normal conditions elevated soluble SSAO activity

was seen in the mice with endothelial expression, and low levels in the mice with adipose expression. A higher level of SSAO activity was found in the mTIEhVAP-1 homozygous compared to heterozygous mice, indicating that gene dose may influence the activity of the soluble enzyme. Their work has also shown that serum SSAO activity can be derived from the expression of the full-length VAP-1 gene, as VAP-1 knockout mice had no detectable SSAO activity, while endothelial cell-specific VAP-1 expression restored enzyme activity to normal.[79] Another recent study by Abella et al. has shown that human adipose tissue explants and also 3T3-L1 adipocytes release VAP-1/SSAO by a matrix-metalloprotease enzymatic cleavage reaction, also called shedding. The same study has shown that partial ablation of internal white adipose tissue reduces soluble SSAO activity.[80]

SSAO is a membrane-bound ecto-enzyme, and it is plausible that its soluble form is derived from shedding from endothelial cells and adipocytes[79], a process that is inhibited by metalloproteases and enhanced by TNF-a[80]. Insulin impairs TNF-a-stimulated SSAO release from adipocytes.[79, 81]

1.4.5 SSAO activity in physiological conditions

All tissues from man, rat and pig tested showed SSAO activity, but in a greatly varying degree. In all three species high SSAO activity was found in the vasculature and in fat tissue as reported before.[82-84] Human tissues are richer in SSAO activity than tissues from rat and pig (Table 3.)

Table 3. The activity of SSAO measured in selected human tissues (activities expressed in nmol benzaldehyde formed per min per mg protein) (See ref. no. [58])

Fat	artery	vein	umbilical cord	Lung	ileum	gall bladder	adrenal	kidney	pancreas
0,71	2,56	7,93	4,63	3,61	2,21	3,52	1,22	0,78	0,58

It is important to note, that MAO activity is absent in human plasma and SSAO is the only enzyme that contributes to oxidative deamination of primary amines.[58] Human plasma does not contain much SSAO activity compared to most other species (but high activity compared to rodents), in healthy adult subjects plasma SSAO activities are relatively stable, with no sex differences.[74] However, in children values are higher from birth until 16 years of age, when activity suddenly drops to the lower level of adults. This is maintained until the age

of 50 years, when SSAO activity slowly increases.[74] The reason for this phenomenon is unknown.

In a recent study involving 24 healthy male subjects, it was shown that insulin might be involved in regulating the soluble form of SSAO.[85] Plasma SSAO activity was not correlated with insulin sensitivity or fasting plasma glucose levels, while it modestly decreased in response to profoundly raised plasma insulin levels during hyperinsulinemic, euglycemic clamping. Using the same technique, a non-significant decrease was observed after both short-term and prolonged moderate hyperinsulinemia. It is known that SSAO activity is unchanged after incubation with insulin in vitro[86], which makes it unlikely that insulin might have an inhibiting effect in vivo[81]. It is speculated that insulin may decrease plasma SSAO activity by mitigating its shedding from cell membranes into the plasma compartment.[86]

As previously mentioned, Imamura et al. have cloned a retina-specific SSAO gene located on chromosome 17q21 (RAO, or AOC2).[68, 69] Recently, Zhang et al. cloned and characterized mouse and rat AOC2, confirming its presence in the retinal ganglion cells in great abundance. Real-time quantitative-PCR of mouse AOC2 showed that it is only expressed in the retina and no other tissues (brain, heart, liver, lung, spleen and testis), with the protein structure being very similar to AOC3. According to their hypothesis, AOC2 evolved evolutionarily from AOC3 to become a retina-specific gene encoding a novel adhesion protein, but its physiological role is not clear yet.[70]

1.4.6 SSAO in adipose tissue

SSAO is highly and preferentially expressed in white and brown adipose tissue. SSAOs account for approximately 1% of total adipocyte membrane proteins (14×10^6 copies per cell), and its level is upregulated concordantly with adipocyte differentiation.[84, 87, 88] Preadipocytes are practically SSAO negative, whereas mature adipocytes express high levels of SSAO protein and activity, which co-localizes with GLUT4 vesicles. Chronic incubation of 3T3 F442A preadipocytes in the presence of SSAO substrates (benzylamine, tyramine, methylamine, ß-phenylethylamine and also histamine) stimulated adipose cell differentiation. This suggests that SSAO is a member of the adipogenic program, and, in addition, that SSAO may contribute to the acquisition of some final characteristics of fully differentiated adipose cells. It is supposed that the enzyme may exert a double biological function on adipose cells:

first, it may play a regulatory role on metabolic processes, and second, it may control cell-to-cell or cell-matrix interaction.[89]

SSAO gene expression and the corresponding enzyme activity are markedly altered by TNF-α, which, besides having an antilipogenic and lipolytic effect on lipid metabolism, potently inhibits adipocyte conversion.[88, 90] The transcript levels and enzyme activity of SSAO were clearly downregulated in white adipose tissue from obese (fa/fa) Zucker rats compared to (Fa/fa) lean Zucker rats. In the same work, an inhibitory effect of TNF-α was seen on SSAO expression in 3T3-L1 adipocytes. In the light of evidence, that TNF-α is overproduced in white adipose tissue from obese humans and animals (including the fa/fa model), it may be speculated that the reduction of SSAO levels in the obese rats might be related, at least in part to an excess of local systemic TNF-α.[88]

As mentioned above, SSAO co-localizes with GLUT-4 in intracellular vesicles. Enrique-Tarrancón et al. have found that this co-localization is partial, as about 18-24% of total intracellular SSAO is present in the intracellular GLUT4 membrane population purified from isolated rat adipocytes.[84] It is also speculated, that SSAO co-localizes with intracellular GLUT4 in an endosomal population, rather than in the specific storage compartment.[89]

1.4.7 SSAO/VAP-1 in the regulation of inflammatory processes

It has been shown that SSAO/VAP-1, acting as a traditional inflammation-inducible adhesion molecule, is supporting leukocyte rolling under physiological shear[71, 91, 92], mediating leukocyte subtype-specific adhesion[91] and transmigration of leukocytes from the luminal surface of the endothelium to the basolateral surface[93]. As previously mentioned, leukocytes are completely devoid of SSAO/VAP-1.[94]

It is also known that SSAO-mediated adhesion and transendothelial migration of leukocytes through endothelial cell layers is mediated by its enzymatic activity and can be blocked by small molecule inhibitors[93]. The lack of the protein in VAP-1 knockout mice leads to increased rolling velocity and a decreased rate of leukocyte transmigration[95]. Recent work has also demonstrated that VAP-1 functions as a regulator of neutrophil transmigration revealing that neutrophils bind to VAP-1 at two sites and that blockade of either site reduces neutrophil transmigration into the tissues.[94]

1.4.8 Pathobiochemistry: toxic products of SSAO activity

Methylamine and aminoacetone have been reported to serve as good substrates for SSAO. Both amines are found at increased levels in diabetes mellitus[96] and especially in type 1 diabetes[97]. Similarly, rats with streptozotocin-induced diabetes show an elevated concentration of methylamine in urine[56].

Aldehyde dehydrogenases, the enzymes responsible for the oxidation of products from reactions catalyzed by SSAO, are essentially absent in the circulation and this might be a partial explanation for the vascular toxicity of aldehydes discussed later[98].

Moreover, hydrogen-peroxide, a reactive oxygen-species, is also formed as a side product of the catalyzed reaction. In several *in vitro* and *in vivo* models it has been shown that hydrogen peroxide may cause or enhance cell damage caused by free radicals[99] and acts as a cell signaling molecule[100].

Considerable research evidence suggest a role of oxidative stress in diabetic complications[101] in which SSAO may play a substantial role throught its metabolites[97, 102].

The generation of methylglyoxal

When aminoacetone is deaminated by SSAO, methylglyoxal is generated, a substance also connected to vascular damage:

$$CH_3COCH_2NH_2 + O_2 + H_2O \rightarrow CH_3COCHO + H_2O_2 + NH_2$$

Methylglyoxal, despite its production via deamination of aminoacetone, could be derived from several pathways and significantly contributes to advanced protein glycation in diabetes.[103] It has been proposed that aminoacetone is formed from threonine and NADP+ in the mitochondrial reaction catalyzed by threonine dehydrogenase. Threonine dehydrogenase also catalyze the formation of glycine and acetyl-CoA from threonine and it has been speculated that aminoacetone production may be dependent on the metabolic state of the cell, i.e. in a state of nutritional deficiency (diabetes) the ratio of acetyl-CoA to CoA increases and this would result in increased formation of aminoacetone and a parallel decrease in glycine and threonine.[104]

The blood concentration of methylglyoxal is increased in diabetes mellitus, and a strong correlation between this concentration and the degree of diabetic complications has

been reported.[105] Methylgyloxal spontaneously reacts with cysteine, arginine and lysine residues of proteins.[106]

An elevated level of methylglyoxal was recently reported in lenses of diabetic rats, suggesting a role in accelerated cataract formation in diabetes. This elevation was significantly reduced with a parallel decrease in SSAO activity in the lens by the administration of a copper chelating agent, trientine (triethylenetetramine), an agent used in the treatment of Wilson's disease.[107]

The generation of formaldehyde

Methylamine can be produced endogenously by the metabolism of sarcosine, creatinine and adrenaline, and probably inhaled from cigarette smoke, and ingested from food and drinks.[102] The primary metabolite of methylamine after deamination by SSAO, formaldehyde, is a potent angiotoxin:

$$CH_3NH_2 + O_2 + H_2O \rightarrow HCHO + H_2O_2 + NH_3$$

Formaldehyde by itself is a well-known protein fixation agent, which is capable of inducing protein cross-linking due to formation of methylene bridges. The increased production of formaldehyde in the blood from deamination of methylamine could be an alternative mode of increasing blood vessel hardening, which is considered to be a major problem associated with diabetic complication and aging.

Formaldehyde is known to form irreversible adducts by reacting with lysine and arginine residues in proteins, thereby causing a permanent modification associated with functional impairment.[108] Furthermore, in vitro studies indicate that formaldehyde may enhance spontaneous advanced glycation.[56] It has also been shown, in rat, that administration of semicarbazide (an irreversible SSAO inhibitor) increases the urine levels of unmetabolized methylamine.[56] In a cell culture study methylamine, at levels close to those found in the blood of healthy controls, caused endothelial cell death.[109] The same study has shown that unmetabolized methylamine was harmless, i.e. methylamine did not cause any cell damage when SSAO was inhibited, which strongly suggests that the cytotoxicity was caused by formaldehyde.

The increased levels of formaldehyde and malondialdehyde were demonstrated in rat urine after chronic administration of methylamine.[102] In another study in STZ-induced diabetic rats, two weeks after methylamine was administered via drinking water, 12-h collected urine contained significantly elevated levels of formaldehyde, methylglyoxal, and malondialdehyde. MDL-72974A, a potent selective SSAO inhibitor, was found to reduce both formaldehyde and malondialdehyde levels and also reduced other aldehyde excretion, suggesting that the SSAO-mediated deamination of methylamine and aminoacetone indeed occurs in vivo. Moreover, the increase of malondialdehyde in methylamine treated and diabetic rats suggests that increased deamination of methylamine may also enhance oxidative stress. The subsequent increases in aldehyde and oxidative stress, may be related to diabetic complications and also atherosclerosis.[110] It may also be involved in the production of non-enzymatic addition of oligosaccharides to proteins during formation of advanced glycosilation end products, typical of diabetes.[56]

There is further evidence for the above processes as the overexpression of SSAO in mTIEhVAP-1 transgene mice is paralleled by increased AGE-formation, as determined by fluorescence spectroscopy in the sera of 64-week-old mice.[76]

Indeed, plasma SSAO activity has been shown to be correlated with advanced glycation end products, hemoglobin A1c (HbA1c) or fructose amine levels in various reports both in human and animal models of diabetes.[97, 111-113]

Incubated together with smooth muscle cells and soluble SSAO enzyme, methylamine induces apoptosis through the production of formaldehyde which raises a possible pathway how SSAO mediated deamination may contribute to vascular complications in diabetes.[114]

It was shown, that formaldehyde formed from the metabolism of adrenaline (via methylamine) may be a potential risk factor for stress-related vascular damage, e.g. stroke.[115] The occurrence of hypoglycemic episodes is common in association with insulin treatment of type 1 diabetes and these episodes are associated with massive adrenaline release. Hence, this may be a contributing factor to development of cardiovascular complications in diabetes.[96]

According to a recent study, formaldehyde and methylglyoxal are both involved in ß-amyloid misfolding, oligomerization and fibrillogenesis.[116, 117] This finding might give a possible explanation why diabetes mellitus is a well known risk factor for Alzheimer's disease. [116, 117]

1.4.9 SSAO and diabetes

A marked increase in soluble SSAO activity was observed in transgenic mice expressing VAP-1 on endothelial cells and adipocytes after 2 and 5 days of STZ-induced diabetes and hyperglycemia, thus indicating that soluble VAP-1 can be released from both endothelial cells and adipocytes in diabetes. In the same set of experiments it was also shown that VAP-1 overexpression increases the lymphocyte adhesion capacity of endothelial cells and the expression of hepatic redox-sensitive proteins. The latter can result from either direct signaling action of VAP-1 or the SSAO reaction byproduct, H_2O_2. Hydrogen peroxide may act as a regulator of gene expression, while at the same time it is a major reactive oxygen species that may be converted to hydroxyl-free radicals and thus increase oxidative stress, which in turn may lead to the observed protein expression changes.[76]

It is known that TNF-α, which plays an important role in linking obesity and insulin resistance, stimulates the release of VAP-1/SSAO, while insulin and benzylamine counteract these effects.[81]

Hyperinsulinemic clamp tests and intravenous glucose tolerance tests in patients with type 1 diabetes have shown that the level of soluble VAP-1 is not regulated by hyperglycemia, instead, insulin levels correlated inversely with the production of soluble VAP-1.[75] That is, correction of the metabolic decompensation restored sVAP-1 levels to normal in ten minutes, while hypoinsulinema resulted in increased sVAP-1 levels. This implies that insulin might be a physiological regulator of the shedding of VAP-1 into the bloodstream.[75]

An increased hepatic expression of redox-sensitive proteins was found in a mouse model overexpressing human VAP-1 fed on a high fat, methylamine diet for 15 months. As excessive H_2O_2 originating from the enzymatic reaction catalyzed by SSAO can be converted to hydroxyl-free radicals via the Fenton reaction, the changes in protein expression may be secondary to SSAO-induced oxidative stress.[79]

1.4.10 The role of SSAO in atherosclerosis and macrovascular complications

Experimental data previously described above in mTIEhVAP-1 transgenic mice showed that methylamine supplementation modified the progression of atherosclerosis, as the

individual lesions were larger with Oil Red O staining.[76] This suggests that the reaction product of SSAO, formaldehyde might indeed promote atherosclerosis.

In another model of obese diabetic KKAy mice fed an atherogenic diet the administration of a highly potent SSAO inhibitor (FPFA – for complete description, see the reference) was capable of reducing atherosclerotic plaques and weight gain.[118]

In patients with type 2 diabetes elevated serum SSAO activity is associated with vascular complications and the severity of carotid stenosis and carotid plaque score.[111, 119] In the sera of type 2 diabetic patients without vascular complications, serum SSAO activity was significantly higher compared to control subjects, while in patients where macro-angiopathy was also present, SSAO activity was significantly higher than in diabetic patients without complications. Interestingly, there were no significant differences regarding other complications.[120] Soluble SSAO activity correlated with the severity of carotid stenosis and also carotid plaque score. In the same study carotid plaque score, total cholesterol level and age-corrected intima-media thickness showed positive correlation.[120]

Both type 1 and type 2 diabetes patients exhibit higher SSAO activity compared with controls and there is a significant positive correlation between serum SSAO activity and the body mass index (BMI), body weight, hemoglobin A1c (HbA1c), fasting plasma glucose, and triglycerides.[111]

Additionally, there is a concentration dependent increase in LDL oxidation using purified diamine oxidase (DAO) as a model enzyme for SSAO in a cell culture with isolated endothelial cells from human umbilical veins.[121]

The above results suggest that determination of soluble SSAO activity might be a candidate biochemical marker of early atherosclerosis and diabetic macrovascular complications.

1.4.11 SSAO activity and microvascular complications of diabetes, diabetic retinopathy

Plasma SSAO activity is elevated in diabetes with microvascular complications compared to that measured in diabetes without any complications, and this applies both to type 1 and type 2 diabetes.[112, 113, 122]

The fact that SSAO/VAP-1 is involved in the direction of NK lymphocytes and CD8+ T cells to sites of inflammation is of particular interest, taking into consideration that local

non-perfusion of capillaries – a hallmark of diabetic microangiopathy – is associated with capillary occlusion by leukocytes adhering to vessel walls.[123]

Among type 1 diabetic patients with either retinopathy or nephropathy or both plasma SSAO activity is higher compared to type 1 diabetes patients without any complications, and is related to glycosylated hemoglobin.[97]

In a large number of consecutive patients with type 1 diabetes (n=287) a correlation between angiotensin-converting enzyme (ACE) and plasma SSAO activity was described recently.[124] An elevated plasma SSAO activity was found in diabetic patients compared to normals, furthermore, among patients with diabetes plasma SSAO was higher in the group with late complications or hypertension. Plasma SSAO and ACE activities were shown to be correlated in patients untreated with ACE inhibitors or angiotensin II receptor antagonists, regardless of the ACE I/D genotype (n=221). These results suggest that a common, however unknown factor is involved in the regulation of both enzymes. Taking into account that ACE is secreted by shedding[124], similarly to that propsed for SSAO, the above results might be explained by the existence of a common sheddase enzyme.[124]

Grönvall-Nordqvist et al. measured plasma SSAO and urinary methylamine in type 2 diabetes patients undergoing follow-up fundus photography 2,8 years after a baseline examination (which was reported by Garpenstrand et al. in ref. [112]) in order to further investigate the role of SSAO in diabetes mellitus and its vascular complications.[125] In both studies plasma SSAO, the mean HbA1c values were significantly higher, while urinary methylamine/creatinine ratio was significantly lower in patients with retinopathy, compared to those without any complications. There was a weak relationship between micrograms methylamine per milligram creatinine and presence of retinopathy ($p=0.05$) suggested by logistic regression. Interestingly, neither HbA1c values from the baseline or the follow-up, nor the duration of diabetes were found to be related to SSAO activity at follow-up. Important to note, that neither SSAO activity, nor methylamine/creatinine ratio were significantly related to tobacco smoking, although the sample was very small (only four patients were smokers). For the level of retinopathy had changed very little since the baseline investigation, the authors could not draw any conclusions regarding the relationship between changes in SSAO activity and development of retinopathy over time.[125]

The work by Dura et al. involved a larger population, 93 patients with type 2 diabetes, compared with 42 control patients. Diabetic patients were divided into 4 subgroups according to the severity of diabetic retinopathy using the ETDRS classification. SSAO activity was

significantly higher in the high-risk proliferative retinopathy group (PDR) than in the non-proliferative group, and also the group without retinopathy. Mean urinary albuminuria was higher in the high risk PDR group compared to both the group without DR and the control group, although SSAO activities were not significantly different between patients with micro- or macroalbuminuria and patients without this symptom belonging to the same subgroups.[113]

There is only few data regarding the connection between nephropathy and soluble SSAO activity, while there is no data on neuropathy and SSAO activity. In the study by Stolen et al. the mTIEhVAP-1 transgene mice (expressing VAP-1 on endothelial cells) were more susceptible to glomerulosclerosis when fed an atherogenic diet, compared to control transgene mice, suggesting that SSAO may play a role in diabetic nephropathy, too.[76]

1.4.12 The insulin-like effect of SSAO in adipocyte homeostasis and its role in diabetes

In the past few years much attention has been drawn to the membrane-bound isoform of SSAO because substrates of SSAO may exert an insulin-like effect on adipose tissue, which plays an important role in glucose homeostasis and the development of insulin resistance.

When artificial SSAO substrate benzylamine, and endogenous substrate tyramine are provided to mature adipocytes in the presence of vanadate (a potent phosphatase inhibitor), glucose uptake in isolated rat adipocytes is significantly enhanced via a GLUT4-dependent mechanism. This metabolic effect apparently depends on hydrogen peroxide formed, which may regulate trafficking of the glucose transporter GLUT4 to the plasma membrane by the complex generated, peroxovanadium, which is known as a potent insulin mimicker.[126] The effect of SSAO activity on glucose metabolism is exerted via stimulation of tyrosine phosphorylation of insulin receptor substrate (IRS) proteins 1 and 3, leading to the activation of phosphatidylinositol-3-kinase (PI-3 kinase).[84, 127] It is proposed, that the activation of the above pathway causes GLUT4 recruitment to the cell surface and stimulation of glucose transport in adipose cells.[127]

Indeed, acute administration of benzylamine together with a low dose of vanadate enhances glucose tolerance in both non-diabetic and in streptozotocin-induced diabetic rats. Chronic administration of benzylamine and vanadate normalized glycemia in STZ-induced diabetic rats, already noted on the fifth day of treatment.[89, 128] Based on these observations and

on the fact, that insulin is present in only low concentrations in STZ-induced diabetic rats, it was proposed that benzylamine and vanadate have insulin-like effects in adipose tissue.[89, 128]

Similar experiments were performed on Goto-Kakizaki (GK) rats, which are hyperinsulinemic, nonobese and hyperglycemic, showing defective insulin secretion and peripheral insulin resistance but normal insulin stimulated glucose transport in adipocytes. The acute intravenous administration of benzylamine and vanadate enhanced glucose tolerance in GK rats, while administrating vanadate or benzylamine alone did not alter glucose tolerance. Chronic treatment for one week with benzylamine and vanadate reduced the hyperglycemia to levels close to those of the nondiabetic group and ameliorated muscle insulin responsiveness. During the treatment period SSAO/VAP-1 or GLUT4 protein expression was not altered in adipose cells, while basal glucose transport and GLUT4 abundance at the plasma membrane have increased. Incubation of soleus muscle preparations from GK rats showed normal basal glucose transport and insulin resistance, while chronic treatment with benzylamine/vanadate reversed the insulin response to normal levels. During the 2-week combined treatment mRNA levels of leptin, TNFα, or resistin in adipose cells were not altered, similar to plasma concentrations of free fatty acids, indicating that the above effects on glycemia and insulin responsiveness were unrelated to changes in gene expression of adipocitokines. In further experiments results have shown that in the presence of adipose tissues or recombinant SSAO/VAP-1 muscles underwent a marked stimulation of glucose transport by benzylamine/vanadate.[129]

More to this, it was also found, that benzylamine and vanadate enhance insulin secretion. Isolated islets from nondiabetic Wistar and GK rats were incubated in the presence of benzylamine/vanadate, which markedly enhanced insulin secretion in pancreatic islets from GK diabetic rats but not from nondiabetic rats. This effect was blocked by semicarbazide. Abella et al. detected a similar abundance of SSAO/VAP-1 protein in extracts from isolated pancreatic islets compared with extracts from total pancreas, though the abundance of the protein was much higher in adipose tissue than in pancreatic islets, with SSAO activity nearly 300-fold higher in adipocytes than in pancreatic islets. It was also found that the generation of peroxovanadium is seen only in the presence of benzylamine/vanadate, causing a marked inhibition of protein tyrosine phosphatase activity, i.e. stimulation of protein tyrosine phosphorylation. None of the above effects were seen after vanadate or benzylamine treatment alone.[129]

The above results show that the local, SSAO-involved reaction may be instrumental to acutely stimulate glucose transport in adipose cells, glucose transport in skeletal muscle, and glucose-stimulated insulin secretion in pancreatic islets from GK rats.[129]

Similar results were found in adipocytes and skeletal muscle cells of mice and rabbits, by the single administering of benzylamine on its own but without the addition of vanadate. However, in contrast, benzylamine was unable to stimulate insulin secretion by isolated pancreatic cells from both species and SSAO activity was hardly detectable in pancreas.[130]

The inhibition of SSAO in the obese diabetic KKAy mouse model by Yu et al. has led to the prevention of weight gain, which was probably a result of a reduction of adipose glucose uptake and subsequent effect on adipose differentiation.[118] Taking into account the previously discussed results of Stolen et al. in transgenic mice expressing human VAP-1 on endothelial cells and adipocytes, it seems reasonable that obese diabetic subjects may have a higher soluble SSAO activity partly because of SSAO originating from adipocytes.

It might be of great importance in the future that glucose transport is increased in intact *human* adipocytes in the presence of SSAO substrates *alone*, as the addition of vanadate did not further enhance this effect. N-acetylcysteine, catalase and glutathione abolished the effects of exogenous H_2O_2, benzylamine and methylamine, suggesting evidence for an involvement of oxygen reactive species in this effect. Semicarbazide also inhibited this effect, further indicating the involvement of SSAO in glucose transport. An indirect demonstration of the involvement of PI3-kinase activation in response to benzylamine was shown by the sensitivity to wortmannin. Benzylamine and methylamine were also able to mimic the antilipolytic action of insulin, which was not influenced by the α2-adrenergic antagonist RX 821002.[131]

It has to be noted, that monoamine oxidase (MAO) activity is also abundantly present in human fat cells as MAO-A, with a minor amount of MAO-B.[132] In a recently published report it has been revealed that besides SSAO, substrate activation of MAO by the same amines may also exert insulin-like effects on 3T3-F442A adipocytes in a short term-treatment period, while one-week treatment had a similar, insulin-like effect on adipogenesis with the involvement of both enzymes.[132] Various SSAO- or MAO-preferring substrates activated glucose uptake and lipid deposition to the same extent, with the effects of pargyline, tyramine and tryptamine being predominantly involved with MAO activity, and benzylamine and methylamine being specific for SSAO. The administration of the substrates together with insulin exerted a slight additive effect on adipogenesis. Histamine was unable to activate glucose uptake or adipogenesis.[132]

2 Aims

The structural changes in diabetic maculopathy have been studied in depth earlier as described above, however, it is still difficult to detect the first changes in diabetic maculopathy. The value of central foveal thickness represents only one aspect of the macula, but does not reflect any overall changes involving the whole macular region.

Analyzing the entire macula is useful for the early detection of subtle thickness changes, ie. the formation of focal edema which can usually not be seen on angiography at this early stage of the disease. Topographic mapping provided by the built-in software of the OCT device may help qualitative analysis, while total macular volume assessment may be a candidate for the quantitative analysis of macular structural changes.

Serous macular detachments (SMD) occur in some cases of macular edema but the effect of SMD on visual function is unknown.

Thickness information of the various cellular layers of the retina may provide more detailed information about the pathological changes in retinal morphology. The quantification of such pathological changes could permit both a better detection and follow-up of layer injury as well as understanding of the diseased retina. Knowing the limitations of StratusOCT™ thickness measurements it would be crucial to know how imaging artifacts may affect the accuracy of the segmentation algorithm of our own design in order to avoid them in future studies.

Morphological changes of the retina are caused by underlying biochemical alterations caused by poor glucose homeostasis in diabetes. Chronic inflammation is observed to accompany diabetes, being an independent risk factor for its late complications.[133] CRP itself exerts direct proinflammatory effects on human endothelial cells, inducing the expression of adhesion molecules.[134] As SSAO is identical with a traditional inflammation-inducible adhesion molecule, VAP-1[67], it is reasonable to suppose that SSAO activity may be correlated with levels of CRP.

The formation of reactive oxygen species (ROS) leading to oxidative stress is also the consequence of bad metabolic control in diabetes, arising from hyperglycemia.[135] Elevated soluble SSAO activity may be a source of ROS as described above.

Therefore we had the following aims in our work:

- To investigate the role of volumetric macular assessment in comparison with central foveal thickness data obtained by OCT in the early detection of retinal changes in patients with diabetes and preserved visual acuity,
- To show the relationship between visual acuity and retinal thickness/macular volume,
- To assess the relationship between visual acuity (VA), macular morphology, certain risk factors and the occurrence of SMD in patients with diabetic macular edema,
- To investigate how cellular layer thickness measurements extracted with our novel segmentation algorithm OCTRIMA (Optical Coherence Tomography Retinal IMage Analysis) are affected by potential artifacts related to OCT operator errors,
- And to suggest strategies for the recognition and avoidance of these pitfalls,
- To study the correlation between soluble and tissue-bound SSAO activity in streptozotocin-induced diabetic rats,
- To assess how different regimes of insulin treatment influence the activity of soluble and tissue-bound SSAO enzyme in STZ-induced diabetic rats,
- And finally, to investigate the levels of serum total antioxidant status (TAS) and CRP in diabetic rats to reveal the correlation between oxidative stress, subclinical inflammation and SSAO activity.

3 Materials and methods

3.1 Optical coherence tomography examinations in patients with diabetes

In a retrospective observational study we analyzed data of 842 OCT examinations performed in eyes of patients with diabetes at our clinic between March 1. 2002. and October 31. 2003. Exclusion criteria were lack of cooperation, opaque media, any other macular pathology except for diabetic maculopathy, previous pars plana vitrectomy, and retinal photocoagulation within four months prior to the visit. We excluded eyes in which the software did not measure correctly (ie. did not find the vitreoretinal border or the RPE as reported previously).[24] The Institutional Review Board previously approved the study.

Optical coherence tomography was performed using a commercially available device (OCT Model 2000, Zeiss-Humphrey Instruments, San Leandro, CA, USA). Six radial scans were obtained in both eyes of all patients through a dilated pupil with a length of 6 mm centered on the foveola, using the automated ETDRS-macular map acquisition protocol of the device. Central retinal (foveal thickness (FT) and total macular volume (MV) were assessed by the built-in software of the scanner (Version A-2, Zeiss-Humphrey). Central foveal thickness represents the average thickness measured automatically by the software in the intersection of all six scans belonging to one scan session, while total macular volume represents the data provided by the software for the macular area with a diameter of 6 mm. In cases where FT measurements had an SD of more than 10% we measured foveal thickness manually by the software.

All patients previously underwent a complete ophthalmologic evaluation, including best corrected Snellen visual acuity, indirect ophthalmoscopy, posterior segment biomicroscopy with slit lamp and a fundus lens. The diagnosis of any stage of diabetic retinopathy (DRP) was made and recorded according to the ETDRS classification.[136]

Altogether 389 OCT scan sessions were selected and two study arms were formed: we divided eyes with preserved (1.0) visual acuity (189 OCT scan sessions in 118 patients) from those with visual acuity worse than 1.0 (200 OCT scan sessions in 126 patients).

Retinal thickness data were compared with the normative database of the software and diffuse retinal thickening (DRT) was diagnosed if retinal thickness exceeded the limits of the normative database in any of the ETDRS macular map regions.

Eyes with preserved visual acuity

The following groups were formed according to retinal thickness and the presence of diabetic retinopathy: the DRT group (DRT, no retinopathy, n=17), the DRP group (DRT, retinopathy present, n=32), while those eyes of diabetic patients with normal thickness and no retinopathy were considered normal (DM group, n=140). As OCT normative data are based on a different population as that represented by Hungarian patients, we adjusted an age- and gender-matched Control group consisting of 38 eyes of 25 healthy volunteers who gave their informed consent to participate in the study. Participants in the Control group underwent the same ophthalmologic evaluation as the patients in order to exclude any possible pathology.

Eyes with decreased visual acuity (worse than 1.0)

Snellen visual acuities were transformed into logMAR units. The presence of diffuse and cystoid edema (DME and CME, respectively) and also SMD was recorded. Diabetes duration longer than 15 years, edema type (CME/DME) and accompanying hypertension were entered in a multiple regression analysis model to find risk factors for the presence of SMD.

Statistical analysis

Because our data for FT, MV and diabetes duration in the cases with preserved visual acuity were non-normally distributed, they are presented as median (interquartile range [IQR]). Differences in FT and MV, diabetes duration, age and sex distribution were compared using the Kruskal-Wallis test one-way analysis of variance. In case of significant result Newman-Keuls post hoc analysis was applied.

In eyes with decreased visual acuity the correlation of FT and MV with logMAR visual acuity was assessed by linear regression analysis. In order to reveal the effect of SMD on visual acuity, the same regression was performed for the eyes with and without SMD and the significance of the regression coefficients was also assessed.

Diabetes duration longer than 15 years, edema type (CME/DME) and accompanying hypertension were analyzed by Fisher exact test in order to reveal risk factors for the presence of SMD. In case of a significant result the odds ration (OR) and relative risk (RR) were computed.

Two-tailed $p<0.05$ was considered significant in all statistical analyses. We used commercially available Statistica 6.0 software for statistical calculations (Statsoft Inc, Tulsa, OK, USA).

3.2 Evaluation of potential image acquisition pitfalls during optical coherence tomography and their influence on retinal image segmentation

Eight normal subjects (3 men and 5 women, age 29±5 years) with normal ocular examination and no history of any current ocular or systematic disease were recruited for this study. Informed consent was obtained from each subject after ethics approval was obtained from the Institutional Review Board. All subjects were treated in accordance with the tenets of the Declaration of Helsinki.

Scanning procedures and operator pitfalls generation

For imaging purposes the commercially available StratusOCT™ unit (software version 4.0; Carl Zeiss Meditec, Inc., Dublin, CA) was used.

A single operator collected all scans per subject in one session. The internal fixation light was used. Since thickness topographic maps depend on accurate determination of retinal thickness in each underlying B-scan, errors in boundary detection in 1 or more of the six line scans obtained with the radial lines protocol will lead to errors in the calculated macular thickness and volume. Thus, instead of acquiring 6 radial B-scans per subject in each experimental condition, only a single B-scan per modeled artifact and optimal scan acquisition was acquired to simplify the quantitative data analysis. Consequently, a total of 8 and 32 horizontal B-scans (7-mm long, horizontal line scan protocol) were obtained under optimal scan acquisition and specific error's operator related artifacts, respectively. Therefore, a total of 40 OCT images (B-scans) were obtained and used in the quantitative analysis. The error's operator related artifacts included: 1) defocusing, 2) depolarization, 3) decentration, and 4) a combination of defocusing and depolarization. First, an optimal scan was acquired with fine adjustment of the focus and automatic optimization of polarization by the StratusOCT™ software. Quality assessment of each initial scan (i.e. of each optimal scan without specific error's operator related artifacts) was evaluated by two experienced examiners (G.M.S. and D.C.F.). Good-quality scan had to have an even distribution of the signal across the full width of the B-scan, an adequate signal strength (≥6), correct alignment and no sign of failure of the algorithm for the detection of the inner and outer boundaries of the retina. The manufacturer-provided image assessment parameter (SS) was collected from the OCT data. We note that SS could be lower than 6 for scans obtained under specific error's operator related artifacts, as we could not get a better signal because of the artifact itself.

Decentration was modeled by manual movement of the fixation point upwards on the StratusOCT™ interface, resulting in a downward gaze. Thus, the macula would get approximately 2 optic disk diameters from its original position as seen on the CCD camera image of the device. The scan line was then manually adjusted to run through the center of the macula. Afterwards, macular fixation was repeated and the scan line readjusted to intersect the foveal center. Defocusing was achieved by turning the focus knob -4.0 Diopters. As a next step, image focusing was readjusted and depolarization was achieved by enhancing polarization by clicking ten times on the increasing button on the StratusOCT™ interface. For the effect of both artifacts, the focus was then simultaneously turned -4.0 Diopters to achieve defocusing and depolarization.

Image analysis

The OCT raw data was exported to a compatible PC and analyzed using an automated computer algorithm of our own design (OCTRIMA) capable of segmenting the various cellular layers of the retina, as described above. Since OCT images suffer from a special kind of noise called 'speckle', which poses a major limitation on OCT imaging quality, the OCT raw data was pre-processed. Specifically, we used a model based enhancement-segmentation approach by combining complex diffusion and coherence enhanced diffusion filtering in three consecutive steps. In particular, the enhancement-segmentation approach starts with a complex diffusion process, which is shown to be advantageous for speckle denoising and edge preservation. A coherence enhanced diffusion filter is then applied to improve the discontinuities in the retinal structure (e.g. gaps created by intraretinal blood vessels) and to obtain the structural coherence information in the raw data.[14] The enhancement segmentation approach ends with the application of a boundary detection algorithm based on local coherence information of the structure.[14]

A total of 7 layers (retinal nerve fiber layer (RNFL), ganglion cell layer (GCL) along with the inner plexiform layer (IPL), inner nuclear layer (INL), outer plexiform layer (OPL), outer nuclear layer (ONL), photoreceptor inner/outer segment junction (IS/OS); and the section including the retinal pigment epithelium (RPE) along with the choriocapillaries (ChCap) and choroid layer) were automatically extracted using the algorithm (see Fig. 9).

Once the various cellular layers of the retina were automatically segmented, the average thickness of these layers at the individual points (i.e. at each of the 512 A-scans) were averaged to yield a mean “raw”measurement of thickness per layer.

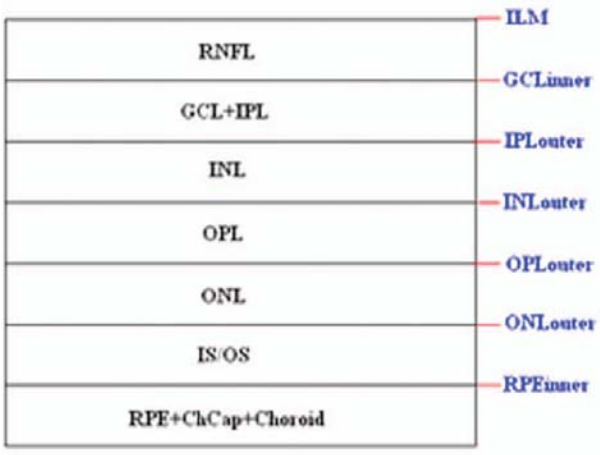

Figure 9. Schematic drawing of the various cellular layers of the retina and their boundaries. For abbreviations see the text or Figure 8.

Image Segmentation Accuracy

Since we are using a new technique of performing image segmentation, a metric geared toward only segmentation needs to be utilized. Thus, an accuracy measure was introduced to evaluate the performance of the new segmentation algorithm. Let us assume that an image obtained from a healthy subject under the optimal scan test is presented to the new segmentation algorithm. The segmentation algorithm then produces a segmented image with detected boundaries *1, 2,.., M* depending on which layers were segmented. At this point, we have the correctly segmented image (the "true" segmentation) assuming that no segmentation errors were observed for any layer segmented under the optimal scan procedure. Let us assume now that a second image obtained for the same healthy subject under a specific error's operator related artifact is presented to the new segmentation algorithm. The segmentation algorithm then produces a segmented image with detected boundaries *1, 2,.., M* depending on which layers were segmented. Then, assuming that we obtain a segmented image with potential errors in the segmentation, we can then measure the performance of the segmentation algorithm per layer (*L*) by using the following segmentation accuracy measure (*SAM*):

$$SAM_L = \frac{Np_{segmented}}{Np_{true}} \qquad (1)$$

where Np_{true} is the total number of boundary pixels detected in the correctly segmented image (i.e. the "true" segmentation). $Np_{segmented}$ is the number of boundary pixels detected in the segmented image with potential segmentation errors that account for the maximum coverage

of the boundary pixels in the "true" segmented image. Note that the maximum coverage measure is actually the fraction of the boundary pixels in the "true" segmented image occupied by the boundary pixels detected in the segmented image with potential segmentation errors. We can measure the overall segmentation accuracy given by the minimum accuracy (i.e. the worst performance) with which individual layers have been identified, i.e. by:

$$SAM_{overall} = \min(SAM_L) \quad (2)$$

The effect of this accuracy measure is illustrated here using an example. Let us assume that two OCT images are obtained from a healthy subject and presented to the segmentation algorithm. One of them is obtained under the optimal scan procedure (i.e. the "true" segmentation image) and the other is acquired under a specific error's operator related artifact (i.e. the image with potential segmentation errors). We note that the total number of pixels along each segmented boundary is 512 because there are 512 A-scans in a B-scan (i.e. along the transverse direction). Thus, Np_{true}=512. Let us also assume that three retinal boundaries (L_1, L_2 *and* L_3) are segmented on each image. For the retinal boundaries identified on the "true" segmented image (L_1, L_2 *and* L_3), consisting of 512 boundary pixels (i.e. Np_{true}=512), the maximum coverage for L_1 is provided in the image with potential segmentation errors by a total of 425 boundary pixels (i.e. $Np_{segmented}$=425), giving SAM_{L1}=0.83 (see Eq. 1). We note that Np_{true} is the same for each boundary identified on the "true" segmented image. The next boundary to be considered is L_2, for which a maximum coverage of 403 boundary pixels is provided in the image with potential segmentation errors, giving SAM_{L2}=0.78. The third boundary is identified by 320 boundary pixels, giving SAM_{L3}=0.62. The overall accuracy measure, given by the minimum of the three boundaries' measures, is therefore 0.62 (see Eq. 2).

The accuracy measures were obtained for all the images acquired under specific error's operator related artifacts (i.e. for 32 B-scans). All of the images were then segmented and subsequently verified by eye to identify algorithm's failures. Then, the maximum coverage of boundary pixels on each boundary detected on the "true" segmented image was calculated by point-wise comparison with the boundary pixels detected on each boundary extracted on the images obtained under operator pitfalls generation. The most accurate segmented image would be one that segment the image with the highest *SAM* and assigns every pixel in the boundaries identified to the corresponding pixels identified in the "true" segmented image.

We note that to obtain the average overall segmentation accuracy values (average $SAM_{overall}$, see Eq.2) for each error's operator related artifact, the accuracy measures per boundary (SAM_L) were first calculated for every subject under each specific error's operator related artifact. Then, the minimum accuracy ($SAM_{overall}$, see Eq.2) with which individual boundaries were identified was obtained for every subject under each specific error's operator related artifact. After that, the average minimum accuracy (average $SAM_{overall}$) was obtained for each specific error's operator related artifact. As a result, a total of 7 segmentation accuracy measures ($SAM_{L1,}$ $SAM_{L2,...,}$ SAM_{L7}) and one minimum accuracy measure ($SAM_{overall}$) were obtained per subject. In the previous sentence we were talking about the average SAMoverall for each artifact derived from the subjects' results) and now again we return to measures per subject. Thus, a total of 8 $SAM_{overall}$ values for each error's operator related artifact was used to calculate the final average $SAM_{overall}$ values.

Statistical analysis

For the statistical analyses of signal strength (SS) and average thickness, Friedman analysis of variance was used. In the case of a significant result, Dunnett post hoc analysis was performed in order to reveal difference from the optimal scan test results. If there was more than one significant difference from the optimal scan test, Newman-Keuls post-hoc analysis was also performed. Statistica 7.0 software was used (StatSoft Inc., Tulsa, OK, USA) in all the statistical analyses performed, $p<0.05$ was considered statistically significant.

3.3 Assessment of SSAO activity in diabetic rats

Animals

Five-week-old male Wistar rats (n=35, body weight 140-160g) were used in our studies. The animal treatments were in compliance with the guidelines established by the Animal Care Committee of Semmelweis University and the Hungarian Guide for the Care and Use of Laboratory Animals. The study was approved by the Regional Ethical Committee of Semmelweis University (TUKEB No. 99/94, 31/1994, 219/94). The rats were housed in wire cages with commercial rat chaw and water ad libitum on a 12-h light/dark cycle (lights on at 6:00 AM) at a temperature of 22 °C, with constant humidity. In 26 animals diabetes was induced by a single intraperitoneal (ip.) injection of STZ (60mg/kg) under pentobarbital

anesthesia. Control group was injected with ip. saline (n=9). All animals were kept under the same conditions and followed for 3 weeks, which time period was determined as "short-term" for diabetes. Only STZ-treated animals with polyuria, polydipsia and plasma glucose concentrations above 15 mmol/l were considered diabetic and involved in the study. Treatment consisted of 2-4 IU subcutaneous insulin (Humulin U) administered once (at 8:00 AM) (DM 1×I, n=8) or twice (at 8:00 AM and 17:00 PM) daily (DM 2×I, n=9), depending on blood glucose levels obtained from the tail of the animals. A group of STZ-treated rats was left without treatment (DM, n=9). At the end of the study blood from the animals was collected in Vacutainer tubes without anticoagulant and centrifuged at 2500 *g* for 10 min. Aortas of all rats were prepared and stored separately from the sera at -80 °C pending assay.

Determination of soluble and tissue-bound SSAO activity

In order to determine serum SSAO activity a radiometric procedure was adapted [23]. The radioenzymatic assay is based on the extraction of ^{14}C-benzaldehyde formed by the enzyme from ^{14}C-benzylamine. Benzylamine, chlorgyline and semicarbazide were purchased from Sigma-Aldrich (Germany). ^{14}C-benzylamine was obtained from Amersham International (United Kingdom; specific activity: 2.04 GBq/mmol). All other chemicals were of analytical grade.

The sera were preincubated in phosphate buffer ($5x10^{-2}$ mol/L; pH=7.4) with chlorgyline (10^{-4} mol/L) at room temperature for 20 min to ensure that any MAO activity, if present, was completely inactivated. The enzyme was then incubated in the presence of ^{14}C-benzylamine (5×10^{-4} mol/L. 2×10^{5} dpm, 0.1 μCi) in a final volume of 200 μl at 37°C for 40 min. The enzyme reaction was stopped by adding 200 μl of 2 mol/L citric acid. The oxidized products were extracted into 1 ml toluene/ethyl acetate (1:1 v/v) mixture, of which 600 μl was transferred to a counting vials containing 5 ml Aquasafe fluid. Radioactivity was determined using a liquid scintillation counter (Beckman LS5000TA).

Rat aortas were carefully cleaned of all adjunct tissues in order to determine tissue-bound SSAO activity more exactly on protein base. Tissue samples were then homogenized and centrifuged at 800 rpm for 10 min. The supernatants were then centrifuged (14000 rpm for 40 min.) and the membrane fractions were incubated for 20 min in phosphate buffer ($5x10^{-2}$ mol/L; pH=7.4), in the presence of chlorgyline (10^{-4} mol/L). The enzyme was then incubated in the presence of ^{14}C-benzylamine (5×10^{-4} mol/L, 5×10^{4} dpm, 0.025 μCi) in a final volume of 220 μl at 37°C for 40 min. All other procedures were carried out as in the case of plasma.

Protein content of the samples was determined according to Lowry, using bovine serum albumin as standard.[137] Serum SSAO activity was expressed in the following unit: pmol substrate oxidized /mg protein/h. Aorta SSAO activity was expressed in nmol substrate oxidized /mg protein/h.

Assessment of serum total antioxidant status (TAS) and high sensitivity C-reactive protein (hsCRP) levels

Serum total antioxidant status was measured by a Randox HA3830 standard kit (Randox Laboratories, Ardmore, UK). The level of serum hsCRP was assessed by an immunoturbidimetric method (Erix Daytona Chemical Analyser, Randox Laboratories, Ardmore, UK).

Laboratory biochemical analyses

Serum glucose concentrations were measured with an automatic analyzer (Hitachi 917, Boehringer-Mannheim Diagnostic Systems, Diagnostic kit). Serum fructosamine concentrations were measured using a reagent kit from Roche Diagnostics GmbH by Hitachi 907. All other chemicals were obtained from Sigma.

Statistics

Results were assessed using ANOVA followed by Newman-Keuls multiple comparisons test. Linear correlation was performed and the Pearson correlation coefficient (r) was calculated for the pairwise relationship between se/aoSSAO, fructose amine, TAS and hsCRP levels as measured in all rats participating in the study. In general, the null hypothesis for all analyses was that the factor has no influence on the measured variable, and significance was accepted at $p<0.05$ level. For the analyses Statistica 6.0 for Windows software was used (Statsoft Inc, Tulsa OK, USA).

4 Results

4.1 Optical coherence tomography examinations in patients with diabetes

Eyes with preserved visual acuity

There was no statistical difference in the gender and age distribution among the groups. Although median duration of diabetes had an increasing tendency with severity of DME, there was no statistical difference in the entire span of the study. Patients in the DRP group had a significantly higher incidence of hypertension. (Table 4.)

Table 4. Clinical characteristics of patients.
Normal Group: diabetes, normal thickness, no retinopathy; DRT Group: diabetes, DRT (diffuse retinal thickening), no retinopathy; DRP Group: diabetes, DRT, DRP (diabetic retinopathy). Abbreviations: SD (standard deviation), IQR (interquartile range).
* p<0,001 compared to Control, Normal and DRT groups

	Control (*n*=38)	Patients with diabetes		
		Normal (*n*=140)	DRT (*n*=17)	DRP (*n*=32)
Sex (% male)	55,2	52,8	58,9	62,5
Age, mean ys±SD (range)	42,3±19,9 (21-79)	49,5±18,8 (29-66)	46,1±19,7 (20-78)	54,3±9,9 (30-72)
Known duration of diabetes, median ys. (IQR)	-	7 (4-14)	10 (7,5-15,5)	14 (5-20)
Antihypertensive treatment (%)	26,3	32,1	23,5	62,5 *

Central foveal thickness did not differ in the control, the DM and the DRT groups, although this latter group had a slightly elevated median thickness. In the DRP group the FT values were markedly higher than in all other groups (Figure 10. A).

In the case of MV both DRT and DRP groups had significantly higher values than the other two groups, and there was significant difference between thee DRT and the DRP groups (Figure 10. B).

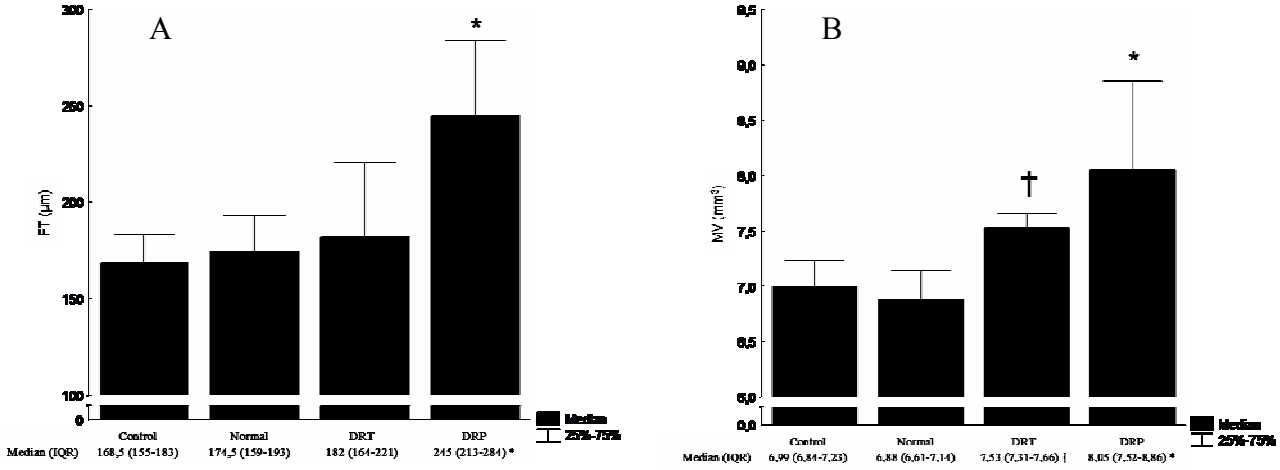

Figure 10. Central foveal thickness (A) and macular volume (B) data in the various groups.
(* p<0,001 compared to Control, Normal and DRT groups; † p<0.001 compared to Control, Normal and DRP groups) Abbreviations: IQR (Interquartile range)

Eyes with decreased visual acuity (worse than 1.0)

Both FT and MV correlated with logMAR VA (Figure 11.). Serous macular detachment was found in 28 eyes (14%). Linear regression was also significant separately in eyes with SMD as well as in eyes without SMD (p<0.001, all cases). Linear regression showed that eyes with SMD had significantly higher FT and MV values compared to eyes without SMD. (Figure 12.).

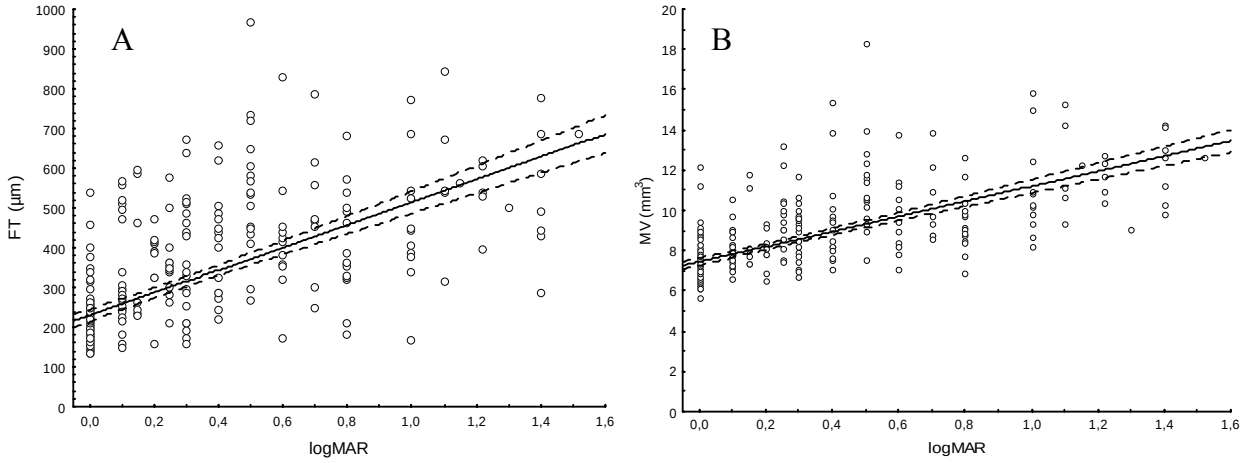

Figure 11. The result of linear regression for logMAR visual acuity and foveal thickness (FT, A) and macular volume (MV, B). (p<0.001 both cases, r=0.65 and r=0.69, respectively.)

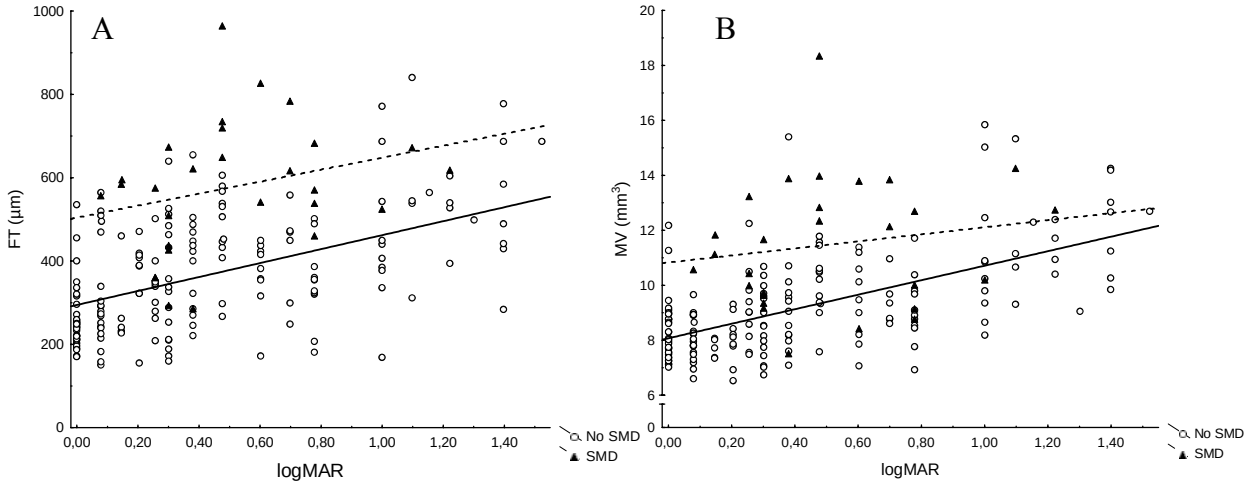

Figure 12. The results of linear regression for logMAR and FT (A) and MV (B) in eyes with and without SMD. In all cases $p<0.001$, for FT $r=0.49$ in eyes without SMD, while in eyes with SMD $r=0.46$. In the case of MV $r=0.60$ in eyes without SMD, while in eyes with SMD $r=0.47$.

The presence of cystoid macular edema and diabetes duration longer than 15 years proved to be significant risk factors for SMD ($p=0.030$, OR=3.15, RR=2.69 and $p=0.047$, OR=2.66, RR=2.32), while the presence of hypertension had no effect.

4.2 Evaluation of potential image acquisition pitfalls during optical coherence tomography and their influence on retinal image segmentation

The SS score obtained under the optimal image acquisition procedure and each error's operator related artifact procedure is shown in Figure 13. Friedman ANOVA ($p<0.001$) and Dunnett post hoc analysis showed significant difference compared to the optimal acquisition protocol in all groups ($p<0.001$ in all cases). In order to reveal intergroup changes, additionally Newman-Keuls post hoc analysis was performed. All groups showed a significant difference compared to each other (data not shown) except for the comparison of decentration with defocus and depolarization ($p=0.19$ and $p=0.13$, respectively).

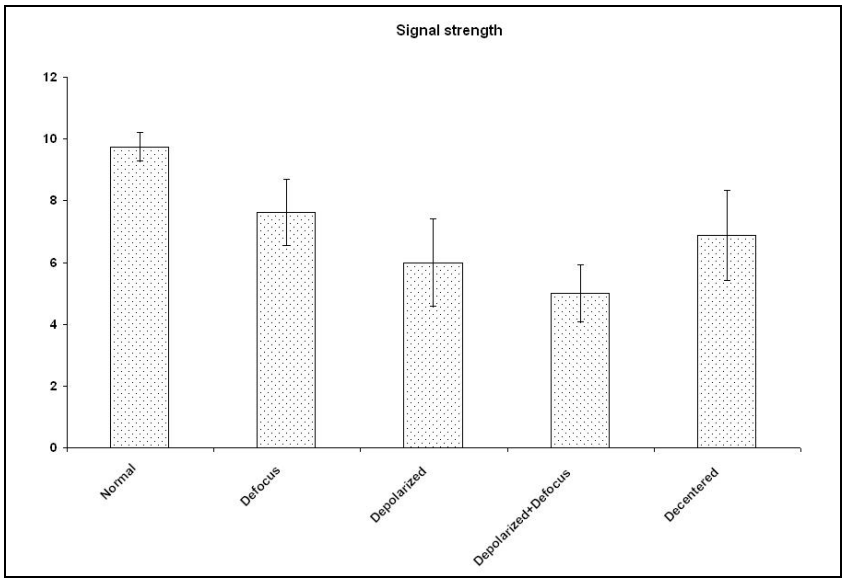

Figure 13. Distribution of the manufacturer provided image assessment parameter (SS) for each specific error's operator related artifacts. Data are represented as mean ± SD.

Of the 32 B-scans with specific error's operator related artifacts, 27 exhibited segmentation errors (84.37%). The lowest and highest segmentation error rate was observed under defocus artifact (9.37%) and depolarized-defocus artifact (25%), respectively. Segmentation error locations were also different for each modeled artifact. We note that segmentation errors were not present in the 8 B-scans obtained under the optimal scan acquisition procedure. (Figure 14.)

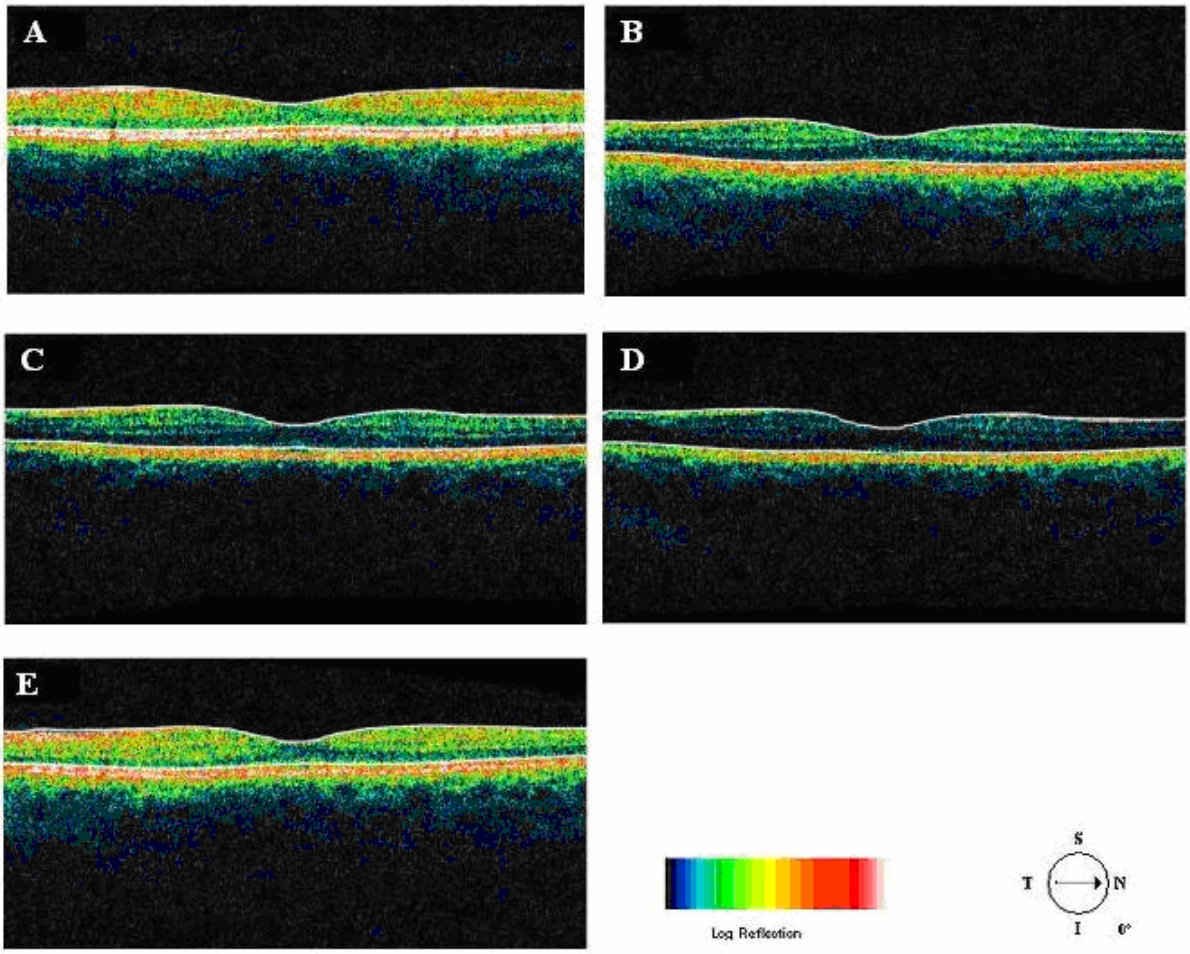

Figure 14. StratusOCT^{TM} images obtained for the normal image acquisition procedure and some error's operator related artifact procedures for a normal eye (OS). **A)** Image obtained with the optimal image acquisition procedure; **B)** Image obtained with the defocusing procedure, **C)** Image obtained with the depolarization procedure, **D)** Image obtained with the combination of defocusing and depolarization procedures; and **E)** Image obtained with the decentration method. The inner and outer retinal boundaries determined by the StratusOCT^{TM} built-in algorithm are marked in white. The OCT signal strength is represented in false color using the normal visible spectrum scale. High backscatter is represented by red-orange color and low backscatter appears blue-black. Note the uneven distribution of signal strength across the full width of the images obtained under error's operator related artifacts.

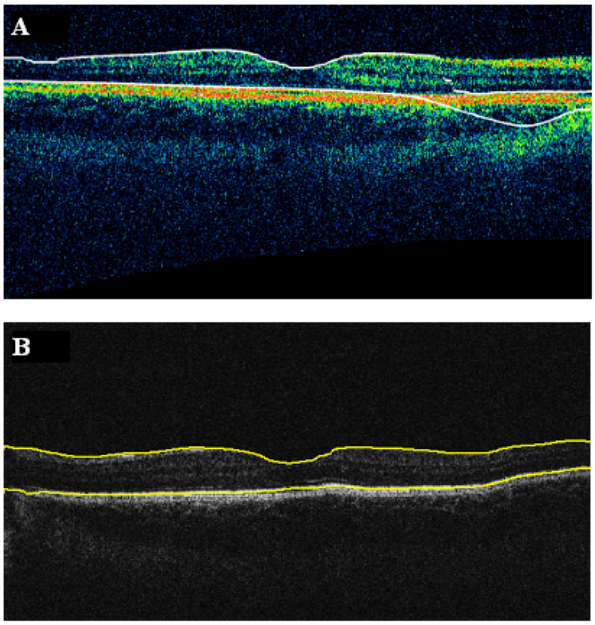

Figure 14. Segmentation results showing the performance of the StratusOCT™ custom built-in algorithm compared to the results using our custom algorithm. **A)** macular scan obtained for Eye 3 under depolarization artifact. Note the misidentification of the outer boundary of the retina (outlined in white). **B)** Results obtained for the same eye (Eye 3, depolarization error) using our methodology. Note that our algorithm was able to correctly detect the outer boundary of the retina.

Table 5. shows the average overall segmentation accuracy measures (average $SAM_{overall}$) obtained per intraretinal boundary and for each specific error's operator related artifact. Note that segmented boundaries with less artifacts (i.e. with highest average $SAM_{overall}$ values) were observed for images obtained under defocus and decentration artifacts (see Table 5). Moreover, inner and outer retina misidentification artifacts were not observed under any error's operator related artifact (see values obtained for ILM and RPE_{inner} boundaries in Table 5).

Thus, these particular boundaries were in very good agreement point-wise with the boundaries detected on images obtained under the optimal scan acquisition procedure. However, the IPL_{outer}, INL_{outer} and OPL_{outer} boundaries showed the worst segmentation performance in all the pitfall cases tested (see Table 5).

Table 5. Segmentation accuracy measures (average $SAM_{overall}$ values) obtained after comparing the segmentation result on images with artifacts with the "true"segmentation.

Scan Acquisition Condition	ILM	GCL_{inner}	IPL_{outer}	INL_{outer}	OPL_{outer}	ONL_{outer}	RPE_{inner}
Defocus	1	1	0.87	0.84	0.83	1	1
Depolarized	1	1	0.79	0.70	0.76	1	1
Depolarized-Defocus	1	0.98	0.64	0.56	0.51	1	1
Decentration	1	1	0.85	0.81	0.84	1	1

Table 6. shows the mean and standard deviation thickness results per layer along with the results of statistical analysis.

The average thickness for each layer segmented is shown in Fig. 16 and Table 6. In this case, a greater – though statistically not significant – effect of depolarization was observed on measurements compared to defocus. However, a statistically significant difference in average thickness was found for depolarization-defocus in the case of GCL+IPL complex and ONL layer segmentation ($p<0.05$, see Table 6). This particular result is in agreement with the lowest average $SAM_{overall}$ values obtained for the IPL_{outer} and OPL_{outer} boundaries (see Table 5). We note that the ONL is bounded by the OPL_{outer} and ONL_{outer} boundaries. As it can be seen, the two artifacts together (depolarized-defocus) had the greatest statistically significant altering effect on all measurements (see Fig.16, Table 5 and Table 6).

Table 6. Mean and standard deviation results per layer compared to optimal scan acquisition conditions (Friedman ANOVA followed by Dunnett post hoc analysis; "*NS"* not significant; † $p<0.05$ compared to Normal).

Scan Acquisition Condition	RNFL Thickness (µm)	GCL+IPL Thickness (µm)	INL Thickness (µm)	OPL Thickness (µm)	ONL Thickness (µm)
Normal	22.04±8.22	71.61±13.40	31.08±4.00	30.59±2.50	84.28±5.80
Defocus	24.11±8.22	63.61±17.94	30.88±0.98	33.95±6.49	89.88±9.78
Depolarized	25.43±6.02	53.87±21.45	26.04±12.21	31.26±4.95	103.30±32.94
Depolarized-Defocus	27.36±14.61	51.43±22.68†	25.83±8.55	29.07±7.22	118.56±33.82†
Decentration	19.59±3.68	51.94±28.33	26.60±10.99	25.94±11.36	120.71±44.37
Friedman ANOVA	NS	$p<0.05$	NS	NS	$p<0.05$

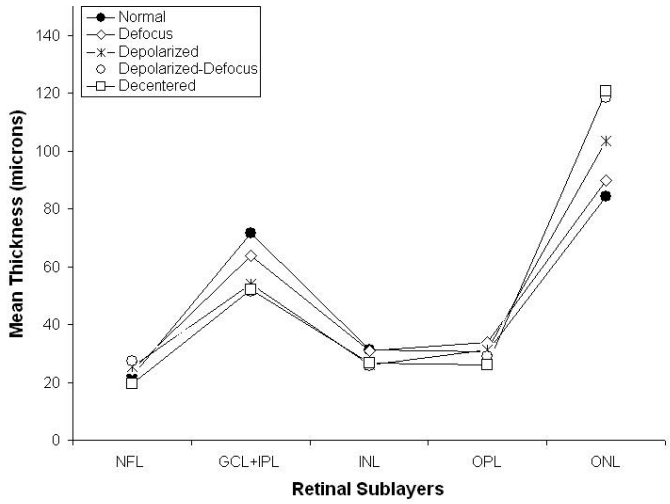

Figure 16. Mean thickness values obtained per layer. Note that a clear thinning and thickening effect was obtained for the GCL+IPL complex and the ONL, respectively. For SD values and statistical analysis results see Table 6. For the abbreviations of the layers see the text.

Decentration had a comparable effect on thickness measurements, however, not reaching statistical significance. These results demonstrate how the accuracy of thickness measurements can be degraded by the variability in measured reflectance under artifacts related to OCT operator errors. It is interesting to note that depolarization resulted in a bigger, significant reduction in SS than defocusing alone, while the combination of the two resulted in an even more pronounced reduction in SS (see Fig. 14). Correspondingly, thickness data were more influenced by depolarization, and most influenced by the combination of the two.

4.3 The correlation between soluble and tissue-bound SSAO activity

The body weight of diabetic rats (DM) and those treated with insulin once daily (DM 1×I) did not reach that of the control group, while animals treated twice daily have shown up equal development of body weights as control animals (Table 7). Serum fructose amine levels were markedly higher in the DM and DM 1×I groups ($p<0.001$ in both cases), while animals with semi-intensive insulin therapy (DM 2x1) showed only modest significant difference compared to Control ($p=0.04$, Table 7). Nevertheless, Newman-Keuls post hoc analysis showed that both DM and DM 1×I groups had serum fructose amine levels significantly higher than the DM 2×I group ($p<0.01$ in both cases, data not displayed).

Table 7. Clinical and laboratory characteristics of control and streptozotocin-induced diabetic rats receiving insulin treatment once or twice daily, or no treatment at the end of the three-week follow-up period (DM 1×I, DM 2×I and DM, respectively). Values are means ± SEM. TAS: serum total antioxidant status; hsCRP: serum high-sensitivity C-reactive protein.
(#p<0.05, and *p<0.001 vs. Control group with Newman-Keuls post hoc analysis)

	Treatment group			
	Control	**DM**	**DM 1×I**	**DM 2×I**
	n=9	n=9	n=8	n=9
Body Weight (g)	359,3 ± 9,76	186,0 ± 12,61*	196,2 ± 7,90*	363,5 ± 7,81
Glucose (mmol/ml)	9,55 ± 0,30	24,32 ± 2,77*	24,65 ± 3,05*	27,93 ± 0,35*
Fructose Amine (µmol/l)	154,39 ± 1,76	289,82 ± 22,56*	285,68 ± 27,02*	216,20 ± 9,74#
TAS (µmol radical/ml)	147,75 ± 9,96	22,60 ± 3,98*	47,24 ± 8,47*	182,07 ± 30,74
hsCRP (mg/l)	0,017 ± 0,009	0,058 ± 0,009#	0,068 ± 0,011#	0,012 ± 0,006

Blood glucose levels measured on the morning of slaughter were significantly elevated in all diabetic rats compared to controls (Table 7). In the DM 1×I group blood glucose levels were similar to the DM group, while in the group of rats with semi-intensive insulin therapy (DM 2×I), blood glucose was even slightly higher than in the previous two diseased cohorts.

Serum SSAO activity had increased five-fold in the DM group and to a lesser degree, in the DM 1×I group, while there was no statistically significant difference between the DM 2×I and the control group (Fig. 17 A). A reversed response in tissue-bound SSAO activity was assessed regarding metabolic state: under poor glycemic control a marked decrease in activity was seen in aorta, while semi-intensive treatment returned aortic enzyme activity closer to, though still significantly lower than control (Fig. 17 B). More to this, serum SSAO activities were in negative correlation with tissue-bound SSAO activities (Table 8).

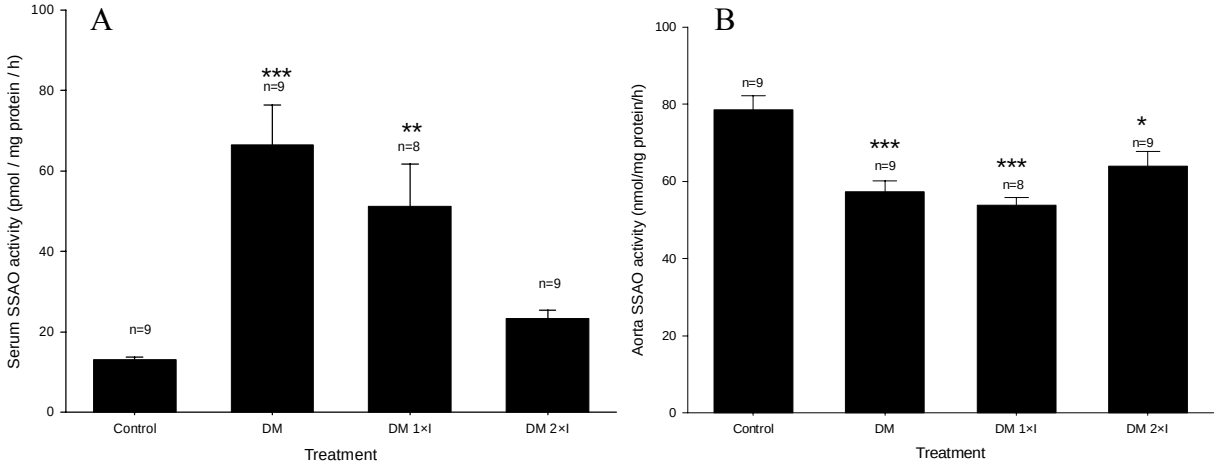

Figure 17 A, B: Serum (A) and aorta (B) SSAO activities measured in control rats, in STZ-induced diabetic rats without treatment, or treated with insulin once or twice daily, after three weeks of treatment (C, DM, DM 1×I and DM 2×I, respectively). The results are expressed as means ± SEM. (*p<0.05, **p<0.01, ***p<0.001 compared to control group by Newman-Keuls post hoc analysis; for regression results see table 7.)

Serum TAS significantly decreased in the DM and DM 1×I groups compared to both the control and the DM 2×I groups, while the control group did not differ significantly from the DM 2×I group. High sensitivity C-reactive protein levels increased both in the DM and the DM 1×I groups, while semi-intensive insulin treatment reduced its concentration back to the level of the control group. Plasma TAS levels showed significant negative correlation with hsCRP and seSSAO (Table 8), while hsCRP and seSSAO were in positive correlation (Table 8).

A very strong positive correlation was found between serum fructose amine and seSSAO, and a strong negative correlation between serum TAS and hsCRP levels. Also strong correlation was revealed in the relationship between hsCRP and seSSAO. Tissue-bound SSAO had no significant relationship with serum TAS, and only weakly correlated with hsCRP. All other parameters have shown significant, though not strong correlation with each other (Table 8).

Table 8. Pairwise linear regression results of variables aortic and serum SSAO activity (aoSSAO and seSSAO, respectively), serum high-sensitivity C-reactive protein (hsCRP), serum total antioxidant status (TAS) and serum fructose amine (FrAm) in all animals. The upper numbers in the boxes indicate the *r* value, the lower numbers in italic indicate the *p* value. NS: not significant.

	aoSSAO	**seSSAO**	**hsCRP**	**TAS**
FrAm	-0,46 *0,0067*	0,73 *0,0000*	0,48 *0,0223*	-0,46 *0,0158*
TAS	NS	-0,56 *0,0023*	-0,71 *0,0004*	
hsCRP	-0,43 *0,0411*	0,63 *0,0018*		
seSSAO	-0,45 *0,008*			

5 Discussion

5.1 Optical coherence tomography examinations in patients with diabetes

Eyes with preserved visual acuity

In our study we have shown that both FT and MV are increased in patients with DRP and preserved visual acuity. More interestingly, we have found increased MV but significantly not different from normal FT in patients with no signs of DRP having marked diffuse thickening of the retina, which means that the increase in macular volume may precede the increase in central foveal thickness in patients with diabetes. A possible reason for this could be that the foveola is not necessarily involved in the first pathophysiological changes of the retina in diabetes. Thus, the measurement of MV seems to be more sensitive for the detection of the first minor macular changes in diabetes as the measurement of FT.

The median and the interquartile range of FT in the DRT group was in the 180-216 μm range previously described as the upper limit of normal thickness[10, 26, 27] which further supports the lack of significant difference from the normal and DM groups. There are no previous data available on the normal range of MV, but according to the results of the DRT group, the upper limit of MV is approximately 7.2 mm^3.

We could also give support that the normative database of the second-generation OCT Model is reliable in predicting normal thickness values also in the Hungarian population, as there were no differences neither in FT nor in MV among the control eyes and the diabetic eyes considered normal with the help of the software. Our data also point to the usefulness and importance of a normative database in order to detect subtle changes of the macula in diabetes which otherwise would be difficult to tell by the human eye.

Eyes with decreased visual acuity

In the case of macular edema we have found a linear correlation between foveal thickness and macular volume. In those eyes, where edema formation was accompanied by SMD visual acuity was better than in eyes with the same FT/MV values but without SMD. One probable reason for this may be the relatively intact neuroepithelial layer in those eyes with SMD compared to the possible destruction caused by excessive edema formation.

Further studies may shed light on the morphological changes accompanying macular edema formation.

The clinical role of angiographically undetectable SMD is somewhat questionable, however, our results show that its presence does not worsen visual acuity. Long diabetes duration and the presence of cystoid macular edema seem to influence the evolution of SMD, but our study was not able to clearly elucidate this.

There were some weaknesses of the above study. First, it was not prospective, however, very strict exclusion criteria were set in order to ensure the enrollment of only precise measurement data obtained by the software (less than 20% of all diabetes cases were included in the study). Second, we used an OCT device with relatively low resolution compared to the latest, commercially available system (Stratus OCT^{TM}). The Stratus OCT^{TM} device makes slightly different thickness measurements and utilizes a newly-developed normative database. This difference has been shown somewhat constant and predictable[138], thus we believe that our results are transferable to the StratusOCT systems, as well.

5.2 Evaluation of potential image acquisition pitfalls during optical coherence tomography and their influence on retinal image segmentation

In our study, the presence and severity of segmentation errors by a novel segmentation algorithm (OCTRIMA) was evaluated under potential OCT image acquisition pitfalls. Our results showed that defocusing and depolarization errors together have a substantial effect on the quality and precision of information extracted from OCT images by using the novel algorithm. As stated in the Results section, the IPL_{outer}, INL_{outer} and OPL_{outer} boundaries were more prone to segmentation errors under the modeled image acquisition pitfalls. The lowest segmentation accuracy was achieved by the combined depolarization-defocus artifact (see the average $SAM_{overall}$ values in Table 5), and accordingly, significant changes in average thickness were due to this type of artifact.

An awareness of these pitfalls and possible solutions is crucial not only for avoiding misinterpretation of OCT images but also for assuring the quality of the quantification of retinal measurements. It is important to note that visual analysis of OCT image quality is affected by intraretinal abnormalities in backscattering that are usually associated to particular ocular diseases. Thus, optimal settings are necessary to avoid measurement errors. For

example, the StratusOCT™ built-in algorithm requires clear delineation of the inner and outer retinal boundaries to accurately identify intraretinal abnormalities. It is well known that StratusOCT™ images are prone to error as a result of inner or outer retina misidentification artifacts. However, our segmentation results for the inner and outer retinal layers showed no misidentification errors for any modeled artifact. Thus, the new segmentation algorithm could provide a more reliable macular volume and thickness measurement than the OCT built-in algorithm under error's operator related artifacts. Though, a further study is needed with a larger sample size to validate these preliminary results and obtain the reproducibility of the retinal measurements extracted by using the novel algorithm. Moreover, the preliminary results should be also validated on the full range of retinal pathologies.

As a consequence of this work and taking into account our experience during the course of scanning a large number of patients per year in our clinic, specific strategies for the recognition and avoidance of image acquisition pitfalls can be now suggested. In order to avoid potential image acquisition pitfalls, it is necessary that first the operator assure the correct placement of the patient's head on the chin and head rest of the StratusOCT™ system. Moreover, it is imperative the lateral canthus markers be lined up with the center of the pupil in primary gaze. Secondly, polarization optimization must be done before and may be repeated during a scanning session. For example, in the case of a radial line scan that is composed of six consecutive scans, the operator should polarize before obtaining the first scan, and then may have to repeat polarization for the fourth and sixth scan if needed. On the other hand, opacities in the eye or corneal drying may change the signal strength on one scan and not the other requiring the operator to repolarize. It is also worth to mention that a target SS $\geq$6 is deemed desirable in identifying a potentially good-quality scan[21], although it is not always possible–because of factors such as media opacity. Significant changes in relative reflectance and thickness were observed under the combined defocus-depolarization artifact where SS was below the above mentioned level which emphasizes our suggestion. For instance, dense cataracts and vitreous opacities limit the image quality no matter how well centered and adjusted could be the scan. We also note that an ideal scan will have an even SS level across the entire scan, with no sections of weak signal.

Furthermore, it is crucial that the operator centers all 6 scans at the fovea when acquiring macular scans for retinal thickness analysis. This is a problem for patients that have poor fixation due to impaired visual acuity. We note that average thickness and standard

deviation of the retinal thickness at the fovea is automatically calculated by the retinal map (single eye) or retinal thickness/volume (OU) analysis protocols. These protocols use the central A-scan of each one of the six radial scans (B-scans) obtained during the acquisition session to calculate foveal thickness. In theory, all six radial scans (B-scans) are to be centered at the same point (fovea) after a perfect acquisition session. Thus, the central A-scan should be the same for all six B-scans and the standard deviation of the retinal thickness at the fovea is to be equal to zero. Depending on the distortions of the macular morphology associated to the disease, standard deviation values of the average foveal thickness higher than 30 microns (or an SD>10% of central retinal thickness)[20] are highly indicative that at least one of the six radials scans is not correctly centered at the fovea. Consequently, a new entire scan acquisition session should be performed.

Although it may seem unusual, the correct focus is not necessarily one that the operator appreciates in the fundus image but one that the operator appreciates in the greater intensity of color saturation in the current scanned image. Thus, it is more important to have a good scanned image than it is to have a good fundus image. The laser and the fundus video camera are not on the same plane, so when one has the best view in one image, in the other may not have the same quality. As it can be seen, an awareness of all these pitfalls is crucial when misinterpretation is to be prevented, which may be important in the planning and evaluation of further studies using the new segmentation algorithm. Moreover, it is important for the use of the new algorithm that physicians be able to trust measurements such as thickness maps of the intraretinal layers and macular thickness and volume. This emphasizes our goal of the present work for the future.

5.3 The correlation between soluble and tissue-bound SSAO activity

In the present study we found that in the short term model of diabetes in STZ-induced rats (1) there is correlation between glucose homeostasis, oxidative stress, inflammation and the activity of soluble and tissue-bound SSAO, and (2) tissue-bound and soluble SSAO activities are inversely correlated with each other.

In our set of experiments, rats receiving insulin twice daily had elevated blood glucose levels compared to the control group. We believe this was because of slight overdosage of the evening insulin, resulting in hypoglycemia during the night. This hypoglycemia – similarly to

the known mechanism in humans – caused an adrenergic reaction, with concomitant increase in blood glucose measurable on the morning of slaughter. This hypothesis is supported by our finding that fructose amine levels were significantly lower in the DM 2×I group than those found in the DM and DM 1×I groups, showing improved carbohydrate turnover in the group of rats on semi-intensive insulin treatment. We did not measure HbA1c levels because of the young age of rats and the short term (3 weeks) of diabetes.

According to the results by Abella et al. adipose tissue is an important contributor to soluble VAP-1/SSAO activity as the membrane-bound form of the enzyme is released by metalloprotease-dependent shedding.[81] This is enhanced in the presence of TNF-α, a cytokine responsible for insulin resistance in obese humans and Zucker obese rats. The ablation of adipose tissue leads to decreased soluble SSAO activities. In our case both diabetic animals, and those receiving insulin treatment only once daily were very lean, did not reach the body weight of the control during the treatment period and had much less adipose tissue in contrast to the other treated or healthy groups. For this reason it is doubtful whether adipose tissue could be the only source of soluble SSAO activity. We have found an inverse change in the activity of tissue-bound SSAO in the vessel wall and soluble SSAO, for this reason we hypothesize that there may be a relationship between the tissue-bound enzyme in the aorta and the soluble form of the enzyme. It is most probable, though, that in other models of diabetes like that seen in obesity and characterized by insulin resistance, SSAO originating from adipose tissue may also play an important role.

Total antioxidant status is a marker of oxidative stress, measured as the total radical scavenging capacity of the plasma. In our study low levels of TAS, that is, high oxidative stress was found in rats with untreated diabetes, and even in rats receiving insulin therapy once daily. Semi-intensive treatment reversed TAS levels back to normal.

A recent study by Ceriello and his co-workers has shown that increased oxidative stress originating from postprandial hyperglycemia has an independent effect on the level of soluble adhesion molecules ICAM-1, VCAM-1 and E-Selectin in the plasma of patients with diabetes.[139] There is evidence, that semicarbazide-sensitive amine oxidase is identical with Vascular Adhesion Protein-1 (VAP-1), which is regulating the adhesion and extravasation of leukocytes.[91] Thus, we suppose that oxidative stress may play an important role in the expression of SSAO (VAP-1).

It is also known that diabetes is associated with chronic subclinical inflammation[140], but the underlying mechanisms are unknown. A number of hypotheses have been put forward including inflammation originating from chronic slow infection, obesity and consequent

insulin resistance, and pre-existing atherosclerosis.[141] However, in our case the diabetic rats were neither obese, nor they had any pre-existing atherosclerosis or slow infection. Hyperglycemia and its biochemical consequences are likely to increase the acute phase response. Such a biochemical consequence may be the increase in free radical reactions, and the translocation of SSAO from the tissue-bound form to plasma. The latter can be facilitated by insulin deficiency, as we observed decreased antioxidant status and increased serum SSAO activity associated with hyperglycemia, while rats in the DM 2×I group had serum SSAO activity lower than the other two diseased groups.

Hyperglycemia leads to increased expression of cytokines interleukin (IL)-1β, IL-6 and tumor necrosis factor (TNF)-α, which increase CRP production in hepatocytes and vascular endothelial cells.[142] C-reactive protein itself is also known to act proinflammatory on human endothelial cells in vitro in the presence of human serum, regulating the expression of various adhesion molecules like vascular cell adhesion molecule (VCAM)-1, intercellular adhesion molecule (ICAM)-1, and E-Selectin, while IL-1β had the same effect alone.[134] In our study increased serum hsCRP was paralleled by an increase in SSAO/VAP-1 levels. This underlines the fact that SSAO protein physiologically acts similarly to the adhesion molecules already known. Taking into account, that we have found significant correlation between hsCRP and soluble SSAO activity, it raises the possibility that hsCRP is a marker of endothelial adhesion molecule expression.

Our results are in concordance with the above mentioned processes, as increased fructose amine levels, indicating long-term hyperglycemia and advanced glycation were correlated with hsCRP levels. We assessed serum CRP levels by a novel, high sensitivity method, which allows reliable measurements even at low serum levels.[143] The increase in hsCRP levels correlated strongly with the increase in soluble SSAO activity.

6 Conclusion

The clinical and laboratory assessment of diabetic microvascular complications is essential not only in the early diagnosis and possible treatment of the condition, but also in the understanding of the disease process.

In our work we aimed to understand the morphological alterations of the macula in diabetic patients with and without visual acuity loss by the help of optical coherence tomography. We investigated what morphological data may give the earliest signs of edema formation and also aimed to describe the role of observed macular edema patterns in visual function.

Future studies will try to elucidate the role played by the various cellular layers of the retina in disease-related thickness changes, therefore we investigated the sensitivity of optical coherence tomography image segmentation for operator-related imaging errors.

Finally, as the observed retinal alterations in diabetes are caused by underlying pathophysiological changes, we focused on soluble and tissue-bound SSAO activity in an experimental rat model. It has been previously described that elevated soluble levels of SSAO are correlated with diabetic retinopathy, therefore we investigated its relationship to insulin treatment and other biochemical markers of disease.

In summary, we have shown the following:

- We have shown the usefulness of high resolution retinal imaging by OCT to detect the earliest macular changes in diabetic retinopathy. Macular volume seems to be a more sensitive indicator of pathological changes than central foveal thickness.
- Visual acuity and retinal thickness/macular volume are strongly correlated in diabetic macular edema.
- Eyes with serous macular detachment have better visual acuity compared to eyes with similar central foveal thickness and macular volume but without SMD. The risk of developing SMD may be higher in the presence of cystoid macular edema and long diabetes duration (longer than 15 years).
- OCT image segmentation by OCTRIMA is sensitive to image artifacts related to OCT operator errors, significantly in the combined cases of decentration and depolarization.

- Careful fine-tuning of imaging settings is important in obtaining a best-possible scan, the value of SS might be of guidance with a target value of ≥6
- Soluble and aorta SSAO activities are inversely influenced by hyperglycemia in diabetes: serum activity increases while that of the tissue-bound form decreases.
- Oxidative stress caused by diabetes triggers inflammatory processes, as there was strong correlation both between oxidative stress related to diabetes, soluble SSAO activity and the increase in the level of hsCRP. As an adhesion molecule, SSAO takes part in these processes, and may facilitate future atherosclerosis.
- Insulin treatment normalizes the above pathobiochemical changes. We suppose, that our results give indirect evidence that soluble and tissue-bound SSAO activity are in negative interrelationship in diabetes. Also, our results are pointing at the importance of tight glucose control in patients with diabetes.

7 Summary

The increasing incidence of diabetes means a growing burden on the societies of developed countries because of the increasing need for disease treatment along with the treatment of complications. In developed countries, among them also in Hungary, the leading cause of legal blindness and visual impairment is diabetes. Optical coherence tomography (OCT) is an imaging method capable of near-histological resolution scanning of retinal tissue. With the use of a custom-built software it is possible to measure not only the total thickness of the retina in the macular area, but also the thickness of the retinal layers. The structural changes of the retina are caused by biochemical-physiological alterations, among which an increasing body of evidence is pointing towards the role of an enzyme, called semicarbazide-sensitive amine oxidase (SSAO). The aim of our work was to investigate how macular volume and central foveal thickness can show early macular changes secondary to diabetes, and also to investigate their relationship with visual acuity in macular edema. We also investigated the risk factors for the occurrence of serous macular detachment (SMD). We investigated the sensitivity of the OCTRIMA (Optical Coherence Tomography Retinal IMage Analysis) software towards operator related image acquisition pitfalls (depolarization, defocusing, the combination of depolarization and defocusing and decentration of the scan). We assessed the activity of soluble SSAO, which is known to be correlated with the degree of retinopathy in humans, and examined its correlation to the tissue-bound aortic SSAO enzyme activity, chronic subclinical inflammation and oxidative stress in streptozotocin-induced male Whistar rats, treated under semi-intensive and intensive insulin regimes. Our results have shown that (1) macular volume seems to be a more sensitive indicator of pathological changes in diabetes than central foveal thickness and (2) macular volume and central foveal thickness are strongly correlated to visual acuity in diabetic macular edema. Eyes with serous macular detachment have better visual acuity compared to eyes with similar central foveal thickness and macular volume but without SMD. The risk of developing SMD may be higher in the presence of cystoid macular edema and long diabetes duration (longer than 15 years). OCT image segmentation by OCTRIMA was significantly influenced by the combined cases of decentration and depolarization. The activity of aortic tissue-bound and soluble SSAO were inversely related, poor glucose homeostasis increased the activity of soluble SSAO and also increased the level of C-reactive Protein (CRP, indicator of chronic subclinical inflammation) and oxidative stress (marked by a decreased Total Antioxidant Status, TAS). The levels of CRP, TAS and soluble SSAO activity were strongly correlated and their pathological changes

were normalized only by intensive insulin treatment. Our results show the usefulness and importance of macular OCT examinations in early diabetes and also in diabetic maculopathy. Careful fine-tuning of imaging settings is important to obtain a best-possible scan in order to make reliable measurements with the use of the OCTRIMA software. Our results give indirect evidence for the source of soluble SSAO activity and emphasize the importance of tight glucose control in patients with diabetes.

8 Magyar nyelvű összefoglaló (Summary in Hungarian)

A cukorbetegség gyakoriságának folyamatos emelkedése komoly terhet ró a fejlett országok társadalmára többek között a kezelés, valamint a növekvő számban megjelenő szövődmények ellátásának a költsége miatt. Hazánkban és a fejlett világban a vakság és a látáscsökkenés egyik vezető oka a cukorbetegség. A diabeteses macula elváltozások szerkezeti vizsgálatára alkalmas eljárás az optikai koherencia tomográfia (OCT), ami a retina nagy felbontású, szövettanihoz hasonló léptékű leképezését teszi lehetővé. Egy, a közelmúltban fejlesztett szoftver használatával az OCT képeken nem csupán a teljes retina, de az egyes rétegek vastagsága is megmérhető külön-külön. A cukorbetegség okozta retina szerkezeti elváltozások hátterében a szervezet biokémiai-élettani eltérései állnak, ezek közül egyre több bizonyíték szól a szemikarbazid-szenzitív aminooxidáz (SSAO) enzim járulékos szerepe mellett. Munkánk során arra kerestük a választ, hogy a macula térfogat vagy a centrális foveoláris vastagság értékek mennyiben lehetnek jelzői a korai diabeteses macula elváltozásoknak, valamint macula oedema esetén a látott eltérések milyen kapcsolatban állnak a látóélességgel, és elemeztük az oedema képződést kísérő serosus macula leválás (SMD) rizikótényezőit. Megvizsgáltuk a maculáról készült OCT képek szegmentálására, a retina sejtrétegeinek vastagsági mérésére alkalmas OCTRIMA (Optical Coherence Tomography Retinal IMage Analysis) szoftver érzékenységét a vizsgáló okozta leképezési hibákra nézve (rossz polarizáció, rossz fókuszálás, ezek kombinációja, valamint a scan helytelen centrálása). A diabeteses retinopathiával ismerten összefüggést mutató szolubilis SSAO enzim aktivitását, valamint annak korrelációját az aortában található szöveti kötött SSAO aktivitással, a krónikus szubklinikai gyulladással, valamint az oxidatív stresszel hím Wistar patkányokban streptozotocinnal előidézett kísérletes diabetesben vizsgáltuk kétféle (félintenzív, valamint intenzív) inzulin kezelés mellett. Eredményeink rámutattak arra, hogy (1) a macula térfogat korai jelzője lehet a macula vastagsági változásainak, és (2) a macula térfogat, illetve a centrális retina vastagság szoros összefüggésben vannak a látóélességgel. Adataink alapján a macula oedemához hosszú diabetes tartam, valamint cystoid oedema jelenléte esetén társul nagyobb eséllyel SMD, ilyenkor a térfogati, illetve centrális retina vastagsági adatokból várhatónál jobb látóélességre lehet számítani. Az OCTRIMA szoftver a rossz polarizáció és fokuszálás együttes előfordulása esetén mért pontatlanul, igaz a trend a mérési hibára nézve a többi leképezési hiba esetén is jelen volt. Az SSAO enzim aktivitása a szérumban és az aortában fordított arányban állt egymással. A rossz cukor háztartás esetén emelkedett C-

reaktív protein (CRP) szintet, valamint megnövekedett oxidatív stresszt (csökent Total Antioxidáns Státuszt, TAS-t) mértünk, ezek szoros összefüggést mutattak a szolubilis SSAO aktivitással. A kóros eltéréseket csak az intenzív inzulinkezelés tudta normalizálni. Eredményeink rámutatnak az OCT vizsgálat fontosságára és hasznosságára mind korai diabetesben, mind pedig kifejezett diabeteses maculopathiában. A jövőben használni kívánt OCTRIMA szoftver esetében fontos odafigyelni a lehető legjobb minőségű leképezések készítésére, hogy megbízható vastagsági elemzések álljanak rendelkezésre. Az SSAO enzim vizsgálatával kapott eredményeink nem csupán a szolubilis enzimaktivitás forrására, valamint az egyéb biokémiai folyamatokkkal való összefüggésekre mutatnak rá, hanem ismételten felhívják a figyelmet az intenzív inzulinkezelés fontosságára.

9 Reference list

1. King H, Aubert RE, Herman WH. Global burden of diabetes, 1995-2025: prevalence, numerical estimates, and projections. *Diabetes Care* 1998;21(9):1414-31.
2. World Health Organization, Diabetes Fact Sheet. *Available from: http://www.who.int/mediacentre/factsheets/fs312/en/index.html. Accessed: March 19, 2008.*
3. American Diabetes Association, Diabetes Dictionary. *Available from: http://www.diabetes.org/diabetesdictionary.jsp?pageID=3&exitDictionaryTo=. Accessed March 19, 2008.*
4. Klein R, Klein BE, Moss SE, Davis MD, DeMets DL. The Wisconsin epidemiologic study of diabetic retinopathy. IV. Diabetic macular edema. *Ophthalmology* 1984;91(12):1464-74.
5. World Health Organization: Global initiative for the elimination of avoidable blindness: action plan 2006-2011. *Available from: URL: http://www.who.int/pbd/publications/blindness_prevention/Vision2020.pdf Accessed 19 March, 2008.*
6. Schneider M SI. Retinopathia diabetica: magyarországi epidemiológiai adatok. *Szemészet (Ophthalmologia Hungarica)* 2005;146: 441-444.
7. Németh J FA, Vastag O, Göcze P, Pető T, Elek I, Adatszolgáltatók. Vaksági okok Magyarországon 1996 és 2000 között. *Szemészet (Ophthalmologia Hungarica)* 2005;146:127-133.
8. Klein R, Moss SE, Klein BE, Davis MD, DeMets DL. The Wisconsin epidemiologic study of diabetic retinopathy. XI. The incidence of macular edema. *Ophthalmology* 1989;96(10):1501-10.
9. Nussenblatt RB, Kaufman SC, Palestine AG, Davis MD, Ferris FL, 3rd. Macular thickening and visual acuity. Measurement in patients with cystoid macular edema. *Ophthalmology* 1987;94(9):1134-9.
10. Hee MR, Puliafito CA, Duker JS, Reichel E, Coker JG, Wilkins JR, Schuman JS, Swanson EA, Fujimoto JG. Topography of diabetic macular edema with optical coherence tomography. *Ophthalmology* 1998;105(2):360-70.

11. Puliafito CA, Hee MR, Lin CP, Reichel E, Schuman JS, Duker JS, Izatt JA, Swanson EA, Fujimoto JG. Imaging of macular diseases with optical coherence tomography. *Ophthalmology* 1995;102(2):217-29.
12. Huang D, Swanson EA, Lin CP, Schuman JS, Stinson WG, Chang W, Hee MR, Flotte T, Gregory K, Puliafito CA, et al. Optical coherence tomography. *Science* 1991;254(5035):1178-81.
13. Jaffe GJ, Caprioli J. Optical coherence tomography to detect and manage retinal disease and glaucoma. *Am J Ophthalmol* 2004;137(1):156-69.
14. Cabrera Fernández D, Salinas HM, Puliafito CA. Automated detection of retinal layer structures on optical coherence tomography images. *Opt. Express* 2005;13(25):10200-10216.
15. Bizheva K, Pflug R, Hermann B, Povazay B, Sattmann H, Qiu P, Anger E, Reitsamer H, Popov S, Taylor JR, Unterhuber A, Ahnelt P, Drexler W. Optophysiology: depth-resolved probing of retinal physiology with functional ultrahigh-resolution optical coherence tomography. *Proc Natl Acad Sci U S A* 2006;103(13):5066-71.
16. Hermann B, Povazay B, Unterhuber A, Lessel M, Sattmann H, Schmidt-Erfurth U, Drexler W. Optophysiology of the Human Retina With Functional Ultrahigh Resolution Optical Coherence Tomography. *Invest. Ophthalmol. Vis. Sci.* 2006;47(5):1672-.
17. Massin P, Vicaut E, Haouchine B, Erginay A, Paques M, Gaudric A, Polito A, Del Borrello M, Isola M, Zemella N, Bandello F. Reproducibility of retinal mapping using optical coherence tomography. *Arch Ophthalmol* 2001;119(8):1135-42.
18. Polito A, Del Borrello M, Isola M, Zemella N, Bandello F. Repeatability and reproducibility of fast macular thickness mapping with stratus optical coherence tomography. *Arch Ophthalmol* 2005;123(10):1330-7.
19. Parikh RS, Parikh S, Sekhar GC, Kumar RS, Prabakaran S, Babu JG, Thomas R. Diagnostic capability of optical coherence tomography (Stratus OCT 3) in early glaucoma. *Ophthalmology* 2007;114(12):2238-43.
20. Ray R, Stinnett SS, Jaffe GJ. Evaluation of image artifact produced by optical coherence tomography of retinal pathology. *Am J Ophthalmol* 2005;139(1):18-29.
21. Stein DM, Ishikawa H, Hariprasad R, Wollstein G, Noecker RJ, Fujimoto JG, Schuman JS. A new quality assessment parameter for optical coherence tomography. *Br J Ophthalmol* 2006;90(2):186-90.
22. Kinyoun J, Barton F, Fisher M, Hubbard L, Aiello L, Ferris F, 3rd. Detection of diabetic macular edema. Ophthalmoscopy versus photography--Early Treatment Diabetic

Retinopathy Study Report Number 5. The ETDRS Research Group. *Ophthalmology* 1989;96(6):746-50; discussion 750-1.

23. Strom C, Sander B, Larsen N, Larsen M, Lund-Andersen H. Diabetic macular edema assessed with optical coherence tomography and stereo fundus photography. *Invest Ophthalmol Vis Sci* 2002;43(1):241-5.
24. Schaudig UH, Glaefke C, Scholz F, Richard G. Optical coherence tomography for retinal thickness measurement in diabetic patients without clinically significant macular edema. *Ophthalmic Surg Lasers* 2000;31(3):182-6.
25. Otani T, Kishi S, Maruyama Y. Patterns of diabetic macular edema with optical coherence tomography. *Am J Ophthalmol* 1999;127(6):688-93.
26. Goebel W, Kretzchmar-Gross T. Retinal thickness in diabetic retinopathy: a study using optical coherence tomography (OCT). *Retina* 2002;22(6):759-67.
27. Sanchez-Tocino H, Alvarez-Vidal A, Maldonado MJ, Moreno-Montanes J, Garcia-Layana A. Retinal thickness study with optical coherence tomography in patients with diabetes. *Invest Ophthalmol Vis Sci* 2002;43(5):1588-94.
28. Giovannini A, Amato GP, Mariotti C, Ripa E. Diabetic maculopathy induced by vitreo-macular traction: evaluation by optical coherence tomography (OCT). *Doc Ophthalmol* 1999;97(3-4):361-6.
29. Panozzo G, Parolini B, Gusson E, Mercanti A, Pinackatt S, Bertoldo G, Pignatto S. Diabetic macular edema: an OCT-based classification. *Semin Ophthalmol* 2004;19(1-2):13-20.
30. Gaucher D, Tadayoni R, Erginay A, Haouchine B, Gaudric A, Massin P. Optical coherence tomography assessment of the vitreoretinal relationship in diabetic macular edema. *Am J Ophthalmol* 2005;139(5):807-13.
31. Otani T, Kishi S. Tomographic assessment of vitreous surgery for diabetic macular edema. *Am J Ophthalmol* 2000;129(4):487-94.
32. Gaucher D, Sebah C, Erginay A, Haouchine B, Tadayoni R, Gaudric A, Massin P. Optical coherence tomography features during the evolution of serous retinal detachment in patients with diabetic macular edema. *Am J Ophthalmol* 2008;145(2):289-296.
33. Giovannini A, Amato G, Mariotti C, Scassellati-Sforzolini B. Optical coherence tomography findings in diabetic macular edema before and after vitrectomy. *Ophthalmic Surg Lasers* 2000;31(3):187-91.

34. Rivellese M, George A, Sulkes D, Reichel E, Puliafito C. Optical coherence tomography after laser photocoagulation for clinically significant macular edema. *Ophthalmic Surg Lasers* 2000;31(3):192-7.
35. Massin P, Girach A, Erginay A, Gaudric A. Optical coherence tomography: a key to the future management of patients with diabetic macular oedema. *Acta Ophthalmol Scand* 2006;84(4):466-74.
36. Lattanzio R, Brancato R, Pierro L, Bandello F, Iaccher B, Fiore T, Maestranzi G. Macular thickness measured by optical coherence tomography (OCT) in diabetic patients. *Eur J Ophthalmol* 2002;12(6):482-7.
37. Massin P, Erginay A, Haouchine B, Mehidi AB, Paques M, Gaudric A. Retinal thickness in healthy and diabetic subjects measured using optical coherence tomography mapping software. *Eur J Ophthalmol* 2002;12(2):102-8.
38. Martidis A, Duker JS, Greenberg PB, Rogers AH, Puliafito CA, Reichel E, Baumal C. Intravitreal triamcinolone for refractory diabetic macular edema. *Ophthalmology* 2002;109(5):920-7.
39. Schaudig U, Scholz F, Lerche RC, Richard G. [Optical coherence tomography for macular edema. Classification, quantitative assessment, and rational usage in the clinical practice]. *Ophthalmologe* 2004;101(8):785-93.
40. Brown JC, Solomon SD, Bressler SB, Schachat AP, DiBernardo C, Bressler NM. Detection of diabetic foveal edema: contact lens biomicroscopy compared with optical coherence tomography. *Arch Ophthalmol* 2004;122(3):330-5.
41. Degenring RF, Aschmoneit I, Kamppeter B, Budde WM, Jonas JB. Optical coherence tomography and confocal scanning laser tomography for assessment of macular edema. *Am J Ophthalmol* 2004;138(3):354-61.
42. Catier A, Tadayoni R, Paques M, Erginay A, Haouchine B, Gaudric A, Massin P. Characterization of macular edema from various etiologies by optical coherence tomography. *Am J Ophthalmol* 2005;140(2):200-6.
43. Ozdek SC, Erdinc MA, Gurelik G, Aydin B, Bahceci U, Hasanreisoglu B. Optical coherence tomographic assessment of diabetic macular edema: comparison with fluorescein angiographic and clinical findings. *Ophthalmologica* 2005;219(2):86-92.
44. Sugimoto M, Sasoh M, Ido M, Wakitani Y, Barakon Y, Takahashi C, Uji Y. Detection of early diabetic change with optical coherence tomography in type 2 diabetes mellitus patients without retinopathy. *Ophthalmologica* 2005;219(6):379-85.

45. Biallosterski C, van Velthoven ME, Michels RP, Schlingemann RO, DeVries JH, Verbraak FD. Decreased optical coherence tomography-measured pericentral retinal thickness in patients with diabetes mellitus type 1 with minimal diabetic retinopathy. *Br J Ophthalmol* 2007;91(9):1135-8.
46. Nilsson M, von Wendt G, Wanger P, Martin L. Early detection of macular changes in patients with diabetes using Rarebit Fovea Test and optical coherence tomography. *Br J Ophthalmol* 2007;91(12):1596-8.
47. Goebel W, Franke R. Retinal thickness in diabetic retinopathy: comparison of optical coherence tomography, the retinal thickness analyzer, and fundus photography. *Retina* 2006;26(1):49-57.
48. Goatman KA. A reference standard for the measurement of macular oedema. *Br J Ophthalmol* 2006;90(9):1197-202.
49. Van Dijk HW, Kok PHB, Abramoff MD, Schlingemann RO, Bernardes R, Verbraak FD. The sensitivity of OCT in the diagnosis of clinically significant macular edema. *Acta Ophthalmologica Scandinavica* 2007;85(s240):0-0.
50. Cabrera D, Salinas HM, Puliafito CA, Knighton RW. Assessment of Internal Reflectivity of the Various Cellular Layers of the Retina Using Optical Coherence Tomography. *Invest. Ophthalmol. Vis. Sci.* 2006;47(5):2630-.
51. Tabor CW, Tabor H, Rosenthal SM. Purification of amine oxidase from beef plasma. *J Biol Chem* 1954;208(2):645-61.
52. Clarke DE, Lyles GA, Callingham BA. A comparison of cardiac and vascular clorgyline-resistant amine oxidase and monoamine oxidase. Inhibition by amphetamine, mexiletine and other drugs. *Biochem Pharmacol* 1982;31(1):27-35.
53. Nilsson SE, Tryding N, Tufvesson G. Serum monoamine oxidase (MAO) in diabetes mellitus and some other internal diseases. *Acta Med Scand* 1968;184(1-2):105-8.
54. McEwen CM, Jr., Harrison DC. Abnormalities of Serum Monoamine Oxidase in Chronic Congestive Heart Failure. *J Lab Clin Med* 1965;65:546-59.
55. Kapeller-Adler R, Toda K. Über das Vorkommen von Monomethylamine im Harn. *Biochem Zeitschrift* 1935;248:403-425.
56. Yu PH, Zuo DM. Aminoguanidine inhibits semicarbazide-sensitive amine oxidase activity: implications for advanced glycation and diabetic complications. *Diabetologia* 1997;40(11):1243-50.

57. Lyles GA. Mammalian plasma and tissue-bound semicarbazide-sensitive amine oxidases: biochemical, pharmacological and toxicological aspects. *Int J Biochem Cell Biol* 1996;28(3):259-74.
58. Boomsma F. Semicarbazide-sensitive amine oxidases: widespread occurrence and many names and faces. *Neurobiology (Bp)* 2000;8(1):1-16.
59. Klinman JP, Mu D. Quinoenzymes in biology. *Annu Rev Biochem* 1994;63:299-344.
60. Wilmot CM, Hajdu J, McPherson MJ, Knowles PF, Phillips SE. Visualization of dioxygen bound to copper during enzyme catalysis. *Science* 1999;286(5445):1724-8.
61. Yu PH, Davis BA. Some pharmacological implications of MAO-mediated deamination of branched aliphatic amines: 2-propyl-1-aminopentane and N-(2-propylpentyl)glycinamide as valproic acid precursors. *J Neural Transm Suppl* 1990;32:89-92.
62. Mure M, Mills SA, Klinman JP. Catalytic mechanism of the topa quinone containing copper amine oxidases. *Biochemistry* 2002;41(30):9269-78.
63. Yraola F, Garcia-Vicente S, Fernandez-Recio J, Albericio F, Zorzano A, Marti L, Royo M. New efficient substrates for semicarbazide-sensitive amine oxidase/VAP-1 enzyme: analysis by SARs and computational docking. *J Med Chem* 2006;49(21):6197-208.
64. Parsons MR, Convery MA, Wilmot CM, Yadav KD, Blakeley V, Corner AS, Phillips SE, McPherson MJ, Knowles PF. Crystal structure of a quinoenzyme: copper amine oxidase of Escherichia coli at 2 A resolution. *Structure* 1995;3(11):1171-84.
65. Mu D, Medzihradszky KF, Adams GW, Mayer P, Hines WM, Burlingame AL, Smith AJ, Cai D, Klinman JP. Primary structures for a mammalian cellular and serum copper amine oxidase. *J Biol Chem* 1994;269(13):9926-32.
66. Zhang X, McIntire WS. Cloning and sequencing of a copper-containing, topa quinone-containing monoamine oxidase from human placenta. *Gene* 1996;179(2):279-86.
67. Smith DJ, Salmi M, Bono P, Hellman J, Leu T, Jalkanen S. Cloning of vascular adhesion protein 1 reveals a novel multifunctional adhesion molecule. *J Exp Med* 1998;188(1):17-27.
68. Imamura Y, Kubota R, Wang Y, Asakawa S, Kudoh J, Mashima Y, Oguchi Y, Shimizu N. Human retina-specific amine oxidase (RAO): cDNA cloning, tissue expression, and chromosomal mapping. *Genomics* 1997;40(2):277-83.
69. Imamura Y, Noda S, Mashima Y, Kudoh J, Oguchi Y, Shimizu N. Human retina-specific amine oxidase: genomic structure of the gene (AOC2), alternatively spliced variant, and mRNA expression in retina. *Genomics* 1998;51(2):293-8.

70. Zhang Q, Mashima Y, Noda S, Imamura Y, Kudoh J, Shimizu N, Nishiyama T, Umeda S, Oguchi Y, Tanaka Y, Iwata T. Characterization of AOC2 gene encoding a copper-binding amine oxidase expressed specifically in retina. *Gene* 2003;318:45-53.
71. Jalkanen S, Salmi M. Cell surface monoamine oxidases: enzymes in search of a function. *Embo J* 2001;20(15):3893-901.
72. Salmi M, Kalimo K, Jalkanen S. Induction and function of vascular adhesion protein-1 at sites of inflammation. *J Exp Med* 1993;178(6):2255-60.
73. Jaakkola K, Kaunismaki K, Tohka S, Yegutkin G, Vanttinen E, Havia T, Pelliniemi LJ, Virolainen M, Jalkanen S, Salmi M. Human vascular adhesion protein-1 in smooth muscle cells. *Am J Pathol* 1999;155(6):1953-65.
74. Boomsma F, Bhaggoe UM, van der Houwen AM, van den Meiracker AH. Plasma semicarbazide-sensitive amine oxidase in human (patho)physiology. *Biochim Biophys Acta* 2003;1647(1-2):48-54.
75. Salmi M, Stolen C, Jousilahti P, Yegutkin GG, Tapanainen P, Janatuinen T, Knip M, Jalkanen S, Salomaa V. Insulin-regulated increase of soluble vascular adhesion protein-1 in diabetes. *Am J Pathol* 2002;161(6):2255-62.
76. Stolen CM, Madanat R, Marti L, Kari S, Yegutkin GG, Sariola H, Zorzano A, Jalkanen S. Semicarbazide sensitive amine oxidase overexpression has dual consequences: insulin mimicry and diabetes-like complications. *Faseb J* 2004;18(6):702-4.
77. Hooper NM, Karran EH, Turner AJ. Membrane protein secretases. *Biochem J* 1997;321 (Pt 2)(Pt 2):265-79.
78. Kurkijarvi R, Yegutkin GG, Gunson BK, Jalkanen S, Salmi M, Adams DH. Circulating soluble vascular adhesion protein 1 accounts for the increased serum monoamine oxidase activity in chronic liver disease. *Gastroenterology* 2000;119(4):1096-103.
79. Stolen CM, Yegutkin GG, Kurkijarvi R, Bono P, Alitalo K, Jalkanen S. Origins of serum semicarbazide-sensitive amine oxidase. *Circ Res* 2004;95(1):50-7.
80. Marti L, Abella A, De La Cruz X, Garcia-Vicente S, Unzeta M, Carpene C, Palacin M, Testar X, Orozco M, Zorzano A. Exploring the binding mode of semicarbazide-sensitive amine oxidase/VAP-1: identification of novel substrates with insulin-like activity. *J Med Chem* 2004;47(20):4865-74.
81. Abella A, Garcia-Vicente S, Viguerie N, Ros-Baro A, Camps M, Palacin M, Zorzano A, Marti L. Adipocytes release a soluble form of VAP-1/SSAO by a metalloprotease-dependent process and in a regulated manner. *Diabetologia* 2004;47(3):429-38.

82. Barrand MA, Callingham BA. Monoamine oxidase activities in brown adipose tissue of the rat: some properties and subcellular distribution. *Biochem Pharmacol* 1982;31(12):2177-84.
83. Lyles GA, Singh I. Vascular smooth muscle cells: a major source of the semicarbazide-sensitive amine oxidase of the rat aorta. *J Pharm Pharmacol* 1985;37(9):637-43.
84. Enrique-Tarancon G, Marti L, Morin N, Lizcano JM, Unzeta M, Sevilla L, Camps M, Palacin M, Testar X, Carpene C, Zorzano A. Role of semicarbazide-sensitive amine oxidase on glucose transport and GLUT4 recruitment to the cell surface in adipose cells. *J Biol Chem* 1998;273(14):8025-32.
85. Dullaart RP, Riemens SC, Boomsma F. Plasma semicarbazide-sensitive amine oxidase is moderately decreased by pronounced exogenous hyperinsulinemia but is not associated with insulin sensitivity and body fat. *Scand J Clin Lab Invest* 2006;66(7):559-65.
86. Boomsma F, Ekberg K, Bruining GJ. C peptide and insulin do not influence plasma semicarbazide-sensitive amine oxidase activity. *Diabetologia* 2001;44(3):388-9.
87. Morris NJ, Ducret A, Aebersold R, Ross SA, Keller SR, Lienhard GE. Membrane amine oxidase cloning and identification as a major protein in the adipocyte plasma membrane. *J Biol Chem* 1997;272(14):9388-92.
88. Moldes M, Feve B, Pairault J. Molecular cloning of a major mRNA species in murine 3T3 adipocyte lineage. differentiation-dependent expression, regulation, and identification as semicarbazide-sensitive amine oxidase. *J Biol Chem* 1999;274(14):9515-23.
89. Zorzano A, Abella A, Marti L, Carpene C, Palacin M, Testar X. Semicarbazide-sensitive amine oxidase activity exerts insulin-like effects on glucose metabolism and insulin-signaling pathways in adipose cells. *Biochim Biophys Acta* 2003;1647(1-2):3-9.
90. Torti FM, Dieckmann B, Beutler B, Cerami A, Ringold GM. A macrophage factor inhibits adipocyte gene expression: an in vitro model of cachexia. *Science* 1985;229(4716):867-9.
91. Salmi M, Tohka S, Berg EL, Butcher EC, Jalkanen S. Vascular adhesion protein 1 (VAP-1) mediates lymphocyte subtype-specific, selectin-independent recognition of vascular endothelium in human lymph nodes. *J Exp Med* 1997;186(4):589-600.
92. Tohka S, Laukkanen M, Jalkanen S, Salmi M. Vascular adhesion protein 1 (VAP-1) functions as a molecular brake during granulocyte rolling and mediates recruitment in vivo. *Faseb J* 2001;15(2):373-82.
93. Yegutkin GG, Salminen T, Koskinen K, Kurtis C, Oroszi N, McPherson MJ, Jalkanen S, Salmi M. A peptide inhibitor of vascular adhesion protein-1 (VAP-1) blocks leukocyte-endothelium interactions under shear stress. *Eur J Immunol* 2004;34(8):2276-85.

94. Jalkanen S, Salmi M. VAP-1 and CD73, endothelial cell surface enzymes in leukocyte extravasation. *Arterioscler Thromb Vasc Biol* 2008;28(1):18-26.
95. Stolen CM, Marttila-Ichihara F, Koskinen K, Yegutkin GG, Turja R, Bono P, Skurnik M, Hanninen A, Jalkanen S, Salmi M. Absence of the endothelial oxidase AOC3 leads to abnormal leukocyte traffic in vivo. *Immunity* 2005;22(1):105-15.
96. Ekblom J. Potential therapeutic value of drugs inhibiting semicarbazide-sensitive amine oxidase: vascular cytoprotection in diabetes mellitus. *Pharmacol Res* 1998;37(2):87-92.
97. Boomsma F, van den Meiracker AH, Winkel S, Aanstoot HJ, Batstra MR, Man in 't Veld AJ, Bruining GJ. Circulating semicarbazide-sensitive amine oxidase is raised both in type I (insulin-dependent), in type II (non-insulin-dependent) diabetes mellitus and even in childhood type I diabetes at first clinical diagnosis. *Diabetologia* 1999;42(2):233-7.
98. Helander A, Tottmar O. Metabolism of biogenic aldehydes in isolated human blood cells, platelets and in plasma. *Biochem Pharmacol* 1987;36(7):1077-82.
99. Frisard M, Ravussin E. Energy metabolism and oxidative stress: impact on the metabolic syndrome and the aging process. *Endocrine* 2006;29(1):27-32.
100. Giorgio M, Trinei M, Migliaccio E, Pelicci PG. Hydrogen peroxide: a metabolic by-product or a common mediator of ageing signals? *Nat Rev Mol Cell Biol* 2007;8(9):722-8.
101. Ceriello A, Motz E. Is oxidative stress the pathogenic mechanism underlying insulin resistance, diabetes, and cardiovascular disease? The common soil hypothesis revisited. *Arterioscler Thromb Vasc Biol* 2004;24(5):816-23.
102. Deng Y, Boomsma F, Yu PH. Deamination of methylamine and aminoacetone increases aldehydes and oxidative stress in rats. *Life Sci* 1998;63(23):2049-58.
103. Thornalley PJ. Glycation in diabetic neuropathy: characteristics, consequences, causes, and therapeutic options. *Int Rev Neurobiol* 2002;50:37-57.
104. Bird MI, Nunn PB, Lord LA. Formation of glycine and aminoacetone from L-threonine by rat liver mitochondria. *Biochim Biophys Acta* 1984;802(2):229-36.
105. McLennan SV, Fisher EJ, Yue DK, Turtle JR. High glucose concentration causes a decrease in mesangium degradation. A factor in the pathogenesis of diabetic nephropathy. *Diabetes* 1994;43(8):1041-5.
106. Thornalley PJ, Westwood M, Lo TW, McLellan AC. Formation of methylglyoxal-modified proteins in vitro and in vivo and their involvement in AGE-related processes. *Contrib Nephrol* 1995;112:24-31.

107. Hamada Y, Nakashima E, Naruse K, Nakae M, Naiki M, Fujisawa H, Oiso Y, Hotta N, Nakamura J. A copper chelating agent suppresses carbonyl stress in diabetic rat lenses. *J Diabetes Complications* 2005;19(6):328-34.

108. Gubisne-Haberle D, Hill W, Kazachkov M, Richardson JS, Yu PH. Protein cross-linkage induced by formaldehyde derived from semicarbazide-sensitive amine oxidase-mediated deamination of methylamine. *J Pharmacol Exp Ther* 2004;310(3):1125-32.

109. Yu PH, Zuo DM. Oxidative deamination of methylamine by semicarbazide-sensitive amine oxidase leads to cytotoxic damage in endothelial cells. Possible consequences for diabetes. *Diabetes* 1993;42(4):594-603.

110. Deng Y, Yu PH. Simultaneous determination of formaldehyde and methylglyoxal in urine: involvement of semicarbazide-sensitive amine oxidase-mediated deamination in diabetic complications. *J Chromatogr Sci* 1999;37(9):317-22.

111. Meszaros Z, Szombathy T, Raimondi L, Karadi I, Romics L, Magyar K. Elevated serum semicarbazide-sensitive amine oxidase activity in non-insulin-dependent diabetes mellitus: correlation with body mass index and serum triglyceride. *Metabolism* 1999;48(1):113-7.

112. Garpenstrand H, Ekblom J, Backlund LB, Oreland L, Rosenqvist U. Elevated plasma semicarbazide-sensitive amine oxidase (SSAO) activity in Type 2 diabetes mellitus complicated by retinopathy. *Diabet Med* 1999;16(6):514-21.

113. Dura E, Meszaros Z, Salacz G, Magyar K, Romics L, Karadi I. [Determination of serum semicarbazide-sensitive amine oxidase activity in diabetic retinopathy in type-2 diabetes]. *Orv Hetil* 2002;143(47):2637-44.

114. Hernandez M, Sole M, Boada M, Unzeta M. Soluble semicarbazide sensitive amine oxidase (SSAO) catalysis induces apoptosis in vascular smooth muscle cells. *Biochim Biophys Acta* 2006;1763(2):164-73.

115. Yu PH, Kis QK, Lai CT, Zuo DM. Formation of formaldehyde from adrenaline in vivo; a potential risk factor for stress-related angiopathy. *Neurochem Res* 1997;22(5):615-20.

116. Chen K, Maley J, Yu PH. Potential inplications of endogenous aldehydes in beta-amyloid misfolding, oligomerization and fibrillogenesis. *J Neurochem* 2006;99(5):1413-24.

117. Jiang ZJ, Richardson JS, Yu PH. The contribution of cerebral vascular semicarbazide-sensitive amine oxidase to cerebral amyloid angiopathy in Alzheimer's disease. *Neuropathol Appl Neurobiol* 2008;34(2):194-204.

118. Yu PH, Wang M, Fan H, Deng Y, Gubisne-Haberle D. Involvement of SSAO-mediated deamination in adipose glucose transport and weight gain in obese diabetic KKAy mice. *Am J Physiol Endocrinol Metab* 2004;286(4):E634-41.

119. Karadi I, Meszaros Z, Csanyi A, Szombathy T, Hosszufalusi N, Romics L, Magyar K. Serum semicarbazide-sensitive amine oxidase (SSAO) activity is an independent marker of carotid atherosclerosis. *Clin Chim Acta* 2002;323(1-2):139-46.

120. Meszaros Z, Karadi I, Csanyi A, Szombathy T, Romics L, Magyar K. Determination of human serum semicarbazide-sensitive amine oxidase activity: a possible clinical marker of atherosclerosis. *Eur J Drug Metab Pharmacokinet* 1999;24(4):299-302.

121. Exner M, Hermann M, Hofbauer R, Kapiotis S, Quehenberger P, Speiser W, Held I, Gmeiner BM. Semicarbazide-sensitive amine oxidase catalyzes endothelial cell-mediated low density lipoprotein oxidation. *Cardiovasc Res* 2001;50(3):583-8.

122. Boomsma F, Derkx FH, van den Meiracker AH, Man in 't Veld AJ, Schalekamp MA. Plasma semicarbazide-sensitive amine oxidase activity is elevated in diabetes mellitus and correlates with glycosylated haemoglobin. *Clin Sci (Lond)* 1995;88(6):675-9.

123. Schroder S, Palinski W, Schmid-Schonbein GW. Activated monocytes and granulocytes, capillary nonperfusion, and neovascularization in diabetic retinopathy. *Am J Pathol* 1991;139(1):81-100.

124. Boomsma F, Pedersen-Bjergaard U, Agerholm-Larsen B, Hut H, Dhamrait SS, Thorsteinsson B, van den Meiracker AH. Association between plasma activities of semicarbazide-sensitive amine oxidase and angiotensin-converting enzyme in patients with type 1 diabetes mellitus. *Diabetologia* 2005;48(5):1002-7.

125. Gronvall-Nordquist JL, Backlund LB, Garpenstrand H, Ekblom J, Landin B, Yu PH, Oreland L, Rosenqvist U. Follow-up of plasma semicarbazide-sensitive amine oxidase activity and retinopathy in Type 2 diabetes mellitus. *J Diabetes Complications* 2001;15(5):250-6.

126. Nolte LA, Han DH, Hansen PA, Hucker KA, Holloszy JO. A peroxovanadium compound stimulates muscle glucose transport as powerfully as insulin and contractions combined. *Diabetes* 2003;52(8):1918-25.

127. Enrique-Tarancon G, Castan I, Morin N, Marti L, Abella A, Camps M, Casamitjana R, Palacin M, Testar X, Degerman E, Carpene C, Zorzano A. Substrates of semicarbazide-sensitive amine oxidase co-operate with vanadate to stimulate tyrosine phosphorylation of insulin-receptor-substrate proteins, phosphoinositide 3-kinase activity and GLUT4 translocation in adipose cells. *Biochem J* 2000;350 Pt 1:171-80.

128. Marti L, Abella A, Carpene C, Palacin M, Testar X, Zorzano A. Combined treatment with benzylamine and low dosages of vanadate enhances glucose tolerance and reduces hyperglycemia in streptozotocin-induced diabetic rats. *Diabetes* 2001;50(9):2061-8.

129. Abella A, Marti L, Camps M, Claret M, Fernandez-Alvarez J, Gomis R, Guma A, Viguerie N, Carpene C, Palacin M, Testar X, Zorzano A. Semicarbazide-sensitive amine oxidase/vascular adhesion protein-1 activity exerts an antidiabetic action in Goto-Kakizaki rats. *Diabetes* 2003;52(4):1004-13.

130. Iglesias-Osma MC, Garcia-Barrado MJ, Visentin V, Pastor-Mansilla MF, Bour S, Prevot D, Valet P, Moratinos J, Carpene C. Benzylamine exhibits insulin-like effects on glucose disposal, glucose transport, and fat cell lipolysis in rabbits and diabetic mice. *J Pharmacol Exp Ther* 2004;309(3):1020-8.

131. Morin N, Lizcano JM, Fontana E, Marti L, Smih F, Rouet P, Prevot D, Zorzano A, Unzeta M, Carpene C. Semicarbazide-sensitive amine oxidase substrates stimulate glucose transport and inhibit lipolysis in human adipocytes. *J Pharmacol Exp Ther* 2001;297(2):563-72.

132. Carpene C, Daviaud D, Boucher J, Bour S, Visentin V, Gres S, Duffaut C, Fontana E, Testar X, Saulnier-Blache JS, Valet P. Short- and long-term insulin-like effects of monoamine oxidases and semicarbazide-sensitive amine oxidase substrates in cultured adipocytes. *Metabolism* 2006;55(10):1397-405.

133. Libby P, Ridker PM. Inflammation and atherosclerosis: role of C-reactive protein in risk assessment. *Am J Med* 2004;116 Suppl 6A(116):9S-16S.

134. Pasceri V, Willerson JT, Yeh ET. Direct proinflammatory effect of C-reactive protein on human endothelial cells. *Circulation* 2000;102(18):2165-8.

135. Mohanty P, Hamouda W, Garg R, Aljada A, Ghanim H, Dandona P. Glucose challenge stimulates reactive oxygen species (ROS) generation by leucocytes. *J Clin Endocrinol Metab* 2000;85(8):2970-3.

136. Early Treatment Diabetic Retinopathy Study design and baseline patient characteristics. ETDRS report number 7. *Ophthalmology* 1991;98(5 Suppl):741-56.

137. Lowry OH, Rosebrough NJ, Farr AL, Randall RJ. Protein measurement with the Folin phenol reagent. *J Biol Chem* 1951;193(1):265-75.

138. Nunes S, Bernardes R, Torrent-Solans T, Soares M, Cunha-Vaz J. Retinal thickness measurements: RTA I vs RTA II, OCT II vs Stratus OCT and RTA II vs Stratus OCT in normal eyes. *Invest. Ophthalmol. Vis. Sci.* 2004;45(5):2374-.

139. Ceriello A, Quagliaro L, Piconi L, Assaloni R, Da Ros R, Maier A, Esposito K, Giugliano D. Effect of postprandial hypertriglyceridemia and hyperglycemia on circulating adhesion molecules and oxidative stress generation and the possible role of simvastatin treatment. *Diabetes* 2004;53(3):701-10.

140. Tan KC, Chow WS, Tam S, Bucala R, Betteridge J. Association between acute-phase reactants and advanced glycation end products in type 2 diabetes. *Diabetes Care* 2004;27(1):223-8.

141. Grimble RF. Inflammatory status and insulin resistance. *Curr Opin Clin Nutr Metab Care* 2002;5(5):551-9.

142. Pradhan AD, Ridker PM. Do atherosclerosis and type 2 diabetes share a common inflammatory basis? *Eur Heart J* 2002;23(11):831-4.

143. Roberts WL, Moulton L, Law TC, Farrow G, Cooper-Anderson M, Savory J, Rifai N. Evaluation of nine automated high-sensitivity C-reactive protein methods: implications for clinical and epidemiological applications. Part 2. *Clin Chem* 2001;47(3):418-25.

10 Publications of the author

10.1 Publications of the author in the scope of the present work

Papers

1. **Somfai GM**, Somogyi A, Nemes J: The relationship between macular morphology and macular function in diabetic patients assessed by optical coherence tomography. (Hungarian) *Ophthalmologia Hungarica* 2004;141(1):45-54.

2. **Somfai GM**, Salacz Gy: Optical biopsy of the retina in vivo: on optical coherence tomography and its clinical use in ophthalmology. (Hungarian) *Orv Hetil* 2005;146(21):1157-63.

3. **Somfai GM,** Knippel B, Ruzicska E, Stadler K, Tóth M, Salacz G, Magyar K, Somogyi A: Soluble semicarbazide-sensitive amine oxidase (SSAO) activity is related to oxidative stress and subchronic inflammation in streptozotocin-induced diabetic rats. *Neurochem Int* 2006 Jun;48(8):746-52. **(IF: 3,159)**

4. **Somfai GM**, Knippel B, Ruzicska É, Stadler K, Tóth M, Salacz Gy, Magyar K, Somogyi A: Soluble semicarbazide-sensitive amine oxidase (SSAO) activity and its role in streptozotocin-induced diabetic rats treated with insulin. (Hungarian) *Metabolizmus,* 2006. Szept(3);4:187-192.

5. **Somfai GM**, Salinas HM, PuliafitoCA, Fernández DC: Evaluation of Potential Image Acquisition Pitfalls during Optical Coherence Tomography and their Influence on Retinal Image Segmentation. *J Biomed Opt.* 2007 July/August, 12: 041209. **(IF 2,870)**

Presentations

1. Nemes J, **Somfai GM**, Salacz Gy: A diabeteses maculopathia vizsgálata optikai koherens tomográffal (OCT). MSzT Éves Kongresszus, Miskolc, 2002.
2. Nemes J, **Somfai GM**, Somogyi A, Salacz Gy: A maculopathia diabetica vizsgálata optikai koherencia tomográfiás készülék segítségével. Fiatal Diabetológusok VI. Országos Találkozója. Gyula, 2003.

3. **Somfai GM**, Knippel B, Ruzicska É, Salacz Gy, Magyar K, Somogyi A: A szemikarbazid-szenzitív aminooxidáz enzim aktivitása cukorbeteg és hypertóniás patkányok aortagyökében. Fiatal Diabetológusok VI. Országos Találkozója. Gyula, 2003.
4. **Somfai GM**, Knippel B, Ruzsicska É, Salacz Gy, Magyar K, Somogyi A: A szemikarbazid-szenzitív aminooxidáz enzim aktivitása cukorbeteg és hypertóniás patkányok aortagyökében. Semmelweis Egyetem PhD Tudományos Napok. Budapest, 2003.
5. Nemes J, **Somfai GM**, Salacz Gy: Diabeteses maculopathia miatt végzett laser photocoagulatio után kialakult strukturális változások vizsgálata optikai koherencia tomográffal. MSzT Éves Kongresszus, Budapest, 2003.
6. **Somfai GM**, Knippel B, Ruzicska É, Magyar K, Salacz Gy, Somogyi A: A szérum és az aorta szemikarbazid-szenzitív aminooxidáz (SSAO) enzim aktivitása kontroll és streptozotocin diabeteses patkányokban. Magyar Szabadgyökkutató Társaság Kongresszusa, Sopron, 2003..
7. **Somfai GM**: Vajon a megnövekedett macula térfogat előfutára-e a korai macula elváltozásoknak diabetesben? Fiatal Diabetológusok VII. Országos Találkozója és Továbbképzése, Siófok, 2005.
8. **Somfai GM,** Nemes J, Somogyi A, Salacz Gy: Serosus macula leválás vizsgálata diabeteses maculopathiában optikai koherencia tomográfia segítségével. MSzT Éves Kongresszus, Szeged, 2005.

Posters, citable abstracts

1. **Somfai GM**, Kovácsvölgyi S, Somogyi A, Nemes J, Salacz Gy: Optikai Koherencia Tomográfiás vizsgálatok diabetes mellitusban. Semmelweis Egyetem PhD Tudományos Napok, Budapest, 2002. (*különdíj*)
2. **Somfai GM**, Salacz Gy: Az Optikai Koherens Tomográf szemészeti alkalmazásáról. MSzT Éves Kongresszus, Miskolc, 2002.
3. Nemes J, **Somfai GM**, Salacz Gy: Structural and functional changes studied by optical coherence tomography in diabetic maculopathy after laser photocoagulation for clinically significant macular edema. 3rd Euretina Congress, Hamburg, Germany, 2003. May 15-17.

4. Nemes J, **Somfai GM**, Salacz G: Examination of diabetic macular edema with optical coherence tomography. 14th Congress of the European Society of Ophthalmology, Madrid, Spain, 2003. June 7-12.
5. Vámos R, Farkas Á, **Somfai GM**, Hargitai J: Multifocal electroretinography and Optical Coherence Tomography in cases with Stargardt's macular dystrophy. 14th Congress of the European Society of Ophthalmology, Madrid, Spain, 2003. June 7-12.
6. **Somfai GM**, Nemes J, Somogyi A, Salacz G: Optical coherence tomography is a new and reliable method for the assessment of diabetic maculopathy. 18th International Diabetes Federation Congress, 24 - 29 August 2003, Paris, France (Diabetologia (2003) 46: [Suppl. 2.]: A393, 1145)
7. **Somfai GM**, Nemes J, Salacz Gy, Somogyi A: Cukorbetegek retinavastagsága és látásélessége közötti összefüggés vizsgálata optikai koherencia tomográfiás berendezéssel. Az MDT XVII. Kongresszusa, 2004. April 22-25. Tihany, Hungary.
8. **Somfai GM**, Nemes J, Ferencz M, Hargitai J, Somogyi A, Salacz G: Is increased macular volume the first sign of minor macular changes in diabetes? Ninth Annual Vision Research Conference – Neuroimaging the retina. April 29-30., 2005, Fort Lauderdale, USA.
9. **Somfai GM**, Nemes J, Ferencz M, Somogyi A., Salacz G: Volumetric measurements obtained by optical coherence tomography may provide a useful clinical tool for the early detection of macular changes in diabetes. 41st EASD Meeting, 12-15 September 2005, Athens, Greece (Diabetologia (2005) 48: [Suppl. 1.]: 989)
10. **Somfai GM**, Nemes J, Hargitai J, Somogyi A, Salacz G: Increased macular volume measured by optical coherence tomography may be the first sign of minor macular changes in diabetes. 15th SOE and 103rd DOG Joint Congress, 25-29 September 2005, Berlin, Germany.
11. **Somfai GM,** Denis CE, Salinas HM, Nagy ZZ, Németh J, Puliafito CA, Cabrera FD: Evaluation of Potential Pitfalls Related to Operator Errors During OCT Image Acquisition. ARVO 2006, April 30-May 4, 2006, Fort Lauderdale, USA., *Invest. Ophthalmol. Vis. Sci.* 2006;47(5):2631-.

10.2 Publications of the author outside the scope of the present work

Papers

1. Nemes J, **Somfai GM**, Hargitai J: Structural changes studied by optical coherence tomography after photocoagulation for diabetic macular edema. (Hungarian) *Ophthalmologia Hungarica* 2004;141(1):41-44.

2. Ferencz M, **Somfai GM**, Récsán Zs: The effect of vitrectomy with peeling of the ILM for treatment of macular edema in diabetic retinopathy. (Hungarian) *Ophthalmologia Hungarica* 2004; 141(1):15-19.

3. Hargitai J, **Somfai GM**, Vámos R, Farkas A, Allikmets R: Foveolar thickness and macular volume changes in Stargardt macular dystrophy. (Hungarian) *Ophthalmologia Hungarica* 2004;141(1):35-39.

4. Ecsedy M, Récsán Zs, Nemes J, **Somfai GM**, Papp M: The role of optical coherence tomography and fluorescein angiography in age-related macular degeneration. (Hungarian) *Ophthalmologia Hungarica* 2004;141(1):55-60.

5. **Somfai GM**, Miháltz K, Tulassay E, Slavei K, Rigó J: The diagnosis of serous macular detachments in patients with severe preeclampsia with the use of optical coherence tomography. (Hungarian) *Magyar Nőorvosok Lapja* 2005;68:5-10.

6. Somogyi A, Herold M, Kocsis I, Nagy G, **Somfai GM**, Studinger P: Effect of vitamin E supplementation on the vitamin content of lipoprotein in young men and women. (Hungarian) *Orv Hetil* 2005;146(35):1813-1818.

7. Tönköl T, **Somfai GM**, Vámosi P: Cogenital pigmentepithelial hypertrophy. (Hungarian) *Ophthalmologia Hungarica* 2005;142(1):45-49.

8. Lengyel M, Debreczeni R, **Somfai GM**, Szigeti Zs, Rigó J Jr.: Post-partum eclampsia complicated by cortical blindness. (Hungarian) *Magyar Nőorvosok Lapja* 2005;68:341-344.

9. Hargitai J, Zernant J, **Somfai GM**, Vamos R, Farkas A, Salacz G, Allikmets R: Correlation of clinical and genetic findings in Stargardt disease patients from Hungary. *Invest Ophthalmol Vis Sci* 2005 Dec;46(12):4402-8. **(IF: 3,643)**

10. **Somfai GM**, Mihăltz K, Tulassay E, Slavei K, Rigó J Jr: Diagnosis of serous neuroretinal detachments of the macula in severe preeclamptic patients with optical coherence tomography *Hypertens Pregnancy* 2006 Mar;25(1):11-20. **(IF: 0,871)**

11. Lesch B., Szabó V, Salacz Gy, Varsányi B, **Somfai GM**, Farkas Á: Up-to date and complex examination of X-linked juvenile retinoschisis. *Ophthalmologia Hungarica*, 2006; 143(3):165-174.

12. Ferencz M, **Somfai GM**, Farkas Á, Kovács I, Lesch B, Récsán Zs, Nemes J, Salacz Gy: Functional assessment of the possible toxicity of indocyanine green dye in macular hole surgery. *Am J Ophthalmol.* 2006 Nov;142:765-70. **(IF 2,468)**

13. Kovács I, Ferencz M, Nemes J, **Somfai GM**, Salacz Gy, Récsán Zs: Intraocular lens power calculations for combined cataract surgery, vitrectomy and peeling of epiretinal membranes for macular edema *Acta Ophthalmol Scand, 2007 Feb;85(1):88-91*.
(IF: 1,458))

14. Varsanyi B, **Somfai GM**, Lesch B, Vamos R, Farkas A.: Optical coherence tomography of the macula in congenital achromatopsia. *Invest Ophthalmol Vis Sci,* 2007 May;48(5):2249-53. **(IF: 3,766)**

15. **Somfai GM**, Ferencz M, Fiedler O, Varga T, Somogyi A, Németh J: Diabetic retinopathy at the beginning of the 21st century: prevention, diagnostics and therapy. (Hungarian) *Magyar Belorvosi Archivum (Journal of the Hungarian Society of Internal Medicine)* 2007;60(2):123-127

Posters, citable abstracts

1. Vamos R, Farkas A, Entz B, **Somfai G**, Salacz G: Functional and morphological evaluation of central areolar choroidal atrophy by multifocal electroretinography and ocular coherent tomography. EVER 2002, Alicante, Spain, 2002. October 2-5.
2. Vamos R, Hargitai J, **Somfai G**, Farkas A, Lesch B, Salacz G: Multifocal electroretinography and optical coherence tomography in cases with Stargardt's macular dystrophy. XXXXI Symposium of the International Society for Clinical Electrophysiology of Vision, Nagoya, Japan, 2003. April 1-5.
3. Hargitai J, **Somfai G**, Vámos R, Farkas Á, Ekesten B, Allikmets R, Gouras P, Salacz G: Foveal thickness and macular volume changes in Stargardt macular dystrophy. ARVO 2003, Fort Lauderdale, Florida, USA, 2003. May 4-9., *Invest. Ophthalmol. Vis. Sci.* 2003;44(5):544-.
4. **Somfai G**, Hargitai J, Vámos R, Salacz G: Optical Coherence Tomography in the study of Stargardt macular dystrophy. 14th Congress of the European Society of Ophthalmology, Madrid, Spain, 2003. June 7-12.
5. **Somfai GM**, Salacz G: Traumatic macular hole with a pseudooperculum in the fellow eye assessed by optical coherence tomography. 6th Meeting of the International Society on Ocular Trauma, September 13-16, 2003, Sopron, Hungary.
6. Gombos K, Kusnyerik Á, Sebestyén M, **Somfai GM**, Salacz G: Volume changes of the macula measured by OCT after phacoemulsification and PCL implantation. EVER, October 8-11, 2003, Alicante, Spain.
7. Vámos R, Hargitai J, **Somfai GM**, Farkas A: Functional and morphologic alterations in Stargardt's macular dystrophy. EVER, October 8-11, 2003, Alicante, Spain.
8. Hargitai J, Zernant J, **Somfai GM**, Vamos R, Farkas A, Nemes J, Salacz G, Allikmets R: Correlation of clinical and genetic findings in Stargardt disease patients from Hungary. ARVO 2004, April 24-29, 2004, Fort Lauderdale, USA, *Invest. Ophthalmol. Vis. Sci.* 2004;45(5):1763-.
9. Barabasi Z, **Somfai GM**, Farkas A, Nemes J, Ferencz M, Salacz G: Bilateral Optical Coherence Tomography abnormalities in patients with central serous chorioretinopathy. ARVO 2004, April 24-29, 2004, Fort Lauderdale, USA, *Invest. Ophthalmol. Vis. Sci.* 2004;45(5):2381-.
10. Varsanyi B, **Somfai GM**, Farkas A: Optical coherence tomography in patients with achromatopsia. EVER 2004, September 24-27, 2004, Algarve, Portugal.

11. **Somfai GM**, Miháltz K, Tulassay E, Slavei K, Rigó J Jr.: Serous neuroretinal detachments of the macula diagnosed by optical coherence tomography in patients with severe preeclampsia. Conference of the International Society for the Study of Hypertension in Pregnancy, November 14-17, 2004, Vienna, Austria. (Young Investigator Award.)
12. **Somfai GM**, Kovács I, Mihátz K, Rigó J, Salacz G: Serous neuroretinal detachments of the macula diagnosed by optical coherence tomography in patients with severe preeclampsia. Ninth Annual Vision Research Conference – Neuroimaging the retina. April 29-30., 2005., Fort Lauderdale, USA.
13. **Somfai GM**, Barabási Z, Nemes J, Somogyi A., Salacz G: The Influence of Serous Macular Detachment on Visual Acuity in Diabetic Macular Edema. ARVO 2005, May 1-5, 2005, Fort Lauderdale, USA., *Invest. Ophthalmol. Vis. Sci.* 2005;46(5):394-.
14. Hargitai J, Zernant J, **Somfai GM**, Vámos R, Farkas A, Nemes J, Salacz G, Allikmets R: ABCR Mutations and Clinical Phenotype in Hungarian Patients With Stargardt Disease. ARVO 2005, May 1-5, 2005, Fort Lauderdale, USA., *Invest. Ophthalmol. Vis. Sci.* 2005;46(5):1638-.
15. Ferencz M, Kovács I, Lesch B,.Farkas A, **Somfai GM**, Barabási Z, Récsán Z, Nemes J, Fiedler O, Salacz G: Assessment of Possible Toxic Effect of Indocianine Dye Applied in Macular Hole Surgery. ARVO 2005, May 1-5, 2005, Fort Lauderdale, USA., *Invest. Ophthalmol. Vis. Sci.* 2005;46(5):4563-.
16. Lesch B, Szabó V, Vámos R, **Somfai GM**, Hargitai J, Varsányi B, Farkas Á: Optical coherence tomography and electroretinography findings in the cases of 4 Hungarian X-linked juvenile retinoschisis families. 15th SOE and 103rd DOG Joint Congress, 25-29 September 2005, Berlin, Germany.
17. Hargitai J, Zernant J, **Somfai GM**, Vámos R, Farkas Á, Salacz G, Allikmets R: Corelation of clinical and genetic findings in Stargardt disease patients from Hungary. 15th SOE and 103rd DOG Joint Congress, 25-29 September 2005, Berlin, Germany.
18. Ferencz M, Kovács I, Lesch B, Farkas Á, **Somfai GM**, Barabási Z, Récsán Z, Nemes J, Fiedler O, Salacz G: Assessment of possible toxic effect of indocyanine dye applied in macular hole surgery. 15th SOE and 103rd DOG Joint Congress, 25-29 September 2005, Berlin, Germany.
19. Varsányi B, **Somfai GM**, Lesch B, Farkas A: Comparison of OCT2 and OCT3 measurements in patients with achromatopsia. EVER 2005, 5-8 September, Vilamoura, Portugal

20. Cabrera FD, Salinas HM, **Somfai GM**, Puliafito CA: Potential use of combining the diffusuion equation with the free Schrödinger equation to improve Optical Coherence Tomography image analysis. APS Meeting, 14-18. March 2006, Baltimore, MD, USA
21. Vámos R, Lesch B, **Somfai GM**, Farkas A: Follow-up of young patients with retinitis pigmentosa by multifocal ERG: 382. Acta Ophthalmologica Scandinavica. 84 Supplement 239:49, October 2006.
22. Lesch B, Szabo V, Pámer Zs, Kenézy K, Salacz G, Papp A, **Somfai GM**, Varsanyi B, Vamos R, Hargitai J, Farkas A: 1 X-linked juvenile retinoschisis - age related macular changes by optical coherence tomography: 323. Acta Ophthalmologica Scandinavica. 84 Supplement 239:34, October 2006.
23. Varsányi B, Lesch B; **Somfai GM**, Farkas A: Age dependence of macular changes in congenital achromatopsia. Acta Ophthalmologica Scandinavica. 84 Supplement 239: October 2006.
24. **Somfai GM**, Fischer E, Ferencz M, Salacz Gy, Nagy Z: Differences in Retinal Thickness Measurements Obtained With the Fast and Slow Scanning Protocols of Stratus OCT. AAO Annual Meeting 2006, November 10-14, Las Vegas, USA
25. Ferencz M, Szepessy Z, **Somfai GM**, Kovács I, Entz B, Récsán Z, Salacz G: Posterior Capsule Opacification and Anatomical Success in Combined Operations for Macular Holes. ARVO 2007, May 6-10, 2007, Fort Lauderdale, USA., *Invest. Ophthalmol. Vis. Sci.* 2007;48(5):4127-.
26. Szepessy Z, **Somfai GM**, Fischer E, Ferencz M, Salacz G: The Assessment of Macular Volume and Thickness Symmetry in Healthy Eyes by Optical Coherence Tomography. ARVO 2007, May 6-10, 2007, Fort Lauderdale, USA., *Invest. Ophthalmol. Vis. Sci. 2007;48(5):156-.*
27. **Somfai GM**, Tatrai E, Ferencz M, Puliafito CA, Cabrera D: Quantifying Retinal Layer Thickness Changes in Eyes With Diabetic Diffuse Macular Edema Using Optical Coherence Tomography. ARVO 2007, May 6-10, 2007, Fort Lauderdale, USA., *Invest. Ophthalmol. Vis. Sci.* 2007;48(5):1426-
28. Ferencz M, Bokrétás G, **Somfai GM**, Kovács I, Fiedler O, Farkas A: The role of multifocal electroretinography in the prognosis of macular hole development. 7th EURETINA Congress, May 17-20, 2007, Monte Carlo
29. Tátrai E, **Somfai GM**, Ferencz M, Puliafito CA, Cabrera D: The assessment of retinal layer thickness and volume subsegmentation reproducibility of optical coherence

tomography images. Annual meeting of the Hungarian Society of Ophthalmology, Debrecen, Hungary 2007. June 21-23.

30. Tátrai E, **Somfai GM**, Puliafito CA, Cabrera FD: The assessment of retinal layer thickness and volume segmentation reproducibility of optical coherence tomography images. Acta Ophthalmologica Scandinavica 85 (supplement 240): 3410. doi:10.1111/j.1600-0420.2007.01062_3410.x (EVER 2007, October 4-7, Portoroz, Slovenia)
31. **Somfai GM**, Tátrai E, Ferencz M, Puliafito CA, Cabrera FD: Retinal layer thickness changes in eyes with diffuse diabetic macular edema. Acta Ophthalmologica Scandinavica 85 (supplement 240): 3381. doi:10.1111/j.1600-0420.2007.01062_3381.x (EVER 2007, October 4-7, Portoroz, Slovenia)

11 Acknowledgement - Köszönetnyilvánítás

Édesanyám kandidátusi disszertációját a család önálló társadalmi-gazdasági szerepéről írta édesapám hathatós segítségével – jelen dolgozatom is az ő igazukat mutatja: eredményeimet nem egyedül értem el, hanem az engem szűkebb-tágabb értelemben körülvevő családom segítségével, akiknek őszinte hálával tartozom:

Témavezetőm, Salacz György professzor úr lehetővé tette a szabad szárnyalást egy olyan, forradalmi berendezés mellett, ami az ideghártya korábban nem látott mélységeit és szépségeit mutatja meg.

Társ-témavezetőm, Dr. Somogyi Anikó egyetemi docens asszony anyai gondoskodásával, türelmével és szeretetével segített végig az időnként göröngyös úton, meglátásai, megérzései nélkül nem születhetett volna meg ez a dolgozat.

Hálával tartozom Magyar Kálmán professzor úrnak az izgalmas beszélgetésekért és a bölcs útmutatásokért, amiket tőle kaptam.

I would like to thank the help and friendship of Dr. Delia Cabrera Fernandez at the Bascom Palmer Eye Insitute in Miami who always encouraged and supported me during our great endeavour.

Köszönöm Németh János intézetvezető professzor úrnak, illetve Dr. Nagy Zoltán Zsolt részlegvezető egyetemi docens úrnak, amiért munkámban végig támogattak és kitartóan biztattak.

Köszönettel tartozom a Mária utcai Szemklinika teljes közösségének, amiért elfogadott és befogadott, tanított és segített eddigi utamon.

Köszönöm a Diabetológia és Anyagcsere Munkacsoportnak a szakmai együttműködést és a barátságukat, valamint a Kardiológiai Intézet Állatkísérletes Laboratórium munkatársainak és vezetőjüknek, Dr. Tóth Mikósnak a rengeteg segítséget, amit tőlük kaptam.

Szeretném megköszönni minden tanáromnak, hogy megtanítottak gondolkodni és segítettek emberré válnom, hivatástudatuk, odaadó munkájuk nélkül biztosan nem tartanék itt.

Köszönöm a Semmelweis Egyetem Doktori Iskola Titkárságán Pintérné Marádi Anna gazdasági ügyintézőnek, Márton Emőke titkárságvezetőnek, valamint Lengyel Anita és Rab Tímea ügyintézőknek, hogy végtelen türelemmel voltak mindig segítségemre, és

kedvességükkel átsegítettek egy-egy bonyolult helyzeten. Lelkes munkájuk közvetve az Egyetem valamennyi doktoranduszának teljesítményében, így a jelen dolgozatban is ott van.

Hálával tartozom édesanyámnak, édesapámnak és nagymamámnak, amiért szeretetben és törődésben neveltek fel, és amiért mindig mellettem (ha pedig kellett, mögöttem) álltak eddigi utamon. Köszönöm testvéremnek, Katának, amiért olyan jó beszélgető partner, mindig számíthatok rá, és rendíthetetlen hittel támogat mindenben. Fogadott nagyszüleimnek, Szentgyörgyi Zsuzsának és Kovács Györgynek hálás vagyok a biztatásért.

Kriszti önzetlen szeretete, támogatása erőt adott és nyugtatott, e nélkül a finisben nehéz dolgom lett volna.

Köszönöm minden barátomnak, hogy a nehéz időszakokban megértőek voltak velem, minden lehetséges eszközzel segítettek és belátással voltak elfoglaltságomra.

Végezetül, munkámat ajánlom Béci bácsi (a néhai Dr. Alberth Béla emeritus professzor) emlékének, Magdi néninek és Maszinak, akiknek a szeretete és figyelő gondoskodása gyerekkorom óta kísér.